11-18-2014

Experiment and Discrete Element Based Modeling of Granular Flow: Tribocharging and Particle Size Reduction in Pharmaceutical Manufacturing

Shivangi Naik
University of Connecticut - Storrs, shivangi.naik@uconn.edu

Experiment and Discrete Element Based Modeling of Granular Flow: Tribocharging and Particle Size Reduction in Pharmaceutical Manufacturing

Shivangi Naik, Ph.D.

University of Connecticut, 2014

Abstract

In the pharmaceutical industry, over 75 percent of all products are in the solid dosage form. Considering their prevalence, the aim of this study was to employ experimental methods and process modeling tools viz. Discrete Element Method (DEM) to ascertain the effect of powder flow and material properties during triboelectrification and particle size reduction. Considering electron exchange to be the dominant mechanism for charge transfer, work function all powders viz. Ibuprofen, theophylline, microcrystalline cellulose and lactose monohydrate was estimated from quantum chemical calculations. Tribocharging of individual powders in a V-blender revealed a higher specific charge for Ibuprofen against all surfaces. Moreover, for mixtures, charge mitigation was observed. To facilitate model development, a hopper-chute assembly was employed to investigate the effect of coefficient of friction (COF) and coefficient of restitution (COR). The specific charge increased with COF due to longer contact time and greater particle-wall collisions. Secondly, the specific charge increased as COR was decreased, suggesting that continuous contacts transfer more charge than bouncing contacts. The model was able to capture the collisional nature of tribocharging although discrepancies were observed between numerical results and experimental observations. Thus, a collective experimental and simulation approach was found to be beneficial in identifying gaps and enabling a comprehensive interpretation of an intricate process.

To study the effect of process parameters on milling, dynamic mechanical analyzer was employed to investigate the effect of damage accumulation during breakage. Damage accumulation was found to be low since the change in breakage force upon repeated impacts was insignificant. High feed rates at lower speeds resulted in flood feed conditions, which changed

the mode of breakage from fragmentation to attrition. Additionally, this effect was verified from the velocity profiles obtained from simulations that revealed stagnation of the powder bed, which consequently reduced the breakage rate. Although, the DEM model does not account for any attrition, simulations could qualitatively capture the effect of impeller speed and feed rate on the average particle size. Consequently, a combined experimental and simulations approach can be employed to direct experiment and equipment design thereby providing a better understanding of a process**.**

Experiment and Discrete Element Based Modeling of Granular Flow: Tribocharging and Particle size reduction in Pharmaceutical Manufacturing

Shivangi Santosh Naik

B. Pharm, University of Mumbai, India, 2007

M. Pharm, University of Mumbai, India, 2009

A Dissertation

Submitted in Partial Fulfillment of the

Requirements of the Degree of

Doctor of Philosophy

At the

University of Connecticut

2014

APPROVAL PAGE

Doctor of Philosophy Dissertation

Experiment and Discrete Element Based Modeling of Granular Flow: Tribocharging and Particle size reduction in Pharmaceutical Manufacturing

Presented by

Shivangi Santosh Naik

B. Pharm, University of Mumbai, India, 2007

M. Pharm, University of Mumbai, India, 2009

Major Advisor _____

Bodhisattwa Chaudhuri

Associate Advisor _____

Montgomery Shaw

Associate Advisor_____

Ramesh Malla

Associate Advisor _____

Robin Bogner

University of Connecticut

2014

Dedication

To all my grandparents, for their affection and support

Acknowledgements

The writing of this dissertation has been one of the most significant academic accomplishments in my life which could not have been achieved by the help and support of family, friends and Almighty. I am deeply indebted to my adviser Dr. Bodhisattwa Chaudhuri for his fundamental role in my doctoral work. Quite simply, his input has been immeasurable. Along with his help in DEM coding, he has kept me focused on the task at hand and provided advice and guidance at all hours. He gave me the freedom for research and at the same time continued to provide valuable feedback, and encouragement. In addition to our academic collaboration, I greatly value the close personal rapport that Dr. Chaudhuri and I have forged over the years.

I am also grateful to my associate advisors, Dr. Montgomery Shaw, Dr. Ramesh Malla and Dr. Robin Bogner for their careful appraisal and direction throughout the project. The good advice, support and friendship of my committee members have been invaluable on both an academic and a personal level, for which I am extremely grateful. I sincerely appreciate their constant motivation and thank them for their belief in me as student. They always encouraged me to "Stay Hungry and Stay Foolish".

I would also like to thank Dr. Bruno Hancock, Dr. Yu Weili and Dr. Yuri Abramov for their critical comments and valuable inputs during my research. Their constant involvement has helped me to gain a better understanding of this subject. A sincere thanks to Dr. Martin Rowland for his suggestions and practical remarks during my research.

I am extremely thankful to the Pharmaceutics faculty for providing a comprehensive graduate curriculum. The graduate seminars, courses and symposiums provided ample training and experience to grow as scientist. I would also like to thank Dr. Burgess, Dr. Xiuling, Dr. Kalonia and Dr. Pikal for useful comments and suggestions throughout my graduate study.

I personally thank Leslie Lebel and Mark Armati for their prompt assistance and special care for international students. I am indebted to my friends including Shweta, Bindu, Raj, Saurabh, Japneet, Masha, Liz, Bruna, Ekneet, Xiaoming, Chaitra, Deepthi, Meera, Sangeetha, Sandhya, Rima, Kinjal, Ruchita, Eric, Dave, Joe, Johanna, Janet and Yan for their support.

I would also like to thank Mark Drobney from Depot Campus. Mark has been a great friend who is always ready to help. I have never heard Mark say the word "Impossible". In fact, his dedication and enthusiasm for his work has been a great inspiration. I am deeply thankful to my family for their love, support, and sacrifices. Without them, this thesis would never have been written. No measure of gratitude is sufficient for their patience, love and understanding.

Table of contents

Chapter 1

Introduction and Organization of Thesis

Processes involving particulate matter are prevalent throughout the pharmaceutical industry where close to 75 percent of pharmaceutical products are formulated as tablets and capsules. These processes often consist of series of unit operations, each intended to alter the properties of material to facilitate processing and imparting desired attributes to the final product. Hence, the need for understanding the behavior of such complex particulate systems is of critical importance. To allow acceptable variations, the importance of mechanistic and parametric factors of the processes should be studied. These aspects of different unit operations pose a challenge owing to the complexities of the process involved [1-4]. For instance, electrostatic charges are known to develop upon interaction between dissimilar surfaces depend. The process of tribocharging is complex and is dependent on many factors such as shape, humidity, contact surface and mechanical factors. It is reported that flow of granular material in a typical unit operation like pneumatic conveying, fluidization, spray deposition, blending can generate 10^{-7} – 10^{-4} C/kg of static charges. Discharge of these charges in the presence of volatile liquid can also lead to explosion hazard [5-6]. Hence, myriads of industries including pharmaceutical expend significantly on safety measures and hazard detection techniques in their processing facilities. Other processes such as milling or particle size reduction are often employed in solid dosage manufacturing to improve flow and enhance solubility. Comminution is a poorly understood process as it depends on complex interaction between the operational parameters and material parameters. Ultimately, a lack of understanding of the flow and process parameters manifests into problems which can jeopardize the final outcome of the product and can also result in product recalls causing significant loss to pharmaceutical industry

A more desirable approach to address such issues is to quantitatively predict flow behavior from fundamental principles, material properties and small-scale laboratory tests, and then to engineer processes accordingly. For this purpose, the use of various process modeling tools is becoming increasingly common and is playing a critical role to gain insight into these processes. Several

computational process modeling tools are available and include computational fluid dynamics (CFD), the finite element method (FEM), and the discrete element method (DEM). In contrast to CFD and FEM models, the discrete element method is a Lagrangian dissipative particle dynamics model that tracks the positions, velocities, and accelerations of each particle individually. This approach is advantageous due to the high level of detail in the output describing the dynamic behavior of the particles. Modeling techniques which simulate unit processes are also considered as current process analytical technology (PAT) tools for process optimization and design space establishment as they can be advantageous compared to experiments with respect to time and costs. It is crucial to remember that combined numerical and experimental efforts often yield the greatest insight into new or poorly understood physical situations. Provided the experiments are well designed, disagreement between model and experiment often identifies gaps in knowledge, fostering a more complete understanding of complex physical situations. Hence, the current study is focused on investigating electrostatic charging and particle size reduction in pharmaceutical industry [7-8].

Objective and Aims

The overall objective of this work is to perform systematic experiments and numerical modeling based on first principles to study the tribo-electrification and particle size reduction in the pharmaceutical industry.

Specific Aims:

1) Investigate triboelectrification during granular flow: Experimental and computational modeling of electrostatic behavior of material in hopper-chute and V blenders**.**

    I. Experimental determination of charge developed for a given pair of material in a hopper chute system
    II. Experimental determination of charge developed for a given pair of material in a V-blender system
    III. Developing a computational model for flow in hopper and V-blender using discrete element method with the incorporation of electrostatic forces. The model will be verified by comparing with the trends obtained from experiments.

2) Investigating particle size reduction of granular material: Experimental and computational modeling of particle size reduction in Wiley mill.

I. A parametric study on Wiley mill to understand the influence of operational parameters on size reduction.
II. Developing a Discrete element model for fragmentation which will be compared with experiments.

Outline

Chapter 2 reviews some fundamental aspects of contact charging, including description of work function, mechansim involved in triboelectrification and techniques of measuring electrostatic charge. It also elucidates the different process and formulation factors involved in tribocharging of pharmaceutical powders. Furthermore, the most used and cited numerical models developed for understanding tribocharging are also described.

Chapter 3 describes the study of contact charging in a hopper-chute system. It focusses on tribocharging due to simple unidirectional flow against a metal and a polymer surface. An attempt has also been made to determine the work function of all materials using semi-empirical approaches. A 3D-DEM model incorporating charge transfer [9-10] and electrostatic forces [11-12] has been presented.

Chapter 4 describes a detailed experimental and simulation study of tribocharging in a V-blender for pharmaceutical powders. A more comprehensive list of contact surfaces has been included owing to the prevalence of tribocharging in aerosol drug delivery [13-16]. The effect of contact time and blender speed on tribocharging has been investigated. The model developed in the previous chapter has been extended for the V-blender geometry. An, effort has been made to correlate tribocharging of pharmaceutical powders to properties such as cohesive energy density (CED) and surface energy [17].

Chapter 5 describes the triboelectrification of mixtures. The mixtures at intermediate concentration exhibited significant charge mitigation. These unanticipated trends previously reported have been explored using process modeling approaches [18-20]. The DEM model developed in Chapter 3 has been extended to include both particle-particle and particle-wall

charge transfer. The particle-particle charge transfer is suspected to actually enhance electrostatic interaction between the drug and excipient and decrease the overall charge transfer between particle and wall.

Chapter 6 describes a review on different approaches for quantifying milling. Despite being ubiquitous in pharmaceutical field, it is one of the least understood processes owing to the complexity of material and machine factors involved during milling. Considering the ongoing initiative of FDA to encourage design in quality, the review is focused on some process analytical tools to characterize particle size distribution as well process modelling tools to simulate particle size reduction. The review highlights on some current experimental and modeling approaches used to quantify and understand the physics behind the process of dry milling.

Chapter 7 describes a model for fragmentation in an impact mill. It employs the concepts of fracture mechanics and single particle breakage to develop a DEM based model for milling. Lactose non-pareil has been used as a model compound in the simulation studies. Additionally parametric studies have been explored using the DEM model and include effect of feed rate, impeller speeds and impeller wall tolerance. Some insights have been provided regarding the mechanism of milling at different operating conditions [21-22]

Chapter 8 provides a summary for the entire thesis

References

1. Bridgewater, J., The dynamics of granular materials – towards grasping the fundamentals. Granular Matter, 4(2003), 175–181.

2. Meier, S.W., R.M. Lueptow, and J.M. Ottino, A dynamical systems approach mixing and segregation of granular materials in tumblers. Advances in Physics, 56(2007), 757-827.

3. Geldart, D., Powder Processing - The Overall View, in Principles of Particle Technology, John Wiley & Sons Ltd, (1990), 1-7.

4. Muzzio, F.J., T. Shinbrot, and B.J. Glasser, Powder technology in the pharmaceutical industry: the need to catch up fast. Powder Technology, 124(2002), 1-5.

5. Wong J., Chan H.-K., Kwok P.C.L., 2013. Electrostatics in pharmaceutical aerosols for inhalation. Ther.Deliv.4, (2013) 981–1002.

6. Glor M. Transfer of powders into flammable solvents overview of explosion hazards and preventive measures, Journal of Loss Prevention in Process Industries, 19(2006), 656-660.

7. Ketterhagen W, Ende M. A., Hancock B. Process Modeling in the Pharmaceutical Industry using the Discrete Element Method, Journal OF Pharmaceutical Sciences, 98(2009), 442-470.

8. Kremer, D.K., Hancock, B.C. Process simulation in the pharmaceutical industry: a review of some basic physical models. Journal of Pharmaceutical Sciences 95 (2006) 517-529.

9. Pei C., Wu C.-Y.,England, D.,Byard,S.,Berchtold,H., Adams M. Numerical analysis of contact electrification using DEM–CFD. PowderTechnol.248, (2013), 34–43.

10. Laurentie J.C., Traoré P., Dascalescu L. Discrete element modeling of triboelectric charging of insulating materials in vibrated granular beds. Journal of Electrostatics 71, (2013), 951-957.

11. Hogue M.D., Calle C.I., Curry D.R., Weitzman P.S. Calculating the trajectories of triboelectrically charged particles using discrete element modeling (DEM), J. Electrost. 66 (2008), 32–38.

12. Hogue M.D., Calle C.I., Curry D.R., Weitzman P.S. Discrete element modeling (DEM) of triboelectrically charged particles: revised experiments, J. Electrost. 67 (2009), 691–694

13. Karner S.,Urbanetz N.A. Triboelectric characteristics of mannitol based formulations for the application in dry powder inhalers. PowderTechnol.235, (2013), 349–358.

14. Karner S., Littringer E. M,, Urbanetz N. A. Triboelectrics : The influence of particle surface roughness and shape on charge acquisition during aerosolization and the DPI performance. Powder Technology 262 (2014), 22–29

15. Kwok P.C.L., Glover W., Chan, H.K. Electrostatic charge characteristics of aerosols produced from metered dose inhalers. Journal of Pharmaceutical Sciences, 94(2005), 2789–2799.

16. Telko M.J.,Kujanpää J., Hickey A.J. Investigation of triboelectric charging in dry powder inhalers using Electrical Low Pressure Impactor (ELPI). Int. J. Pharm. 336 (2007) 352–360.

17. Ahfat, N.M., Buckton, G., Burrows, R., Ticehurst, M.D., 2000. An exploration of interrelationships between contact angle, inverse phase gas chromatography and triboelectric charging data. Eur. J. Pharm. Sci. 9(2000), 271–276.

18. Engers D.A., Fricke M.N., Storey R.P., Newman A.W., Morris K.R. Triboelectrification of pharmaceutical relevant powders during low-shear tumble blending. Journal of Electrostatics, 64(2006), 826–835

19. Engers D.A., Fricke M.N., Storey R.P., Newman A.W., Morris K.R. Triboelectric charging and dielectric properties of pharmaceutically mixtures. Journal of Electrostatics, 65, (2007), 571–581.

20. Murtomaa M., Laine E. Effect of surface coverage of a glass pipe by small particles on the triboelectrification of glucose powder. Journal of Electrostatics, 54, (2001), 311–320.

21. D.E. Grady, Fragmentation under impulsive stress loading, in: W.L. Fourney, et al., (Eds.), Fragmentation by blasting, Society for Experimental Mechanics, Connecticut, USA, (1985), 63–72.

22. Naik, S., Malla R., Shaw M., Chaudhuri B. 2013. Investigation of Comminution in a Wiley Mill: Experiment and DEM Simulations Powder Technol. 237(2013), 338-354

Chapter 2

Triboelectrification: A review of experimental and mechanistic modeling approaches with a special focus on pharmaceutical powder

Shivangi Naik [1], Bodhisattwa Chaudhuri [1,2*]

[1]Department of Pharmaceutical Sciences, University of Connecticut, Storrs, CT, 06269, USA

[2] Institute of Material Sciences, University of Connecticut, Storrs, CT, 06269, USA

*Corresponding Author

Email: bodhi.chaudhuri@uconn.edu

Abstract

Pharmaceutical processing inevitably involves relative movements of particles against solid surfaces, thus providing ample opportunities for triboelectrification. The charged particles can cause problems such agglomeration, segregation during flow or adhesion to process equipment. In addition, if particles are excessively charged, an electrostatic discharge may occur, which can pose a risk of fire and explosion hazards. Despite its prevalence, the electrostatic charging process is not fully understood, owing to the numerous factors that affect the phenomenon. The current review, briefly examines some of the basic concepts involved in charge transfer. It highlights the different experimental approaches employed in measuring electrostatic charges and summarizes the various factors involved in tribocharging. To theoretically analyze the process of particle charging, relevant numerical models have also been discussed.

Keywords: work function, insulators, DEM, electrostatic forces.

1. Introduction

Electrostatic effects on solids have been known for a long time; the ancient Greeks in the sixth or seventh century B.C. had already observed that amber attracts small objects after rubbing. Contact electrification is defined as the transfer of electric charge from one to the other when two different materials are brought into contact and separated. When the two materials are rubbed against each other, the process of charge transfer can be called 'frictional electrification' or 'triboelectric charging [1,2]. Such contact electrification or tribocharging which has been known for many years now, is often significant in industrial processes. For instance, the ability of electrostatic forces to control the motion of charged particles has been exploited in many applications such, e.g. electrophotography, electrostatic precipitation and particle separation [3-7]. As powders and particulate solids are extensively used in solid dosage manufacturing, electrostatic effects are also significant in the pharmaceutical industry. For example, electrostatic dry coating has been used as an alternative coating technique to obtain uniform coating for solid oral dosage forms as well as intravascular stents [8-11]. Although powder charging is found to be beneficial in these coating processes it is often considered as a nuisance for other powder operations such as mixing, micronization, pneumatic transport and silo discharge. The electrostatic forces generated in such cases are a concern since the accumulated charge on these particles can cause adhesion or agglomeration leading to processing difficulties [12]. Electrostatic forces may also result in undesirable adhesion of charged drug particles to drug devices such as inhalers and hence affect the trajectory and deposition of aerosols within the lungs[13]. Moreover, if the particles are excessively charged, an electrostatic discharge can occur, which can pose a risk of fire and explosion hazards [12]. While, contact charging has been known for many years, there are still many uncertainties, and in some cases, inconsistent results have been reported. This is because there are several factors, viz. chemical, physical, electrical properties and environmental conditions, which affect the process. [14-17] In light of these potential effects, different approaches have been applied to the characterize tribocharging, with different objectives and to varying degrees of success. The current review summarizes these methods and the basic mechanisms involved in charge transfer between solid surfaces. It highlights the various factors and different experimental approaches utilized to measure the electric charge of

pharmaceutical powders. To this end, numerical methods based on first principle such as Discrete element Method (DEM) incorporating charge transfer has been deliberated.

2. Concepts and Mechanism of Charge transfer

2.1. Work Function

One of the fundamental properties involved in charging of materials is their work function and is defined as the minimum energy needed to extract an electron from a material. The experimental methods routinely employed to determine work function of surfaces are Photoemission spectroscopy (PES) and Kevin-Zisman method [18-20]. PES refers to measurement of energy of electrons emitted from solids by the photoelectric effect. It is sensitive to the surface region due to the short range of the emitted photoelectrons and measures the kinetic energy spectra of photoelectrons emitted by molecules to determine orbital energies and work function. The Kevin-Zisman method, on the other hand, (Fig.1) employs, an electric circuit consisting of a vibrating capacitor, a DC bias voltage supply, and an electrometer to determine the work function of the sample material. The material whose work function is to be determined is placed into the concavity of the lower electrode and the upper electrode made of gold oscillates vertically above the sample. When the voltage applied on the upper electrode is equal to the potential difference between the sample and the upper electrode, the induced currents detected by the electrometer become zero. The work function can be calculated from this applied voltage and from the known work function of gold. Thus, the Kevin-Zisman method determines the work function relative to probe used, whereas PES allows the measurement of the absolute value of work function [20]. Besides these limited experimental approaches, computational tools are also available to determine the work function of surfaces. For instance, Yanagida et al [21] and Trigwell *et al.* [22] have determined the electronic states of polymers by computational molecular orbital calculations and found these values to be almost proportional to the threshold energy of photoemission that corresponds to the work function of polymers. Ab initio calculations have been employed by Yoshida et al. [23] to determine work function and study the charge transfer for insulators. Their results indicate that the C atom with a dangling bond is more effective to transfer electrons than the fluorine atom.

2.2. Mechanism of charge transfer

Metal contact electrification has been studied for many years and is well understood to be a process of the transfer of electrons.

$$\Delta q = C_o V_c = -C_o (\emptyset_1 - \emptyset_2)/e \qquad (1)$$

Φ_1 and Φ_2 represent the different work functions of the materials, while *e* refers to the elementary electronic charge (1.62×10^{-19}C), C_o is the capacitance between the two contacting bodies and V_c is the contact potential difference (CPD) [17]. However, the charging mechanisms in case of insulators are still poorly understood despite of extensive research. This is because insulator surfaces are difficult to characterize and the electron energies are ill-defined. Based on experimental evidence, the concept of work function or electron transfer has also been extended to nonmetals. For example, in case of metal-insulator contacts, linear relationships have been found between charge density of polymers and metal work functions that support an electron exchange mechanism [17, 24-25]. Moreover, theoretical relationships between work function, dielectric constant and particle size of polymers by Gallo and Lama, also support the concept of electron transfer for tribocharging of insulators [26]. These studies suggest that when two substances with different dielectric constants or work function establish a contact, the material with a higher dielectric constant would donate electrons to the other and thus become positively charged (Table 1). The overall trends indicate that larger particles tend to be electron donors and become positively charged whereas the smaller particle of the same material accept electrons and become negatively charged. In a similar manner, experimental evidence suggests that charging of polymers also depends upon the chemical nature of the side group existing on carbon chain backbone. Certain chemical functional groups have been identified to be involved in tribocharging and in decreasing order of donor tendency. These include: OH > OCOR > C_6H_5 > COOH > CN [27]. To investigate the effect of functional groups on tribocharging, Gibson [28-30] employed a cascade method, where metal beads were flown over an inclined plate coated with a film made of salicylaldehyde or substituted polystyrenes. Linear correlations were observed for the specific charge and Hammett substituent constant of the functional group. These results strongly reinforced the investigation between chemical structure and triboelectrification of insulators. Thus, plasma modification of polymer surfaces has been extensively studied and has been shown by X-ray photoelectron spectroscopy (XPS) to modify the functional groups on the

polymer backbone hence altering the chemical structure. As an example, quantum chemical calculations revealed a decrease in work function of PFTE upon substitution of the fluorine group by hydroxyl or carbonyl group. Consequently, for many organic compounds, the charging tendency can be determined by the energy level of HOMO and LUMO since they depend on the functional groups present in the chemical structure [22, 31].

Besides electrons, some researchers have also suggested that electrolytic ions and adsorbed water play an important role in the charging process. Diaz *et al.* demonstrated that for dyes containing a large organic cation and a small inorganic anion, charge transfer would result in a positively charged toner due to transfer of the mobile ion [32-33]. Law *et al.* have successfully verified ion transfer mechanism by employing toners coated with a cesium salt as a negative charge control agent. The linear correlation between the toner charge and the amount of cesium transferred, as determined by surface analysis XPS (x-ray photoelectron spectroscopy), serve as an evidence for ion transfer charge mechanism [34]. This mobile ion mechanism cannot be applied to non-ionic polymers since they do not contain any mobile ions and yet exhibit charge exchange just as much as mobile ion containing polymers. For these non-ionic polymers it has been proposed that hydrophobic surfaces such as fluorocarbons can adsorb water from the air. The presence of water on these surfaces can affect surface conductivity and hence contact electrification under ambient conditions. Whiteside et al. proposed that hydroxide ions, generated from rapid equilibration of hydroxide and hydronium ions within the thin water layer between polymers can be preferentially adsorbed to one of the surfaces, though it is not yet understood why some polymers have greater affinity than others for hydroxide ion [35]. Recently, however, in experiments designed to verify this hypothesis it has been demonstrated that contact charging can occur between nonionic polymers even in the total absence of water. Other reports have also demonstrated that charging can take place in vacuum between freshly cleaved polymer surfaces that were never exposed to the atmosphere. Thus, although the ion transfer mechanism has been demonstrated for ionic polymers it yet has to be verified for non-ionic polymers [36]. Nonetheless, for most materials, electron transfer has been assumed to be involved in tribocharging. Some general trends have been observed in the interaction of different materials; part of this information has been captured in triboelectric series, which ranks materials in their propensity of acquiring positive (and negative) electric charge [22]. A combination of new surface-specific spectroscopic techniques that can be used under ambient conditions and increasingly

sophisticated computer simulations may be able to test the different hypothesis viz. electron v/s ion transfer which has been suggested for triboelectrification.

3. Electrostatic Charge Measurement techniques

A diverse range of electrostatic measurement devices have been described in the literature for powders and aerosolized particles. These devices were individually designed by separate research groups and operate on different mechanistic principles. The simplest instrument for measuring electrostatic charge is the Faraday pail or Faraday well. It consists of two metal containers, one situated inside the other. The outer well is grounded to provide shielding from interferences by stray charges or electric fields in the vicinity. The inner well, connected to an electrometer, is electrically insulated to prevent charge leakage. A charged object in the inner well induces a flow of electrons to or from earth through the electrometer to balance the charge in the well. To measure the charge on powders, the Faraday cup can be used in different ways. In some studies, after tribocharging under different conditions the powder has been directly poured into the Faraday cup to measure the resultant charge. The Faraday cup measurement system is a very sensitive device and hence this method should be avoided as manual pouring of the powders into cup can itself generate charges. The preferable technique is to convey the powders directly into the Faraday cup following tribocharging [37-41]. Besides powders, the Faraday cup can has also been used for characterizing charging behavior of aerosols. In these measurements, the powders are first drawn out and the residual charge on the inhaler is then determined. The limitation of this setup is that the charges among different size fractions cannot be determined [42]. Another modification is a through-type Faraday cage utilized by Watanabe *et al.* to study the tribocharging of pharmaceutical particles by impact. The entire experimental assembly involved two through-type Faraday cages, the first installed to measure the particle charge before impact and the second within the collection chamber to measure the particle charge after impact [37]. An array of Faraday cages mounted vertically in cascade has been utilized by Zhao *et al.* [43] to study triboelectrification in a fluidized bed. This series of Faraday cages have open holes and the measurements are performed during the free falling of particles. The charge and mass of particles are measured with each Faraday cage. Since this technique allows studying charge distribution it can be used to study complex bipolar system. Besides, the Faraday cup newer techniques have evolved to measure particle charges for bulk powder. These non-intrusive

and real-time techniques are able to generate signals that give electrostatic parameters for processes such as mass flow rate, volume loading and velocity For instance, Kwek *et al.* [44] employed a non-intrusive experimental procedure involving a vibrating capacitive probe to analyze the triboelectric chargeability of pharmaceutically powders such as adipic acid and α-lactose monohydrate under controlled environmental conditions.

To measure the aerodynamic diameter and charge for aerosols; electrical low pressure impactor (ELPI) [44-45] or the electrical-single particle aerodynamic relaxation time (E-SPART) [47] analyzer can be employed. The ELPI is a cascade impactor that can classify particle size fractions and measure the charge on each impactor. Unlike conventional cascade impactors, ELPI detects particle deposition by measuring electrical current resulting from dissipation of the particle's charges. The collected particles can be measured simultaneously on all stages using a multichannel electrometer and reported in real-time on a computer. Since impactor stages are electrically isolated, size specificity of charging can be evaluated. For example, Kwok *et al.* [45] used the ELPI to investigate the effect of different inhaler devices and observed a positive charge on the fine fractions and a shift to negative charge on the coarser fractions. Since ELPI provides both mass and charge distribution it can be used to evaluate inhaler devices as well as the deposition behavior from a temporal perspective.

An ESPART device generates an oscillating electric field within the device that causes particles to oscillate and the particle's response to these oscillations results in information about the particle's count mean aerodynamic diameter and its charge-to-mass ratio. Unlike the ELPI, that measures the average charges for mass deposited, E-SPART can obtain charges for individual particles [47]. Saini et al. [48] recently used the E-SPART to study aerosol particle electrostatics. Inhalers were actuated into a collection chamber from which the E-SPART sampled particles over the course of several minutes. The study illustrated bipolar particle charging and suggested that charging was a result of interaction between inhaler surfaces and formulation.

Electrostatic grid-probes have also been employed to measure charge distribution on aerosols. The measurement system consists of three conducting grids through which the charged aerosol passes. When the distance between the grids is relatively small, the probe gives information about the charge distribution as a function of time. Murtoma *et al.* [49] employed an

electrostatic grid probe to study charge distribution in dry powder inhalers (DPI). The study concluded that if the generated charge on particles is due to separation of drug and additive particles then particles always carry opposite charges. On the other hand, if the charge of the aerosol is mainly due to contacts with the inhaler surfaces, drug and additive particles tend to carry similar charges. Thus, the electrostatic grid was also capable of separating charge signals from the drug and additive particles. Such quantitative information has the potential to reduce aggregation and enhance deposition in the lung for DPI delivery.

4. Influencing variables

As tribocharging is by influenced by the interplay of material properties and environmental factors (Table 2 and Table 3), it is often difficult to envisage the extent of charging. It is difficult to predict in which way the sign and magnitude of the charge might change. Hence, the electrostatic charging of a powder in a given process may not be applicable to the same powder in a different process. Despite these difficulties, some factors have been recognized to affect electrostatic charging and include surface properties viz shape [50], surface roughness [51-53], process and formulation factors [54-63] and atmospheric conditions such as relative humidity [64-66]. Some of these factors will be discussed in the following sections

4.1. Surface

As triboelectrification arises from interactions between surfaces, the geometry and composition of surfaces would directly affect charging. With respect to geometry, Ireland [67] investigated the effect of particle shape on tribocharging by examining the interaction of particulate flow over a solid surface. According to these studies, spherical particles tend to roll and gather more charges than sliding contacts, as compared to irregular shaped particles. As a rolling particle presents a fresh surface area every time it flows, they have a greater capacity to accumulate charge. Kraner *et al.* [53] also observed similar results for mannitol particles; particles with higher aspect ratios were found to charge much more than particles with lower aspect ratios. Besides particle shape, the effect of surface roughness has also been investigated. For instance, Kwek *et al.* [52] compared the tribocharging of rough and smooth surfaces of mannitol generated by spray drying at different conditions. Subsequent triboelectrification studies revealed rough and smooth particles to accumulate specific charges of 3.23 ± 0.54 and 1.35 ± 0.30 nC/g, respectively. This differential charging between mannitol particles has been attributed to significantly higher

surface potential of rough particles (~ −5.91 kV/m^2) as compared to smooth particles (~ −1.42 kV/m^2). Moreover, surface roughness of a particle also influences the contact area with the surface and can hence affect the overall charge transfer.

Based on the concept of work function, contact surfaces can also affect the extent of charging. For example, Carter et al. [68] experimentally determined the charge on lactose following tribocharging against brass, steel, and cellulose. Stainless steel was found to impart a more electronegative charge on lactose than brass due to a difference in work function. Similarly, Eilbeck et al [51] investigated the charging of lactose particles by blowing through a cyclone apparatus with interchangeable internal surface materials. They observed that polyvinylchloride (PVC) generated positively charged particles whereas acetal and stainless steel produced negative charges. Polypropylene imparted a minimal charge on the particles and thus was suggested to be a suitable material for avoiding charges during processing. Coating of surfaces by particulate material also affects charging process. In such cases, particle deposits can promote particle-particle and decrease particle-wall interactions. For instance, Elajnaf *et al.* [69] examined the effect of coating of stainless steel mixing vessels on tribocharging of powders. A considerable decrease in triboelectrification of salbutamol sulphate and ipratropium bromide was observed following film coating with the same drug viz. salbutamol sulphate and ipratropium bromide respectively. These studies suggest that charge transfer between like surfaces is minimal. As most DPI formulations consist of micronized drug blended with larger carrier particles, the electrostatic interactions between drug and carrier have been recognized as a major determinant of DPI performance. Telko *et al.* [46] characterized the electrostatic behavior of DPI powders using ELPI and generated a triboelectric series that follows the order (from most negative to most positive charge): Budesonide < glucose < calcium phosphate < milled lactose < sieved lactose < albuterol. Consequently, such triboelectric series can be very useful to estimate the relative charging capacity of many materials and hence facilitate the choice of materials for storage and packaging of powders as well as for the components of dry powder inhaler (DPI) devices.

4.2. Process and Formulation parameters

Dense powder flows characterized by multiple particle-particle and particle wall contacts are often are encountered in powder handling operations such as pneumatic conveying, sieving,

mixing and milling. Hence, in addition to aforementioned surface properties, the extent of the charging also depends on various process and formulation parameters. To understand the electrostatic behavior of powders during these handling stages, Engers et al. [70] employed a low-shear stainless steel blender and measured the charge by dispensing the powder directly into a Faraday pail. The surface charge density for all powder compounds was determined after 40 blender rotation. Different grades of MCC were observed to charge to a different extent and this behavior was attributed to the microstructure of these porous particles, which are commonly manufactured by spray-drying with differences in amorphous–crystalline content. Parameters such as hold time after processing and composition of the formulation were found to be the most effective means of dissipating charge, whereas the use of grounding straps were less effective. Colloidal silicon dioxide was found to be the most effective excipient in reducing the surface charge density in comparison to other excipients such as lactose monohydrate.

The charging kinetics of particles in mixers has been examined by Zhu et al [71]. Various operating conditions, particle characteristics, mixer type, had an impact on the triboelectrification of adipic acid, microcrystalline cellulose, and glycine. The accumulated charge on the powders was found to increase as the blender speed was increased from 34 rpm to 72 rpm. Greater tribocharging with blender speed was believed to be due to an increase in particle-wall contacts as well as a decrease in charge relaxation since the interval between successive collisions decreases with increase in blender speed. Tribocharging was also found to be greater for sliding motion in a horizontal oscillating mixer than the impact motion in a turbula mixer. The increase in tribocharging in horizontal oscillating mixer was recognized to be due to an increase in apparent contact area owing to sliding motion. For all powders, it was observed that the charge increased monotonically with mixing time until reaching saturation. The charging profiles for fine adipic acid particles were found to be different from those of coarse adipic acid and was recognized to be due to adhesion of particles onto the mixer wall that can alter the particle–wall contacts and slower the charging kinetics.

As particle charging due to multiple contacts is difficult to analyze, Watanabe *et al.* explored charging due to a single impact for aspirin, ethyl cellulose and lactose monohydrate [37]. These powders were impacted against a stainless steel target at velocities ranging from 0-30 m/s. For all powders, the impact charge increased linearly with impact velocity. The equilibrium

charge on softer materials such as aspirin and ethyl cellulose was found to be higher due to greater contact areas upon impact. The equilibrium charge was also found to be linearly related to the contact potential difference of the sample powders.

Statistical DOE studies have been carried out by Karner *et al.* [72-73] to investigate the influence and interactions of particle size, container size and concentration of fines. Detailed studies of a range of particle sizes, suggested that the magnitude of the charge increases continuously with decrease in particle size. Rowley *et al.* also observed a similar result (Table 3). Tribocharging was also found to increase upon addition of fines (<40 μm) to coarse particles (100 μm–125 μm). This strong increase in the net charge was believed to be due to the adhesion of fine particles to coarse particles that eventually lead to an enhancement of the surface roughness of the coarse particles. Interaction effects were observed for particle size and container size. Additional studies also demonstrated the effect of aerosolization on triboelectrification of powders. The strongest effect was observed upon increasing the air flow rate through the inhaler from 60 l/min to 90 l/min. This behavior was attributed to the higher impact and shear velocity of particle–particle and particle–wall contacts generated at higher air flow rates.

4.3. Relative Humidity

Since moisture has a strong effect on the electrical conductivity of the surface of particles, relative humidity plays an important role in tribocharging of powders. As such in many cases, particle charging has been found to decrease with increasing ambient relative humidity (RH) [64, 74-75]. It has been suggested that moisture can reduce the surface contact, change the conductivity or other bulk properties of the particles, and hence facilitate charge neutralization. In a similar manner, the volume resistivity and charge decay half-life of pharmaceutical powder compacts were also found to decrease with increasing humidity [76].

Relative humidity and electrostatic charge can also influence the fine particle fraction and the emitted dose of a DPI. Kwok and Chan [77] measured the electrostatic charge of an aerosol released from two commercial DPI devices viz. Pulmicort (Budesonide) and Bricanyl (terbutaline sulfate) at different RH-levels. Bricanyl followed the expected trend and the absolute specific charges decreased with increasing RH up to 90%. In case of Pulmicort a similar decrease in charge was observed up to 65%. However, the absolute specific charges then increased at RH greater than 65%. The authors suggested that this increase in charging was due to greater

cohesive forces between agglomerates. Thus, at higher RH only those particles that can be successfully dislodged from the agglomerate became dispersed and are suspected to be carrying more charges. As terbutaline sulfate is more hygroscopic and electrically more conductive than Budesonide, such a behavior was not observed from Bricanyl inhalers.

5. Numerical Simulations

The aforementioned factors affect tribocharging, as they can influence the contact area, pressure, duration and contacting frequency between surfaces, which are difficult to quantify experimentally [60]. Secondly, when a large number of particles are present, the charge on the nearby particles can affect the motion of particles. For instance, if all the particles have the same charge then the particles tend to repel each other and deposit on nearby surfaces. This is known as the space charge effect [78]. These forces cannot be evaluated without accounting for the position of all charged particles. With respect to numerical methods, discrete element method (DEM) serves as a powerful tool that can predict particle trajectories from Newton's law of motion. It continuously calculates inter-particle and particle-boundary forces and can hence simulate the collisional nature of powder flow. These approaches are more flexible than Monte Carlo simulations as they permit a direct relation between material properties and model parameters [79]. For example, Watano *et al.* [80] employed a three-dimensional discrete element method (DEM) to study electrification during pneumatic conveying of powders. The effect of particle load and fluidization velocity on triboelectrification was evaluated using a simple charge transfer model. This model (Eq. 2) assumed the electrification of particles to be proportional to the vertical collision velocity.

$$\Delta q = \sigma * S(v) \qquad (2)$$

Thus the charge on the particle for a single collision, has been calculated from the contact area *S(v),* and the charge density, *σ.* The contact area was calculated using Hertz theory and extension by Masui and Murata [81] for plastic deformation was employed. The charging model also assumed the contact surface to get a constant charge density σ, which was derived from experiments. No electrostatic forces were incorporated into the DEM model. In these simulations, as the charge transfer occurs mainly by particle collisions against the pipe wall, the specific charge was found to decrease with the initial load. Increase in fluidization velocity

increased the specific charge up to a maximum value and then followed a decrease due to the turbulent airflow. Although, the experimental results were well explained by these numerical calculations, the predicted charges were a factor of three to five times higher. Matsuyama et. al [82] employed a similar to Watano *et al.* for charge transfer in vibrating cylindrical container. They observed that the resemblance between simulations and experiments improved when coulombic forces were incorporated into the DEM model. A comprehensive model on tribocharging incorporating both charge transfer and the effect of electrostatic forces has also been employed by Hogue et al [83-84]. The DEM model simulates charge transfer during flow of glass spheres along an inclined chute of different materials viz. were aluminum, polyvinyl chloride (PVC), low density polyethylene (LDPE), nylon, and polytetrafluoroethylene (PTFE). The charging of the particles in the simulations was modeled using a time dependent semi empirical relation (Eq.3) with a charging rate constant α, the saturation charge of the particle q_{sat} and the initial charge on the particle q_{in}.

$$\frac{dq}{dt} = \alpha(q_{sat} - q_{in}) \qquad (3)$$

The simulations performed without any electrostatic forces produced the smallest amount of separation across the incline while the unscreened electrostatic force (Coulomb's forces) produced the greatest. For the screened electrostatic forces (Eq.4), q_1 and q_2 represent the charges of two particles, r is the distance between their centers, ε is the relative permittivity of medium, ε_o is the permittivity of the free space (8.85×10^{-12} F/m) , τ is the screening factor, e is the charge of the electron(1.602×10^{-19} C), ε is the relative permittivity of the medium, , T is the temperature in Kelvin, K_B is the Boltzmann's constant (1.38×10^{-23} JK^{-1}), and n_i is the number of particles with charge q_i in the near vicinity.

$$F_{sc} = \frac{q_1 q_2}{4\pi\varepsilon_o}\left(\frac{\tau}{r} + \frac{1}{r^2}\right)e^{-\tau r} \qquad \tau = e\sqrt{\left(\frac{1}{\varepsilon\epsilon_0 T K_B}\sum_i n_i q_i^2\right)} \qquad (4)$$

Addition of a screened electrostatic force to DEM calculations illustrated a reasonable similarity for flow width between the experimental digital frames and the simulation snapshots. Moreover, the comparison between experimental and simulations results for the total charge/mass obtained for different chute inclinations was also found to be reasonable. However, in this simulation model, the effect of chute inclination was investigated by maintaining the charging efficiency constant for different chute materials. Consequently, this charging constant ensured that the particles would charge negatively whereas the inclined plane would charge positively upon contact.

A charging process can also be described by a capacitor or condenser model where it is assumed that the accumulation of charge on the surface of the contacting particles is analogous to the build-up of charge on a capacitor. Thus, the surfaces in contact are viewed as two parallel plates which are charged by a potential difference V. This potential is caused by the difference in work function of the dissimilar surfaces [85]. Tanoue et al. [86] employed a condenser model within the DEM–CFD framework to simulate powder tribocharging in a gas–solid two-phase flow. Although there was a good agreement between particle diameter and acquired charge, it was found that the effects of air velocity and pipe diameter on the impact charge are qualitatively different from those of the experimental results. A lack of electrostatic forces in the numerical model could explain these discrepancies since the influence of space charges was found to increase at a denser flow. As these were not included in the model, it may explain some of the incorrect trends. Another probable reason for this discrepancy is that the DEM model considered charge transfer as long as the particle was in contact with the wall. This can also result in overcharging of the system owing to the explicit nature of DEM model.

Pie et. al [87] employed a 2D DEM model to analyze the charge transfer during pneumatic flow. To compute the charge transfer in a collision, a condenser model (Eq.5) was introduced, where

$$\Delta q = kS\Delta V \qquad (5)$$

$$\nabla V = V_i - V_j - V' \qquad (6)$$

ΔV is the total potential difference for a collision, S is the contact area, k is the charging constant during contact electrification and is of the order of 10^{-4} C · m^{-2} · V^{-1}. The total potential (Eq.6)

difference was determined by the work function potentials (V_i, V_j) of the materials and the induced potentials generated (V') during collisions. Additionally, charge transfer was considered only for the maximum contact area for a given collision which was determined by comparing the value of the contact area at each time step during the collision. No electrostatic forces were incorporated in the DEM model. This simulation model was employed to investigate the effect of particle size and air fluidization on contact electrification. It was demonstrated that, in successive impacts, the charge on the particle increased and eventually reached equilibrium. The charge/mass ratio was also found to increase with decrease in particle size. Moreover, the transferred charge decreased as the accumulated charge on the particle increased. It was also observed that during the initial stage of the fluidization, regions near the walls of a pipe have higher charge densities than particles in the center of the bed, due to frequent particle-wall collisions. Additionally, higher superficial gas velocity resulted in a faster charge accumulation due to increased collision frequency and impact velocity. Laurentie et al. [88] also employed a similar 2D condenser model for electrostatic separation of polymer particles in a vertically-vibrated bed. The charge exchange between colliding particles as well as the Coulomb force acting on particles was computed from the electric field based on superposition principle. The total electric field was obtained from the vector addition of the electric field due to charged particles and the external electric field generated from a high-voltage supply to facilitate separation of granular plastics. The numerical results were found to fit very well to the experimental data following fine tuning of the work function of the polymers employed in the experimental set up. Although, numerical modeling for tribocharging is limited, the findings presented from these models are relevant to industrial processes as they provide insight on parameters that affect charge transfer at particle level.

6. Conclusions

Triboelectrification of powders is a multifaceted process that has been recognized to play a substantial role in powder processing. As such, conflicting observations have been reported and consistency between labs has often been lacking. Evidently, cleanliness and environmental conditions play an important role and should be carefully controlled. Another challenge for these experimental studies of triboelectric charging is to obtain data that can be linked to theoretical predictions. As such the inherent complexity of the process necessitates the application of new

analytical tools. Sensitive surface analyses could provide a powerful approach to recognize the charge transfer carriers as well identify the most relevant factors involved in tribocharging. Additionally, the development of dynamic measurement techniques to monitor charge accumulation during manufacture of powder formulations can elucidate the effect of different operational factors involved in tribocharging. Although such analysis is scarce, some general trends have been observed from bulk measurements and are summarized in the form of triboelectric series. Some attempts have also been made to model the charging of an ensemble of particles in different configurations. In most cases, charge transfer is modeled as simple capacitor or condenser. Numerical methods such as DEM have been employed to quantify tribocharging during powder flow as they can capture the collisional nature of tribocharging viz. mechanical factors that are difficult to measure experimentally. Further research should focus on the improvement of the charge exchange model by taking into account the effect of the ambient relative humidity. In closing, the information assembled from such experimental and computational approaches could potentially improve the understanding of triboelectrification; thereby improving theoretical predictions.

Nomenclature

Φ	Work Function
V_c	Contact potential difference
V’	Induced potential
C_o	Capacitance
ε_o	permittivity of the free space
ε	the relative permittivity of the medium
s	Contact area
k	Charging constant
e	Charge of an electron
q	Charge of particle
T	Temperature
K_B	Boltzmann Constant
F_{sc}	Screened Coulombic forces
τ	Screening factor
r	Distance
σ	Charge density

Abbreviations

CPD	Contact potential difference
DPI	Dry powder inhaler
DOE	Design of experiments
HOMO	Highest occupied Molecular orbital
LUMO	Lowest occupied Molecular orbital
ELPI	electrical low pressure impactor
ESPART	electrical-single particle aerodynamic relaxation time
MCC	Microcrystalline cellulose
PES	Photoelectron Spectroscopy
XPS	X-ray Photoelectron Spectroscopy

7. References

1. Hendricks C.D., Charging macroscopic particles. In Moore AD, editor Electrostatics and its Applications. New York, NY: John Wiley & Sons. (1973) 57-85.
2. Peart J 2001. Powder electrostatics: Theory, techniques, and applications. Kona 19, (2001) 34-45.
3. Gupta R., Gidaspow D., Wasan D.T., Electrostatic separation of powder mixtures based on the work functions of its constituents. Powder Technology 75, (1993) 79–87.
4. Lawless P.A., Electrostatic precipitators. In: Webster, J.(Ed.),Wiley Encyclopedia of Electrical and Electronics Engineering,vol.7.JohnWiley& Sons, Inc. (1999)1–15.
5. Mazumder M.K., In: Webster.(Ed.),Wiley Encyclopedia of Electrical and Electronics Engineering,vol.7. JohnWiley & Sons, Inc., (1999)15–39.
6. Schein L.B., Electrophotography and Development Physics, 2nd ed. Springer-Verlag/Laplacian Press, Berlin (1992/1996).
7. Schein L.B., Recent advances in our understanding of toner charging. Journal of Electrostatics 46,(1999) 29–36.
8. Pfeffer R., Dave R.N., Wei D., Ramadhan M., Synthesis of engineered particulates with tailored properties using dry particle coating. Powder Technol.117, (2001) 40–67.
9. Luo Y.F., Zhu J., Ma Y.L., Zhang H., Dry coating, a novel coating technology for solid pharmaceutical dosage forms. Int. J. Pharm. 358, (2008)16–22.
10. Qiao M., Zhang L., Ma Y., Zhu J., Xiao, A novel electrostatic dry coating process for enteric coating of tablets with Eudragits L100-55. Eur. J. Pharm. Biopharm. 83, (2013) 293–300.
11. Nukala R., Boyapally H., Slipper I., Mendham A., Douroumis D., The application of electrostatic dry powder deposition technology to coat drug- eluting stents. Pharm. Res.27, (2010) 72–81.
12. Gibson N., Static electricity – an industrial hazard under control. J. Electrostat. 40(1), (1997), 21–30.
13. Wong J., Chan H.-K., Kwok P.C.L., 2013. Electrostatics in pharmaceutical aerosols for inhalation. Ther. Deliv. 4, (2013) 981–1002.
14. Lowell J., Akande A.R., Contact electrification—why is it variable? Journal of Physics D:Applied Physics 21, (1988) 125–137
15. Jones T.B., Electromechanics of Particles. Cambridge University Press, Cambridge, (1995)

16. Bailey, A. G., Charging of Solids and Powders. Journal of Electrostatics 30, (1993)167-180
17. Harper W.R., Contact and Frictional Electrification. Clarendon Press, Oxford. (1967)
18. Itakura T., Masuda H., Ohtsuka C., Matsusaka S., The contact potential difference of powder and the tribo-charge. J. Electrostat. 38, (1996), 213–226.
19. Murata Y., Photoelectric emission and contact charging of some synthetic high polymers. Jpn. J. Appl. Phys,. 18(1979) , 1–8
20. Matsusaka S., Maruyama H., Matsuyama T., Ghadhiri M., Triboelectric charging of powders: a review.Chem.Eng.Sci.65, (2010), 5781–5807.
21. Yanagida K., Okada O., Oka K., Low-energy electronic states related to contact electrification of pendant-group polymers: photoemission and contact potential difference measurement. Japanese Journal of Applied Physics 32, (1993), 5603–5610
22. Trigwell S., Grable N., Yurteri C.U., Sharma R., Mazumder M.K., Effect of surface properties on the tribocharging characteristics of the polymer powder as applied to industrial processes, IEEE Transactions in Industry Applications 39 (2003) 79–86
23. Yoshida M., Ii N., Shimosaka A., Shirakawa Y., Hidaka J., Experimental and theoretical approaches to charging behavior of polymer particles. Chemical Engineering Science 61, (2006), 2239–2248.
24. Davies D. K., Charge generation on dielectric surface. J. Phys. D: Appl. Phys., Ser. 22, (1969) 1533-1537
25. Lowell J., The electrification of polymers by metals. J. Phys. D: Appl. Phys. **9**, (1976) 1571-1577
26. Gallo C.F., Lama W.L., Some charge exchange phenomena explained by a classical model of the work function. Journal of Electrostatics 2 (1976), 145-150.
27. Deryagin BV, Krotova NA, Smilga VP, Adhesion of Solids. New York, NY: Consultants Bureau. (1978)
28. Gibson, H.W., Linear free energy relationships—triboelectric charging of organic solids. Journal of the American Chemical Society 97, (1975) 3832–3833.
29. Gibson H.W., Bailey F. C., Linear free energy relationships. Triboelectric charging of poly(olefins). Chem. Phys. Lett., 2 (1977) 352–355.
30. Gibson, H.W., Control of electrical properties of polymers by chemical modification. Polymer 25 (1984), 3–27.

31. Morra M., Occhiello E., and Garbassi F., "Aging of plasma-treated polytetrafluoroethylene surfaces," Surf. Inter. Anal., 16 (1990), 412–415.
32. Diaz A.F., Fenzel-Alexander D., 1993. Anion transfer model for contact charging. Langmuir 9, (1993) 1009–1015.
33. Diaz A.F., Guay J., Contact charging of organic materials: ion vs. electron transfer. IBM Journal of Research and Development 37, (1993) 249–259.
34. Law K.-Y., Tarnawskyj I. W., Salamida D., Debies T., Investigation of the Contact Charging Mechanism between an Organic Salt Doped Polymer Surface and Polymer-Coated Metal Beads. Chem. Mater. 7, (1995) 2090-2095.
35. McCarty L.S., Whitesides G.M., Electrostatic charge due to separation of ions at interfaces: Contact electrification of ionic electrets. Angew. Chem. Int. Ed. 47, (2008) 2188- 2207.
36. M. W. Williams. Triboelectric charging of insulating polymers–some new perspectives. AIP Advances 2, (2012) 1-9.
37. Watanabe H., Ghadhiri M., Matsuyama T., Ding Y.L., Pitt K.G., Maruyama H., Matsusaka S., Masuda H., Triboelectrification of pharmaceutical powders By particle impact. International Journal of Pharmaceutics 334, (2007 a) 149–155.
38. Brown C., Tutorial review: simultaneous measurement of particle size and particle charge. Journal of Aerosol Science, 28, (1997) 1373–1391.
39. Šupuk E., Zarrebini A., Reddy J.P., Hughes H., Leane M.M., Tobyn M.J., Timmins P., Ghadiri M., Tribo-electrification of active pharmaceutical ingredients and excipients. Powder Technol. 217, (2012) 427–434.
40. Šupuk E., Ghori M.U., Asare-Addo, K., Laity P.R., Panchmatia P.M., Conway B.R.,The influence of salt formation on electrostatic and compression properties of flurbiprofen salts. Int. J. Pharm. 458, (2013) 118–127.
41. Sarkar S., Cho J., Chaudhuri B., Mechanisms of electrostatic charge reduction of granular media with additives on different surfaces. Chem. Eng. Process. 62, (2012)168–175.
42. Chow K.T., Zhu K., Tan R.B.H., Heng P.W.S., Investigation of electrostatic behavior of a lactose carrier for dry powder inhalers. Pharmaceutical Research, 12, (2008) 2822–2834.
43. Zhao H., Castle G.S.P., Inculet I.I., 2002. The measurement of bipolar charge in poly-disperse powders using a vertical array of Faraday pail sensors. Journal of Electrostatics 55, (2002) 261–278.

44. Kwek J.W., Jeyabalasingam M., Ng W.K., Heng J.Y.Y., Tan R.B.H., Comparative study of the triboelectric charging behavior of powders using a nonintrusive approach. Ind. Eng. Chem. Res. 51, (2012) 16488–16494.
45. Kwok P.C.L., Glover W., Chan, H.K., Electrostatic charge characteristics of aerosols produced from metered dose inhalers. Journal of Pharmaceutical Sciences, 94, (2005) 2789–2799.
46. Telko M.J., Kujanpää J., Hickey A.J., Investigation of triboelectric charging in dry powder inhalers using Electrical Low Pressure Impactor (ELPI). Int. J. Pharm. 336, (2007) 352–360.
47. M. Ali, Reddy R. N., Mazumder M. K., Electrostatic charge effect on respirable aerosol particle deposition in a cadaver based throat cast replica. Journal of Electrostatics 66 (2008) 401–406
48. Saini D., Trigwell S., Srirama, P.K., Sims R.A., Sharma R., Biris A.S., Mazumder M. K., Portable free-fall electrostatics separator for beneficiation of charged particulate materials. Part. Sci. Technol. 26, (2008) 349–360
49. Murtomaa M., Strengell S., Laine E., Bailey A., Measurement of electrostatic charge of an aerosol using a grid-probe.J.Electrostat.58, (2003 a) 197–207.
50. Murtomaa M., Mellin V., Harjunen P.,Lankinen T., Laine E.,Lehto V.-P., Effect of particle morphology on the triboelectrification in dry powder inhalers. Int. J. Pharm. 282, (2004) 107–114.
51. Eilbeck J., Rowley G., Fletcher J., Smith I., Investigation of the effects of contact surface on triboelectrification in pharmaceutical powders. In: 11th Pharmaceutical technology conference, 2, (1992) 358.
52. Kwek J.W., Heng D., Lee S.H., Ng W.K., Chan H.K., Adi S., Heng J., Tan R.B.H., High speed imaging with electrostatic charge monitoring to track powder deagglomeration upon impact. J. Aerosol Sci. 65, (2013) 77–87.
53. Karner S., Littringer E. M., Urbanetz N. A., Triboelectrics : The influence of particle surface roughness and shape on charge acquisition during aerosolization and the DPI performance. Powder Technology 262, (2014) 22–29
54. Murtomaa M., Harjunen P., Mellin V.,Lehto,V.-P., Laine E., Effect of amorphicity on the triboelectrification of lactose powder.J.Electrostat.56, (2002c) 103–110.

55. Murtomaa M., Laine E., Electrostatic measurements on lactose–glucose mixtures. J. Electrostat. 48, (2000)155–162.
56. Murtomaa M., Ojanen K., Laine E., Poutanen J., Effect of detergent on powder triboelectrification. Eur. J. Pharm. Sci.17, (2002 a) 195–199.
57. Murtomaa M., Ojanen K., Laine E., Effect of surface coverage of a glass pipe by small particles on the triboelectrification of glucose powder. J. Electrostat. 54, (2002 b) 311–320.
58. Pingali K.C., Shinbrot T., Hammond S.V., Muzzio F.J., An observed correlation between flow and electrical properties of pharmaceutical blends. Powder Technol.192, (2009b) 157–165.
59. Pu Y., Mazumdar M., Cooney C., Effects of electrostatic charging on pharmaceutical powder blending homogeneity.J.Pharm.Sci.98, (2009) 2412–2421.
60. Rowley G., Quantifying electrostatic interactions in pharmaceutical solid systems. Int. J. Pharm. 227, (2001) 47–55.
61. Staniforth J.N., Rees J.E., Electrostatic charge interactions in ordered powder mixes. J. Pharm. Pharmacol. 34, (1982) 69–76.
62. Wong J., Kwok P., Noakes T., Fathi A., Dehghani F., Chan H., Effect of crystallinity on electrostatic charging in dry powder inhaler formulations. Pharm. Res., (2014)1–9.
63. Hoe S., Traini D., Chan H.-K., Young P., The influence of flow rate on the aerosol deposition profile and electrostatic charge of single and combination metered dose inhalers. Pharm. Res. 26,(2009b) 2639–2646,
64. Rowley G., Mackin L.A., The effect of moisture sorption on electrostatic charging of selected pharmaceutical excipient powders. Powder Technology, 135&136, (2003) 50–58.
65. Kwok P.C.L., Noakes T., Chan H.K., Effect of moisture on the electrostatic charge properties of metered dose inhaler aerosols. Journal of Aerosol Science 39, (2008) 211–226.
66. Young P., Sung A., Traini D., Kwok P.C.L., Chiou H., Chan H.-K., Influence of humidity on the electrostatic charge and aerosol performance of dry powder inhaler carrier based systems. Pharm. Res.24, (2007) 963–970.
67. Ireland P.M., Triboelectrification of particulate flows on surfaces: Part II—mechanisms and models. Powder Technology, 198, (2010) 199–210.

68. Carter P.A., Rowley G., Fletcher E.J., Hill E.A., An experimental investigation of triboelectrification in -cohesive pharmaceutical powders. Drug Dev. Ind. Pharm. 18, (1992)1505–1526.
69. Elajnaf A., Carter P., Rowley G. Electrostatic characterization of inhaled powders: effect of contact surface and relative humidity. European Journal of Pharmaceutical Sciences, 29, (2006) 375–384.
70. Engers D.A., Fricke M.N., Storey R.P., Newman A.W., Morris K.R., Triboelectrification of pharmaceutically relevant powders during low-shear tumble blending. J. Electrostat. 64, (2006) 826–835.
71. Zhu K.W., Tan R.B.H., Chen F.X., Ong K.H., Heng P.W.S., Influence of particle wall adhesion on particle electrification in mixers. Int. J. Pharm.328, (2007) 22–34.
72. Karner S., Urbanetz N.A., Arising of electrostatic charge in the mixing process and its influencing factors. Powder Technol. 226, (2012) 261–268.
73. Karner S., Urbanetz N.A., Triboelectric characteristics of mannitol based formulations for the application in dry powder inhalers.PowderTechnol.235, (2013) 349–358.
74. Gold D, Palermo BT, Hopper flow electrostatics of tableting material I. Journal of Pharmaceutical Sciences 2 (1965) 310-312.
75. Eilbeck J, Rowley G, Carter PA, Fletcher EJ, Effect of contamination of pharmaceutical equipment on powder triboelectrification. International Journal of Pharmaceutics 195 (2000) 7-11.
76. Grosvenor MP, Staniforth JN, The influence of water on electrostatic charge retention and dissipation in pharmaceutical compacts for powder coating. Pharmaceutical Research 13(1996) 1725-1729.
77. Kwok P.C.L., Chan H.K., Effect of relative humidity on the electrostatic charge properties of dry powder inhaler aerosols. Pharmaceutical Research 25, (2008) 277–288.
78. Finlay W., The mechanics of inhaled pharmaceutical aerosols. Academic Press, San Diego (2001).
79. Ketterhagen W.R. Am Ende, M.T., Hancock B.C., Process modeling in the pharmaceutical industry using the discrete element method. J. Pharm. Sci. 98, (2009) 442–470.
80. Watano S., Mechanism and control of electrification in pneumatic conveying of powders, Chem. Eng. Sci. 61 (7) (2006) 2271–2278.

81. Noriaki Masui, Yuji Murata, Electrification of polymer particles by impact on a metal plate, Jpn. J. Appl. Phys. 22 (1983) 1057–1062.
82. Matsuyama T., ˇSupuk E.,Ahmadian H.,Hassanpour A.,Ghadiri,M., Analysis of tribo-electric charging of spherical beads using distinct element method. Powders and Grains 2009.AIP, NewYork, (2009) 127–130.
83. Hogue M.D., Calle C.I., Weitzman P.S., Curry D.R., Calculating the trajectories of triboelectrically charged particles using discrete element modeling (DEM), J. Electrost. 66 (2008) 32–38.
84. Hogue M.D., Calle C.I., Weitzman P.S., Curry D.R., Discrete element modeling (DEM) of triboelectrically charged particles: revised experiments, J. Electrost. 67 (2009) 691–694.
85. Matsuyama T., Yamamoto H., Characterizing the electrostatic charging of polymer particles by impact charging experiments, Advanced Powder Technology 6 (1995) 211–220.
86. K.-I. Tanoue, H. Tanaka, H. Kitano, H. Masuda, Numerical simulation of triboelectrification of particles in a gas–solids two-phase flow, Powder Technol. 118 (2001) 121-129.
87. Pei C., Wu C.-Y., England D., Byard S.,Berchtold H.,Adams M., Numerical analysis of contact electrification using DEM–CFD. PowderTechnol.248, (2013) 34–43.
88. Laurentie J.C., Traoré P., Dascalescu L., Discrete element modeling of triboelectric charging of insulating materials in vibrated granular beds. Journal of Electrostatics 71, (2013) 951-957.

Tables

Table 1: Triboelectric series for polymers[26]

Material	Work Function (eV)	Dielectric Constant (K)
PFTE	5.75	2.1
Polyvinly chloride (PVC)	5.13	3.4
Polysulfone	4.95	3.0
Polystyrene	4.90	2.6
Polyethylene	4.80	2.4
Polycarbonate	4.68	3.17
Polymethylmethacrylate (PMMA)	4.54	4.2
Polyvinly acetate	4.38	5.5
Nylon	4.3	6.3
Polyethylene oxide	3.98	7.6

Table 2: Effect of contact surface on tribocharging

% (RH)	Process	Triboelectric series
20	Cyclone charger [64]	Stainless steel <Acetal <Lactose <PP < PVC
5-25	Bin Blender [70]	Pseudoephedrine HCl< Stainless steel<Dicalcium phosphate dihydrate<MCC<Lactose monohydrate<acetaminophen
30-35	Hopper-Chute [41]	Aluminum < glass < lactose < PVC
25-30	Turbula mixer [71]	MCC<Glycine<Stainless Steel<Adipic acid
5-15	Vibratory Shaker	Lactose monohydrate< Hydroxy Propyl cellulose<PFTE
50-60	Impact [37]	Ethyl cellulose<stainless steel<Sucrose<Aspirin<PFTE

Table 3: Effect of process parameters on tribocharging

Factors	Effect
Mixing speed [70-72]	Equilibrium charge independent of blender speed.
Contact time [37,71-73]	Charge increases exponentially with time and then plateaus.
Relative humidity [64-66,74-77]	Powders: ▪ Decreases with increase in RH for all bulk powders. ▪ Significant for hygroscopic powders Aerosols: ▪ the charge behavior depends on FPF ▪ may increase or decrease

Table 4: Effect of particle size on tribocharging[60]

Particle size (μm)	Charge (nC/g)
335-500	10
250-355	28
125-150	50
90-125	65

Figures

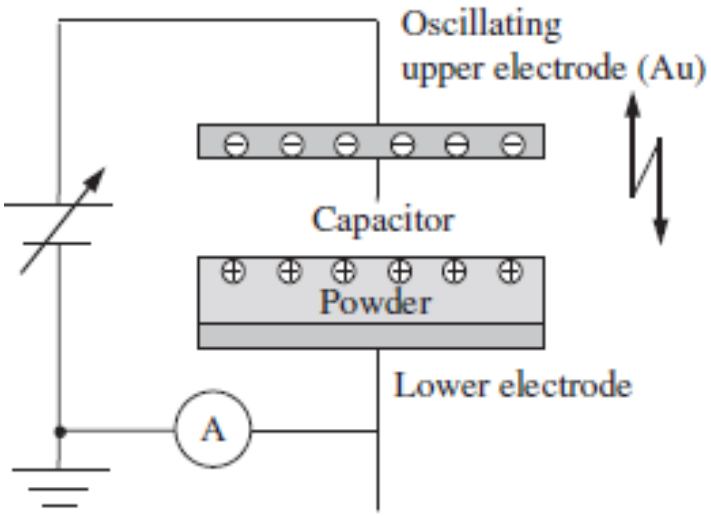

Figure1. Equivalent electric circuit of the Kelvin–Zisman method [20]

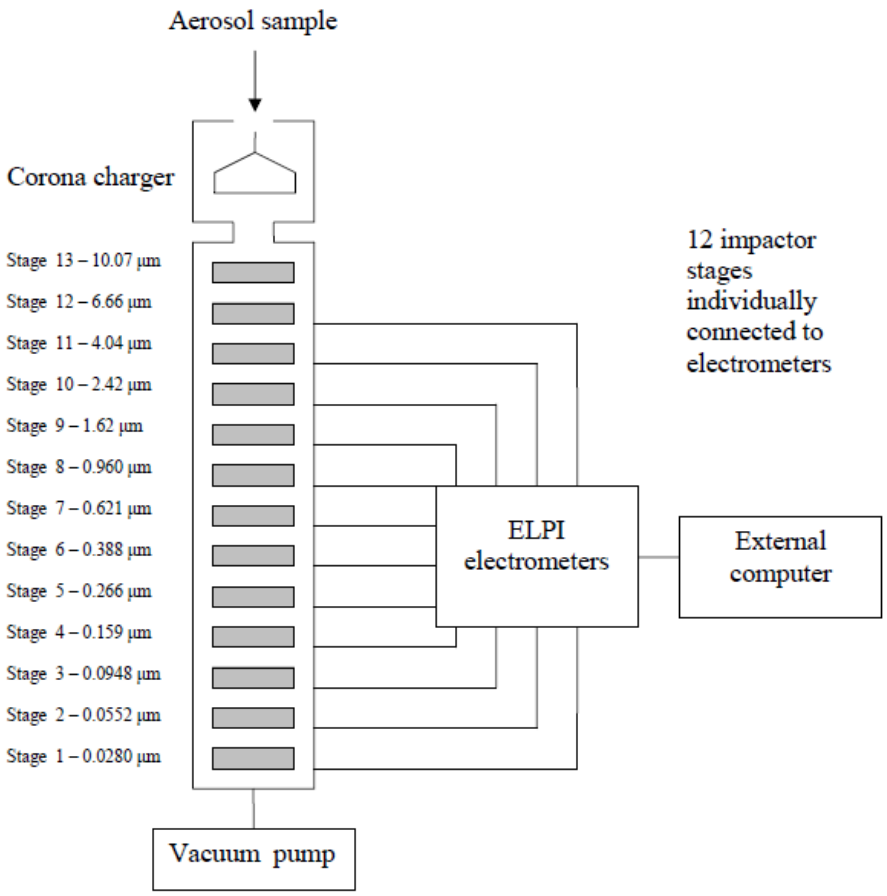

Figure 2. Schematic diagram of the ELPI [46]

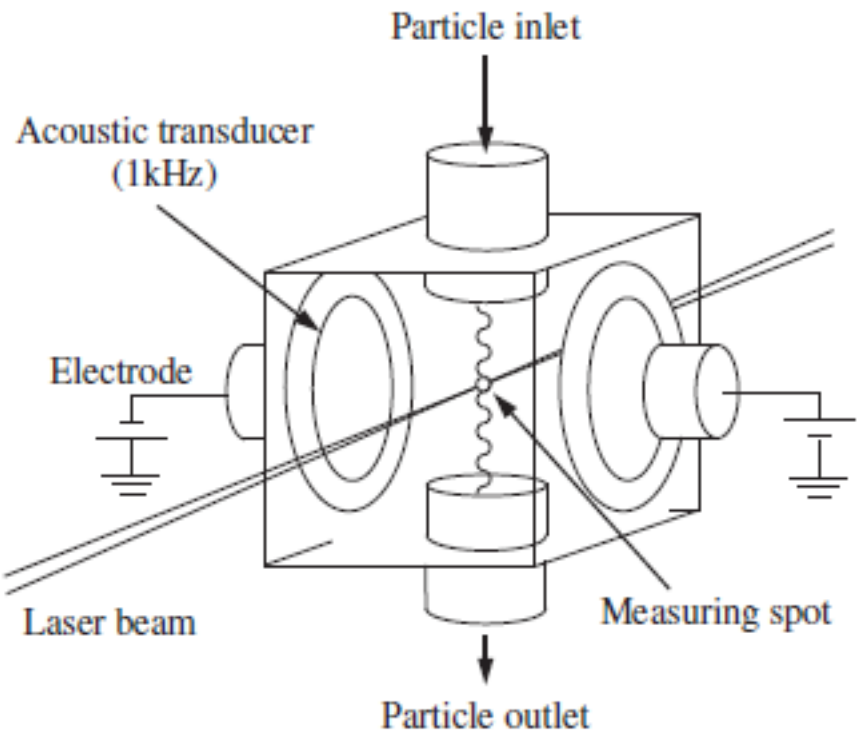

Figure 3. Electrical-single particle aerodynamic relaxation time (E-SPART) analyzer[20].

Chapter 3

An experimental and numerical based study of tribocharging during granular flow

Shivangi Naik[1], B.C. Hancock[2], Y. Abramov[2], Yu Weili[2], Bodhi Chaudhuri[1,3*]

[1]Department of Pharmaceutical Sciences,

University of Connecticut,

Storrs, CT, 06269, USA.

[2]Pfizer Inc,

Groton CT 06340, USA.

[3] Institute of Material Sciences,

University of Connecticut,

Storrs, CT, 06269, USA.

*Corresponding Author

Email: bodhi.chaudhuri@uconn.edu

Abstract

Electrostatic charging via contact electrification or tribocharging refers to the process of charging of two solid surfaces when they are brought into contact with each other and separated. Charging of continuous particulate flows on solid surfaces is poorly understood and has often been empirical. This study aims towards understanding the tribocharging of pharmaceutical excipients using a simplified geometry of unidirectional flow in a hopper-chute assembly. Assuming electron transfer to be the dominant mechanism of electrification, a triboelectric series was generated using work functions estimated from quantum chemical calculations. A 3D-DEM model has been developed employing charge transfer and electrostatic forces. Using numerical simulations the charge accumulation for an assemblage of particles during flow was determined under different conditions. To theoretically analyze the process of charging, parametric studies affecting powder flow have been investigated. A higher charge accumulation per mass was observed at larger friction coefficients and lower restitution coefficients. The results obtained from the simulation model reinforce the collisional nature of triboelectrification. The simulation results revealed similar trends to experimental data. However, to enable a priori prediction the model needs to be tested for additional materials or extended to other process operations.

Keywords: work function, DEM, friction, electrostatic forces.

1. Introduction

When two materials are touched or rubbed together, electrical charges can be transferred from one material to another. This charging process is described as triboelectrification or tribo-charging since sliding/frictional contacts are invariably involved. Such contact electrification or tribocharging which has been known for many years now, is often significant in industrial processes (Bailey, 1993). It is ubiquitous in dry particulate systems and can influence the mechanical behavior of particles resulting in adhesion to vessels or pipes (Jones *et al*., 1991). Although tribocharging is considered beneficial in some particulate processing operations such as xerography or electrostatic powder coating, (Bailey, 1998, Castle, 2001) the food, defense and the pharmaceutical industries often strive to minimize triboelectrification (Adhiwidjaja *et al.*, 2000) that can cause process problems such as jamming, segregation during powder flow.

The triboelectric charging of metals has been well established and it is known to arise from the difference in work function of two surfaces. The absolute value of chemical potential i.e. the work function of a surface can be described as the minimum energy required to remove the weakest bound electrons away from the surface. Thus, electrons are transferred between two metal surfaces till thermodynamic equilibrium has been attained. In case of metals, however triboelectrification is usually imperceptible since the charge transferred moves away from the contact point due to their high conductivity (Inculet, 1980). There have been different mechanisms proposed for charge transfer involving insulators. With respect to tribocharging of insulators, the charge transfer carriers are thought to be either electrons or ions. Electron exchange has been suggested for insulator tribocharging based on experimental evidence. (Davies, 1970; Fabish *et al*., 1976; Lowell *et al*., 1986, Bailey, 2001). Recently, electrochemistry has been employed to provide evidence for an electron transfer mechanism for insulators. In these studies, the surface charges developed after tribocharging of insulators were employed for different chemical redox reactions and chemiluminescence, reactions which can be induced only by electrons (Lui *et al*., 2008, 2009). For ionic polymers, evidence suggests that the sign of the charge exchanged has been found to be consistent with transfer of the mobile ion. It is believed that these mobile ions are available for charge exchange at insulator surfaces in a similar manner as the electrons are deemed to be available in metal-metal charging (Diaz *et al*., 1993). Non-ionic polymers also exhibit substantial tribocharging and in this case ion transfer mechanism may not

hold true as they lack mobile ions. Although some theories have suggested the preferential adsorption of hydroxide ions from the atmosphere on the polymer surfaces, it is still unknown why some polymers have greater affinity for hydroxide than others (McCarthy *et al*., 2008). Moreover, it has been demonstrated that charging can occur between nonionic polymers even in the total absence of water (Baytekin *et al*., 2011). Thus, tribocharging can be considered as a combination of these aforementioned processes and particularly for non-electrolytes, electrons can be considered as the important charge transfer carriers (Karner *et al*., 2011).

Pharmaceutical powders are usually insulators with a relatively small particle size and low bulk density, thus providing ideal conditions for tribo-electric charging (Huber & Wirth, 2003). A net charge on a powder is often generated in processes such as transport, sieving, mixing and milling due to inter-particle and particle-wall collisions with different surfaces. A majority of research to quantify tribocharging has been made using Faraday cages, or Faraday cups. A Faraday cup consists of a receiving surface contained within a cup enclosure that shields the material inside from the effect of any external electric fields. The Faraday cup is quite versatile and can be used in different ways for charge measurements. The most common technique is to pour the powder or directly convey it into the Faraday cup following tribocharging (Byron *et al*., 1997). The latter technique has been most commonly used by different investigators to describe tribocharging. Murtoma *et al*., (2000), performed a simple study of sliding lactose and glucose powders across an inclined plane of glass and measured the total charge. He suggested that in frictional contact these powders develop positive charges against glass. Tribocharging of lactose was found to higher than glucose and was believed to be due to lower resistivity of lactose than glucose. Rowley and Mackin (2003) studied tribocharging in a cyclone charger with removable walls materials using a Faraday cup. They generated a triboelectric series inclusive of α-lactose monohydrate and dextrose monohydrate that charged negatively against steel and positively against PVC and polypropylene. Sodium starch glycolate was found to charge negatively against all surfaces. They extended their experiments to study the effects of relative humidity on charge accumulation. These factors were also investigated by Elajnaf *et al*. (2006) and Zhu *et al*. (2007) who demonstrated that the magnitude of the net charge decreases with increase in relative humidity. A critical challenge for such experimental studies of triboelectric charging is to obtain data that can be linked to theoretical predictions. Ireland (2010) developed a simple 2D capacitor model for charge accumulation using silica particles to relate the triboelectrification of a flowing

powder to the mechanical characteristics of the flow. Rather than considering the actual contact mechanics or individual events viz. collisions, the study attempted to relate tribocharging to general average characteristics such as average time. Thus, the present lack of a quantitative understanding of charging during such interaction purports the need of developing more fundamental approaches to quantify tribocharging and support experimental evidence.

These inadequacies have propelled the development of numerical methods to model tribocharging for an ensemble of particles. Such approaches have been adopted by Klinzing *et al*. (1986), Abel *et al*. (2002) and Bottner *et al*. (2002) for pneumatic conveying, segregation and powder coating using continuum approaches. One of the drawbacks of these models is that they ignore the discrete nature of powders and do not account for any electrostatic forces. Watano *et al*. (2003) has used a 2D discrete element model to analyze particle flow during pneumatic conveying. The model is restricted as it uses a limited number of particles and assumes that electrification of particle is proportional to the collision velocity. Their charging model also assumed a constant charge density which was derived experimentally. Hogue *et al*. (2009) has used 3D DEM to analyze the electrification of polymeric particles moving down an inclined plane. However this method employs a time-dependent semi-empirical approach to quantify electrification and hence, a priori prediction may not be possible. Taking into account the complexity of powder tribocharging in industrial operations, this paper intends to gain insight by rendering the geometry of interaction as simple as possible i.e. a unidirectional flow on flat surface. Based on the condenser model of Matsusaka *et al.* (2000) a 3D DEM model incorporating electrostatic forces has been developed. The ability of simulations to account for mechanical factors affecting tribocharging viz. COF (coefficient of friction) and COR (coefficient of restitution) has been exploited. Moreover, the estimation of work function of all materials by in silico computations has been attempted. The multi-scale model has been verified with experimental runs similar to pharmaceutical processing.

2. Materials and Methods

2.1. Materials

Materials used in this study were two commonly used pharmaceutical excipients, sucrose non-pareil from Paular Incorporation and microcrystalline cellulose (MCC) non-pareil from Cellets.

The excipients were sieved using B.S. test sieves, to produce a narrow particle size fraction for use in triboelectrification experiments. The experimental set up used in this study is a hopper-chute assembly (Fig. 1) with two contact surfaces viz. Aluminium and polyvinylchloride (PVC)

2.2. Material Characterization

Tribocharging is known to be sensitive to the surface properties and any changes in surface state due to atmospheric contamination can significantly affect the charge transfer process. In this study an attempt was made to characterize the material by measuring some of these properties. The particle size (Table 1) of both the materials was determined by Malvern Mastersizer (2000E) using the Scirocco unit for dry measurements. Moisture sorption isotherms obtained by dynamic vapor sorption (DVS) analysis is one of the simplest means to study the interaction of water molecules with powder materials. In a typical DVS experiment ,the relative humidity (%RH) is stepped from a low initial level (either ambient or 0 %RH) to a high level (90-95 %RH), then back down to a low level, and finally increased again to a higher level. The above study was carried out by placing ca. 15 mg of each test sample on the sample pan of DVS. Then each test sample was allowed to equilibrate at increasing R.H for 600 min, and the change in weight at each R.H was calculated. The temperature was kept constant at 25℃ throughout the run.

2.3. Work function estimation

The tendency of an insulator getting charged positively or negatively in contact with another insulator or metal can be evaluated using a triboelectric series (Matsusaka & Masuda, 2003). The materials higher up in this series generally have a lower work function than those located below and thus tend to release electrons and accumulate positive charge. There are a few experimental techniques such as photoelectron emission spectroscopy (PES) and Kevin Zisman method that can be used to actually measure work function. While PES allows the measurement of the absolute work function, Kevin Zisman method only gives the contact potential difference (CPD) between the actual probe and the sample surface. Additionally, PES can be combined with scanning electron microscopy (SEM) to obtain high spatial resolution maps of work function. Besides these limited experimental approaches, computational tools are also available to determine the work function of surfaces. For instance, Yanagida et al (1993) have determined the electronic states of polymers by computational molecular orbital calculations and found these

values to be almost proportional to the threshold energy of photoemission that corresponds to the work function of polymers. Similarly, Gibson *et al.* (1984) has shown the triboelectric charging efficiency to be dependent on functional groups on the polymer backbone. Although the quantitative analysis is still limited, the molecular orbital calculations suggest a strong relationship between work function and chemical structure in order to understand the charge transfer between surfaces. Accordingly, in this study, the estimation of work functions of all materials (Eq. 1), based on quantum chemical calculations were attempted. Semi-empirical quantum calculations (Trigwell *et al.*, 2003; Sarkar *et al.* 2012) were performed using MOPAC 2012, a restricted Hartree Fock (RHF) PM7 methodology to determine the band gap (E_g) and ionization potential (χ)

$$\Phi = \chi - 0.5E_g \qquad (1)$$

2.4. Experimental Section

The pharmaceutical materials along with the hopper-chute assembly (Fig.1) were equilibrated at 20% RH for 24-36 hours inside a humidity controlled glove box. The materials were spread in thin layers onto wax paper to condition them at 20% RH. At the beginning of each experiment the initial charge on the material was measured in a Faraday's cup connected to a nano-Coulomb-meter (Monroe Electronics, NJ, Model 284). The particles were then loaded into the hopper and any residual charges on the material or hopper-chute assembly was neutralized using overhead anti-static ionizing bars (Meech International, Witney, Oxfordshire, UK). The material was then released through a dam in the base of the hopper to flow over the chute and then directly into the faraday cup. Following each experimental run, the hopper-chute assembly was thoroughly cleaned using isopropyl alcohol (Fischer Scientific, MA) and then deionized. All experiments were done in triplicate at ambient temperature (22 ± 2 ◦C) and humidity (20 ± 3% RH) within the glove box.

3. Discrete Element Method

In DEM, the trajectory of each particle inside the system can be calculated by considering all the forces acting on it. Once the forces have been calculated, new position and orientation can be obtained by integrating Newton's second law of motion and the kinematic equations. This soft-particle approach can be used to investigate long-lasting and multiple particle contacts

characteristic of pharmaceutical powders as it is not limited by the instantaneous contact time assumption of the hard-particle model (Cundall and Strack, 1979). The contact model used in this study is based on the work of Walton and Braun (1986). In this model each particle may interact with its neighbors or with the boundary only at the contact points through normal and tangential forces. The partially latching hysteretic spring model is used to calculate the normal forces based on extent of overlap between the particles and tangential forces are calculated using the incrementally slipping model based on loading and unloading history of the contact (Mindlin and Deresiewicz; Walton, 1993). Thus the total forces and torques acting on each of the particles is calculated as

$$\sum F_i = m_i g + F_N + F_T \qquad (2)$$

$$\sum T_i = r_i \times F_T \qquad (3)$$

As in this study, triboelectrification during flow is also being considered, besides contact mechanical forces, the electrostatic forces between particles ($F_{ep,i}$) and between particle and wall ($F_{ew,i}$) need to be calculated to determine the trajectories of all particles.

Modeling Electrostatic flow behavior of material

In this study a condenser model introduced by Matsusaka *et al.* (2000) has been employed to compute the charge transfer during a collision. According to the condenser model, the total potential between two surfaces can be expressed as a difference in the contact potential difference and the induced potential difference. The contact potential difference depends upon the work function of the surfaces whereas the induced potential depends upon the charge of the approaching particles. The potential for a charge particle is given by (Eq.4) where q is the

$$V = \frac{q}{4\pi\epsilon_0 r^2} \qquad (4)$$

charge on the particle, ε_0 is the permittivity of vacuum. (Pie *et al.*, 2013). In the current DEM model, the electric field (Eq.5) of the charged particles is determined based on superposition principle since it also accounts for the presence of other charges in the system (Laurentie J.C. *et al.* (2013).

$$E_i = \sum_{k=1}^{M} \frac{q_k}{4\pi\varepsilon_0 \, l_{i,k}{}^3} \vec{l_{i,k}} \qquad (5)$$

In Eq. (5), M is the total number neighbors of particle *i*, $l_{i,k}$ is the position vector between particle i and its neighbor k. Thus the charge accumulated (Eq.6) on the particle is then given by

$$q_{new} = q_{initial} + \frac{s\varepsilon_0}{ze} \left[\varphi_i - \varphi_j - (E_{ii}.\frac{d_{ij}}{||d_{ij}||})ze\right] \qquad (6)$$

After each collision, the charge on materials *i* and *j* will become $q_i - \Delta q$ and $q_j + \Delta q$, respectively. In Eq. 5, *s* represents the contact area, ϕ is the work function, *e* is the electron charge, E_{ii} is the electric field of the incoming particle, d_{ij} is the position vector between particle and wall. The cutoff distance for charge transfer (z) considered in this study is 250 nm (Lowell and Roseinnes, 1980). The implementation of the Discrete Element Method requires generally a very small time step to predict the trajectories of particles. As a result, the contact between two particles may occur over numerous time steps and could result in excess charging. Hence for a given collision, charge transfer is considered to occur only for maximum force between particles (Matsusaka *et al*., 2000; Watanabe *et al*., 2007). As the charge decay times can be longer at relative humidities less than 30%, the effect of charge relaxation has not been considered in this model (Chubb, 2002).

When a large number of charged particles are involved in a system, the charge on nearby particles can affect the motion of a particle. This is referred to as the 'space charge" effect. The force of Coulombic repulsion (Eq.7) of two neighboring particles with charges q_l and q_2, is given by,

$$F = \frac{q_1 q_2}{4\pi\epsilon_0 r^2} \qquad (7)$$

r is the distance between the particles and ε_0 = 8.85 x 10^{-12} C ^{2} N^{-1} m^{-2}. The actual force on a particle will be the sum of all the Coulombic forces of its neighboring particles. Thus, we cannot evaluate this force exactly without knowing the position of all particles. As the electrostatic force is approximately four times higher for its nearest neighbor, the force can be evaluated only for its

nearest neighbors (Finlay, 2001). Considering this electrostatic interaction between charged particles, a screened Coulomb force ($F_{ep,i}$) has been computed (Eq.8, Eq. 9) (Hogue *et al*., 2008).

$$F_{ep,i} = \frac{q_1 q_2}{4\pi\varepsilon_o}\left(\frac{\tau}{r} + \frac{1}{r^2}\right) e^{-\tau r} \qquad (8) \qquad \tau = q_e\sqrt{\left(\frac{1}{K_B T \varepsilon \epsilon_0}\sum_i n_i q_i^2\right)} \qquad (9)$$

In this equation q_e is the charge of the electron (1.602×10^{-19} C), ε is the relative permittivity of the medium, ε_o is the permittivity of the free space, T is the temperature in Kelvin, K_B is the Boltzmann's constant (1.38×10^{-23} JK^{-1}), and n_i is the number of particles with charge q_i in the near vicinity. To account for the electrostatic interaction between wall and particles, the boundary has been discretized into rectangular grids. The electrostatic force on a charged particle, i located near a wall may then be calculated as $F_{ew,i} = E.q_i$, where E represents the electric field due to continuous charge distribution on the chute wall (Lim EWC *et al.*, 2012)

4. Results and Discussion

4.1. Estimation of Work function

In silico computations were performed using MOPAC 2013 (Trigwell *et al.*, 2000) that solves for Schrödinger's equation of multiple electron system for molecular structures. AVOGADRO, an advanced molecule editor and visualizer used in computational chemistry, bioinformatics, materials science, and related areas was used for importing the molecular structures. From the semi-empirical calculations (Table 2) the triboelectric series appears to be in the order Aluminium, sucrose, MCC and PVC.

4.2. Effect of loading mass

The first part of the study was to develop a method to study tribocharging for the experimental assembly under investigation. This also encompasses the task of assessing the sensitivity and the reproducibility of nano-coulomb meter using simple faraday pail method. The study was conducted using MCC and sucrose spheres against Aluminium chute for which the total charge was determined at the end of each run. For both the materials, the magnitude of charge obtained increased with increase in the sample load (Fig 2a & Fig 2b), illustrating the collisional nature of tribocharging. Loading mass greater than 20g, seem to display the least statistical variability for

both the cases. Higher mass loadings i.e. greater than 120 g were not possible as the detection limit of the nano-coulomb meter was 200 nC.

4.3. Effect of chute Inclination

The mechanical nature of the interaction between a particle and a solid surface can strongly influence the exchange of charge. Consequently, the time the particle might spend in actual contact with the surface becomes an important determinant for charge transfer. The contact time could depend on whether the particle just bounces on the surface as opposed to roll or slide. A rolling particle can progressively makes its entire area available for contact and may charge more than sliding contacts. However, a temperature rise caused through sliding contacts may also enhance charge transfer. Hence the effects of rolling and sliding contacts on triboelectrification are difficult to comprehend (Ireland, 2010). To investigate the effect of contact time, the particles were fed from the hopper onto a flat tilted chute at different angles (30º, 40º and 50º). The charge acquisition data was represented as the total charge to mass ratio at the end of each run. The charge accumulated (Fig. 3a & Fig 3b) at 30º was found to be higher ($p<0.05$) than cases with 40º and 50º inclination of chute. The extent of charge accumulation is governed by the normal force acting on particles and the overall particle-wall collisions. A greater normal contact force can be predicted intuitively with decrease in chute angle, which would allow superior charge transfer between the contacting surfaces. Thus, the accumulated charge was found to decrease at steeper chute angles.

4.4. Effect of Humidity

It is well-known relative humidity plays a role in the discharge of insulators. Since moisture has a strong effect on the electrical conductivity of the surface of particles, relative humidity is an important influencing parameter of charging processes of powder. The dielectric constant of air also increases with RH, but the effect is negligible. Under ambient temperature (22ºC) and pressure (1 atm), the dielectric constant of air only increases by 0.017% if the RH increases from 15 to 90%. Hence interaction of moisture with the contacting surfaces is thought to be a major factor as it changes the particle surface conductivity (Koga, 1940; Rowley *et al.*, 2003). The effect of relative humidity on electrification was studied at 20%RH, 40%RH and 60%RH as depicted by the experimental method in section 2.2. For both MCC (Fig. 4a) and sucrose (Fig.

4b), there was decrease in charge accumulated upon increasing RH. However, the decrease in tribocharging of sucrose was found to be much smaller as compared to MCC ($p<0.05$). If dynamic vapor sorption is considered (Table 2) then the moisture sorption for MCC was found to be higher than sucrose. Thus, the enhanced charge dissipation rates are perhaps due to the facilitated movement of charges through the moisture layer on particle surfaces, which can contribute to greater charge mitigation for MCC as compared to sucrose.

5. Discrete Element Modeling

The collisional nature of tribocharging was further investigated by a 3D-DEM electrostatic model as it incorporates the effects of contact area, time and frequency which are difficult to quantify experimentally. Initially 30,000 spherical inelastic, frictional particles were deposited in the non-discharging hopper of same dimension to that of the experiment. No tribocharging was considered during deposition of particles in hopper. Following deposition, charge transfer and electrostatic forces described in section 3 were incorporated into the DEM model and the particles were then discharged.

5.1. Effect of Chute Angle

To determine the effect of contact time or contact mode, simulations were run at different hopper-chute inclinations viz. 30º, 40º, and 50 º. The DEM simulation parameters used in this study are depicted in Table. 4. The DEM snapshots (Fig. 5a-5c) illustrate the particle dynamics of flow and tribocharging along the chute at a given time. In these simulations the particles have been color coded for charge. The uncharged particles are represented by a cold blue color. As particles flow along the chute charge transfer occurs. Depending on the scope of particle-wall collisions particles are charged to different extents viz. -5e-14 C to 4e-14 C (light blue), -7e-14 C to -4e-13 C (light green to yellow), -1e-12 to -5e-12 (orange to red). Similar to experiments, the charge/mass values (Fig. 6) were calculated after all particles were discharged from the chute into Faraday cup. Besides a decrease in the charge at higher chute inclinations, DEM simulations also show some avalanching or bouncing of particles at steeper chute angles. To elucidate this effect further, the coefficient of restitution was varied viz. 0.9 to 0.4. As observed in Fig. 7a there is considerable bouncing of particles at COR of 0.9 as compared to a COR of 0.4 (Fig. 7b). Also, the accumulated charge per unit mass (Fig.8a) was found to increase upon decreasing COR. This

behavior is further corroborated by the increase in chute collisions (Fig. 8b) following a decrease in COR. Thus, despite an expected greater instantaneous normal force for bouncing contacts, simulations suggest these contacts do not contribute much, to overall charging. Consequently, continuous contacts transfer more charges as compared to bouncing contacts.

5.2. Effect of Chute-Particle friction coefficient

To determine the effect of coefficient of friction, the simulations were run using static different friction coefficients viz. 0.1, 0.4 and 0.7. It can be concluded from the simulation snapshots at a given time instant (Fig.9a-9b) and from the charge/mass values at different friction coefficients (Fig 10), there is an increase in charge accumulation. A simplified approach was employed to understand the effect of COF on contact mode i.e. to identify between sliding and non-sliding contacts such as rolling. To determine sliding contacts, the coulomb's friction criterion was applied. It was observed that the fraction of the sliding contacts decreased from 0.82 to 0.36 upon increasing coefficient of friction. In comparison to irregular particles, the difference in the apparent contact area for rolling and sliding contacts is not considerable for spherical particles (Ireland, 2010). Moreover in the simulation model, charge distribution is considered to be uniform on the surface. Consequently, the increase in tribocharging cannot be attributed to difference in rolling/non-sliding and sliding contacts in this case. Thus, the increase in tribocharging in this case irrespective of type of contact is due to the greater contact time with the chute.

In this study, the chute-wall has been discretized into 5 X 20 rectangular grids to account for charge accumulation. If the charging of wall is considered, (Fig 11a & Fig.11b) there is distinct region where charge accumulation seems to be maximum. This is the region where all the particles impact the chute from the hopper and will have the strongest electric field. This region is likely to be the cause of adhesion of particles to surfaces. However, in case of hopper-chute system, charging on the chute is for a short period (<4secs) and not quite high. Hence the extent of adhesion to chute wall was not practically significant. Moreover as the friction coefficient was increased, the collisions to the side walls also increased (Fig 11b). This might be due to increased space charge effect at higher friction values that results in relatively greater repulsion between particles.

5.3. Model Verification

Experimental observations for charging of MCC and sucrose spheres against aluminum and PVC indicate that these materials charged in accordance to triboelectric series. To study these effects of contact surface on tribocharging, DEM simulations were performed against aluminum and PVC chute at 30º angle. The results (Fig 12) were found to correlate well for both the excipients, although some differences were observed against PVC surface. These differences cannot be explained based on the collisional nature of tribocharging alone and are still under investigation. It is suspected that this effect might be due to dangling bonds or surface defects that provide electron trapping sites resulting in faster tribocharging. In order to develop a more robust model, more materials need to be considered along with different process operations.

6. Conclusion

For complex processes such as tribocharging, numerical methods such as DEM can serve as a powerful tool to explore the dynamic charging behavior of particles during powder processing. Hence in this study, 3D –DEM model for charge transfer and electrostatics was developed. Additionally, contact mechanical aspects of tribocharging were investigated with this model. To verify the model, a simplified geometry viz. chute assembly with a Faraday cup was employed in the experiments to quantify tribocharging for pharmaceutical excipients. Assuming electron transfer to be the dominant mechanism of electrification, a triboelectric series was generated using work function estimated from quantum chemical calculations. Different interacting surfaces viz. Aluminium and PVC produced charges of opposite polarity in accordance to the triboelectric series. The DEM model captured the effect of chute inclination on tribocharging with a decrease in charge per unit mass at steeper chute inclines. Moreover, the effect of bouncing and continuous contacts revealed that the latter are more effective in charge transfer. Although some discrepancies were observed between the simulation and experimental results; a combined experimental and multi-scale approach was found to be more useful in quantifying electrostatic charging.

Nomenclature

Φ	Work Function
V	Electric potential
z	Cut off distance for charge transfer
ε_o	permittivity of the free space
E	Electric field
E_g	Band gap
χ	Ionization potential
s	Contact area
e	Charge of an electron
q	Charge of particle
T	Temperature
K_B	Boltzmann Constant
d	Position vector
F_N	Normal Force
F_T	Tangential Force
$F_{ep,i}$	Electrostatic force between particles
$F_{ew,i}$	Electrostatic forces between particle and wall

Abbreviation

COR	Coefficient of restitution
COF	Coefficient of friction
MCC	Microcrystalline cellulose
PES	Photoelectron spectroscopy

7. References

Adhiwidjaja, I.,Matsusaka,S.,Yabe,S.,Masuda,H.,2000.Simultaneous phenomenon of particle deposition and re-entrainment in charged aerosol flow—effects of particle charge and external electric field on the deposition layer. AdvancedPowderTechnology11,221–233.

Al-Adel, M.F., Saville, D.A., Sundaresan, S., 2002. The effect of static electrification on gas–solid flows in vertical risers. Industrial and Engineering Chemistry Research 41, 6224–6234

Bailey, A.G., 1993. Charging of solids and powders. Journal of Electrostatics 30, 167–180.

Bailey, A.G., 1998. The science and technology of electrostatic powder spraying, transport and coating. Journal of Electrostatics 45, 85–120.

Bailey, A.G., 2001. The charging of insulator surfaces. Journal of Electrostatics 51/52, 82–90.

Baytekin H. T., Baytekin B., Soh S., Grzybowski B. A.,2011. Angew. Chem. Int. Ed. **50**, 6766-6770

Bottner, C.U., & Sommerfeld, M. (2002). Numerical calculation of electrostatic powder painting using the Euler/Langrage approach. Powder Technology, 125(2-3), 206-216.

Castle, G. S. P. Industrial applications of electrostatics: the past, present and future. Journal of Electrostatics 51, 1-7 (2001).

Chubb J., 2002. New approaches for electrostatic testing of materials, J. Electrostat. 54, 233–244

Cundall, P.A.,Strack,O.D.L.,1979.A discrete numerical model for granular assemblies. Geotechnique29,47–65.

Davies, D.K., 1969. Charge generation on dielectric surfaces. British Journal of Applied Physics: Journal of Physics D 2, 1533–1537.

Diaz, A.F., Guay, J., 1993. Contact charging of organic materials: ion vs. electron transfer. IBM Journal of Research and Development 37, 249–259.

Elajnaf, A.,Carter,P.,&Rowley,G.(2006).Electrostatic characterization of inhaled powders: effect of contact surface and relative humidity. European Journal of Pharmaceutical Sciences, 29, 375–384.

Fabish, T.J., Duke, C.B., 1977. Molecular charge states and contact charge exchange in polymers. Journal of Applied Physics 48, 4256–4266.

Finlay, W., 2001. The mechanics of inhaled pharmaceutical aerosols. Academic Press, San Diego

Gibson, H.W., 1984. Control of electrical properties of polymers by chemical modification. Polymer 25, 3–27.

Hogue, M.D., Calle, C.I., Curry, D.R., & Weitzman, P.S. (2008). Calculating the trajectories of triboelectrically charged particles using Discrete Element Modeling (DEM). Journal of Electrostatics 66, 32–38

Hogue, M.D., Calle, C.I., Curry, D.R., & Weitzman, P.S. (2009). Discrete element modeling of triboelectrically charged particles: Revised Experiments. Journal of Electrostatics, 67(4), 691-694.

Huber,G.,&Wirth,K.E.(2003).Electrostatically supported surface coating of solid particles in liquid nitrogen for use in dry-powder-inhalers. Powder Technology, 134, 181–192

Inculet, I. I. in Electrostatics and its applications (ed. Moore, A. C.) 86-114 (John Wiley & Sons, New York, 1973).

Ireland, P.M.(2010).Triboelectrification of particulate flows on surfaces:Part II—mechanisms and models. Powder Technology, 198, 199–210

Jones, T.B., King, J.L., 1991. Powder Handling and Electrostatics: Understanding and Preventing Hazards. Lewis, Chelsea.

Karner, S., Anne Urbanetz,N.,2011.The impact of electrostatic charge in pharmaceutical powders with specific focus on inhalation-powders.J.AerosolSci.42, 428–445.

Klinzing, G.E., 1986. Clustering under the influence of electrostatic forces. International Journal of Multiphase Flow 12, 853–857

Koga I 1940. Dielectric constant of moist air. Electrotechnical Journal 4:108-110

Laurentie J.C., Traoré P., Dascalescu L., 2013. Discrete element modeling of triboelectric charging of insulating materials in vibrated granular beds. Journal of Electrostatics 71, 951-957

Liu C., Bard A. J., 2008. Electrostatic electrochemistry at insulators. Nature Materials **7**, 505-509

Liu C., Bard A.J., 2009. Electrons on dielectrics and contact electrification. Chem. Phys.Lett. 480, 145–156.

Lowell, J., Rose-Innes, A.C., 1980. Contact electrification. Advances in Physics 29, 947–1023.

Lowel J. and Truscott W. S., 1986. Triboelectrification of identical insulators: I. An experimental investigation. Phys. D: Appl. Phys. **19**, 1281-1298

Mackin, L.A.,Rowley,G.,Fletcher,E.J., Marriott,R.(1993). An investigation of the role of moisture on the charging tendencies of pharmaceutical excipients. In: Proceedings of the 12th pharmaceutical technical conference, Vol.2,pp.300–317.

Matsusaka, S., Ghadiri, M, Masuda, H., 2000. Electrification of an elastic sphere by repeated impacts on a metal plate. Journal of Physics D: Applied Physics 33, 2311–2319

Matsusaka, S., Masuda, H., 2003. Electrostatics of particles. Advanced Powder Technology 14, 143–166.

McCarty L.S., Whitesides G.M.,2008. Electrostatic charge due to separation of ions at interfaces: contact electrification of ionic electrets, Angewandte Chemie: International Edition in English 47 2188–2207

Mindlin, R.D.,Deresiewicz,H.,1953.Elastic spheres in contact under varying oblique forces.J.Appl.Mech.Trans.ASME20,327–344

Murtomaa, M., Laine,E.(2001).Effect of surface coverage of a glass pipe by small particles on the triboelectrification of glucose powder. Journal of Electrostatics, 54, 311–320

Pei, C.,Wu,C.-Y.,England,D.,Byard,S.,Berchtold,H.,Adams,M.,2013.Numerical analysis of contact electrification using DEM–CFD. PowderTechnol.248, 34–43.

Rowley G, Mackin LA 2003. The effect of moisture sorption on electrostatic charging of selected pharmaceutical excipient powders. Powder Technology 135-136:50-58

Sarkar, S., Cho, J., Chaudhuri, B., 2012. Mechanisms of electrostatic charge reduction of granular media with additives on different surfaces. Chem. Eng. Process. 62, 168–175.

Trigwell S., Grable N., Yurteri C.U., Sharma R., Mazumder M.K., 2003. Effect of surface properties on the tribocharging characteristics of the polymer powder as applied to industrial processes, IEEE Transactions in Industry Applications 39, 79–86.

Walton,O.,Braun,R.,1986.Viscosity,granular-temperature and stress calculations for shearing assemblies of inelastic,frictional disks.J.Rheol.30,949–980.

Walton,O.R.,1993.Numerical simulationof inclined chute flows of monodisperse, inelastic, frictionalspheres.Mech.Mater.16,239–247.

Watanabe,H., Ghadiri,M., Matsuyama,T. ,Ding,Y.L. ,Pitt,K.G., Maruyama,H., Matsusaka, S., Masuda, H., 2007. Triboelectrification of pharmaceutical powders by particle impact. Int. J. Pharm.334, 149–155.

Watano, S., Saito, S., Suzuki, T., 2003. Numerical simulation of electrostatic charge in powder pneumatic conveying process. Powder Technology 135–136, 112–117.

Yanagida, K., Okada, O., Oka, K., 1993. Low-energy electronic states related to contact electrification of pendant-group polymers: photoemission and contact potential difference measurement. Japanese Journal of Applied Physics 32, 5603–5610

Zhu, K.,Tan,R.B.H.,Chen,F.,Ong,K.H.,&Heng,P.W.S.(2007).Influence of particle wall adhesion on particle electrification in mixers. International Journal of Pharmaceutics, 328, 22–34

Tables

Table 1: Particle size of pharmaceutical excipients

Material	d_{50} (μm)
Sucrose spheres	1100
MCC spheres	950

Table 2: Moisture sorption of pharmaceutical excipients determined by DVS

R.H (%)	Sucrose (%w/w)	MCC (%w/w)
10	0.001	0.109
20	0.008	0.216
45	0.015	0.72
70	0.026	1.507

Table 3: Calculated work functions of materials used to study tribocharging

Material	Work Function (eV)
Aluminium	4.33
Sucrose spheres	4.80
MCC spheres	5.11
PVC	5.33

Table 4: DEM simulation parameters for MCC against Aluminum chute

DEM Parameters	Values
Total number of particles	30,000
Particle size	1000μm
Chute angle	30,40,50
Coefficient of restitution: Particle/particle	0.7
Coefficient of restitution: Particle/wall	0.7
Friction coefficient: particle/particle	0.2
Work function: Surface	4.33eV
Work function particle	5.11eV
Friction coefficient: particle/wall	0.3
Time step	$5.0 * 10^{-6}$

Figures

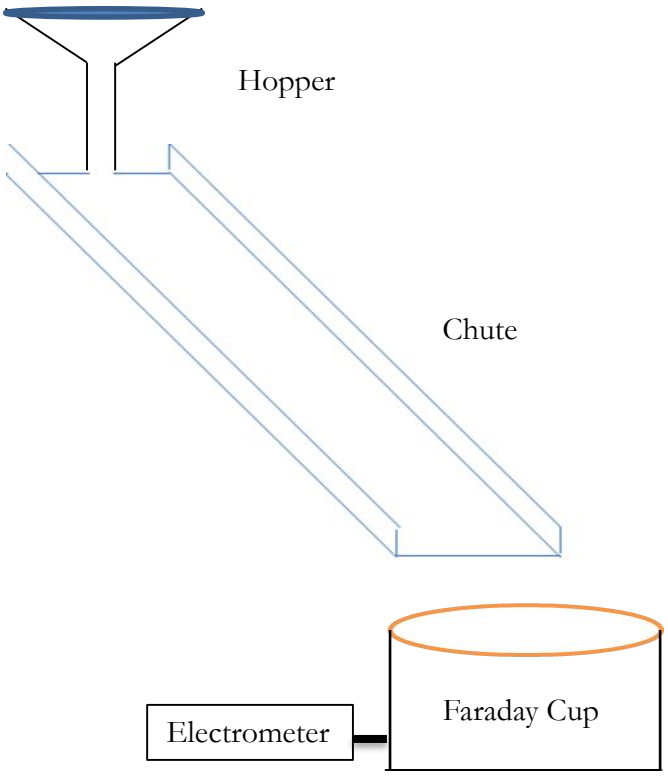

Figure 1. Schematic of Hopper-Chute assembly

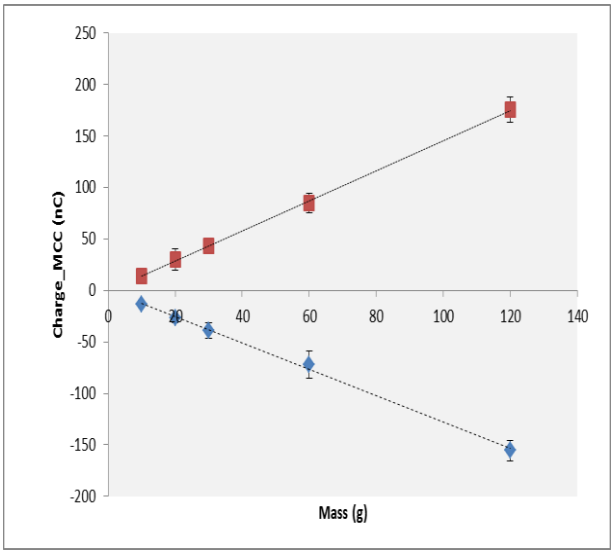

Figure 2a: Effect of loading mass on tribocharging MCC against Aluminum and PVC chutes

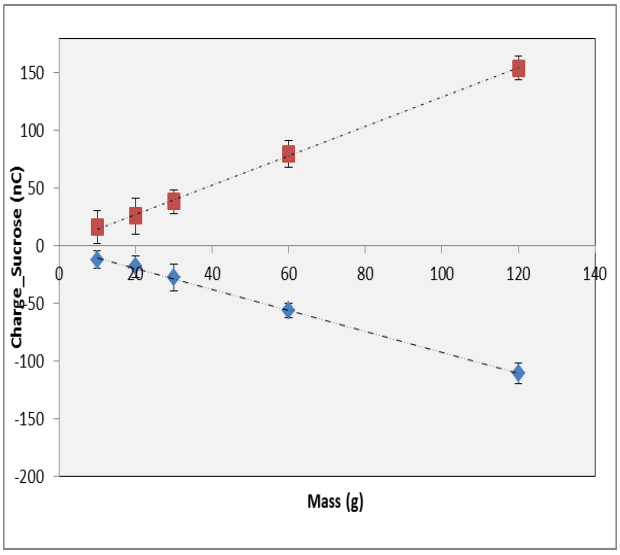

Figure 2b: Effect of loading mass on tribocharging Sucrose against Aluminum and PVC chutes

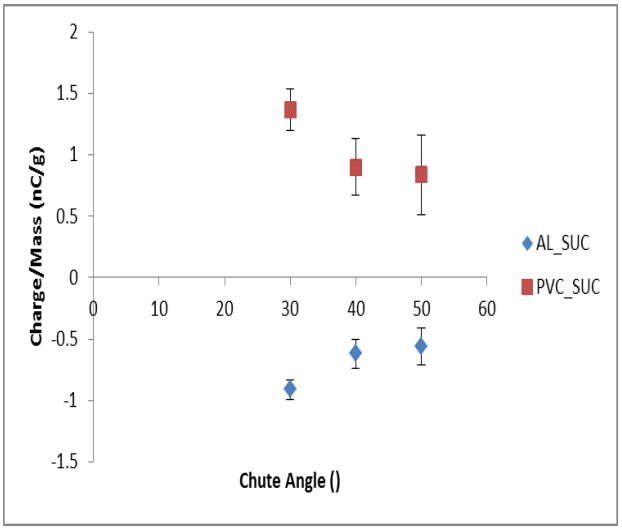

Figure 3a: Effect of chute angle on tribocharging of sucrose against Aluminum and PVC chutes

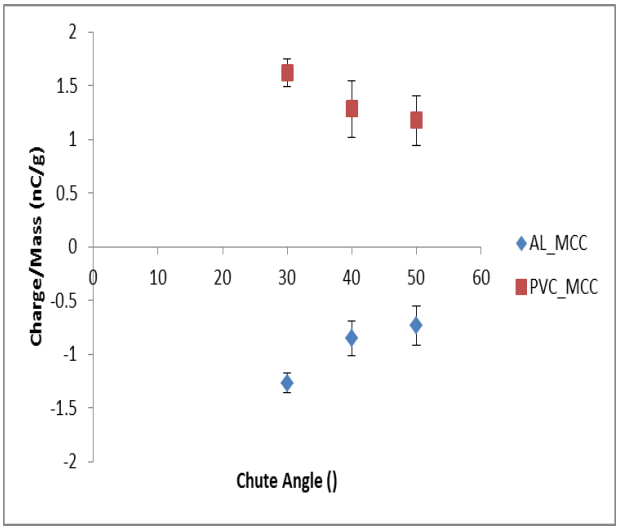

Figure 3b: Effect of chute angle on tribocharging of MCC against Aluminum and PVC chutes

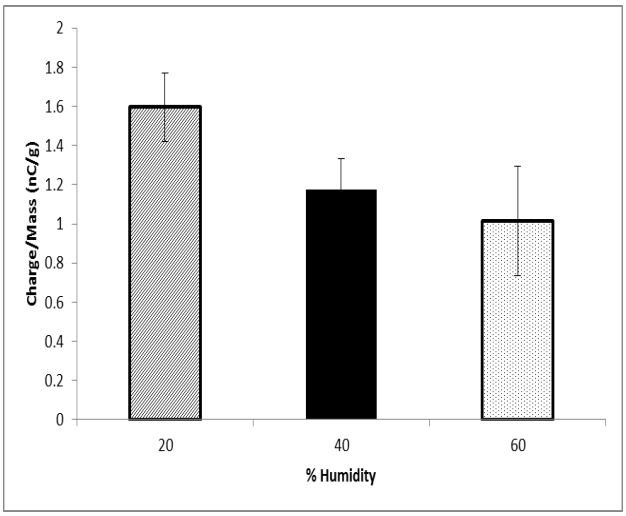

Figure 4a. : Effect of humidity on tribocharging MCC against PVC chutes

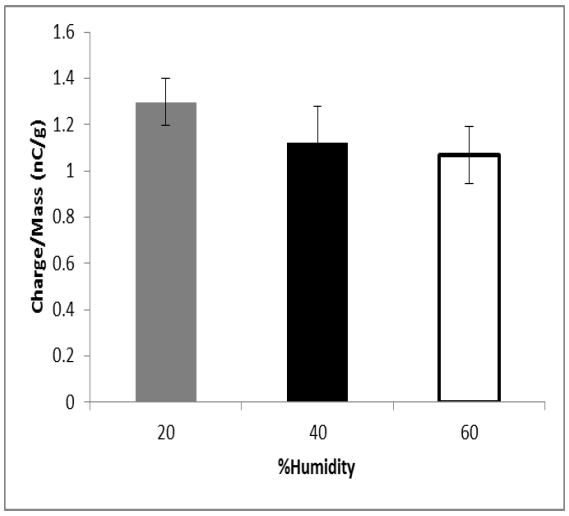

Figure 4b. : Effect of humidity on tribocharging sucrose against PVC chutes

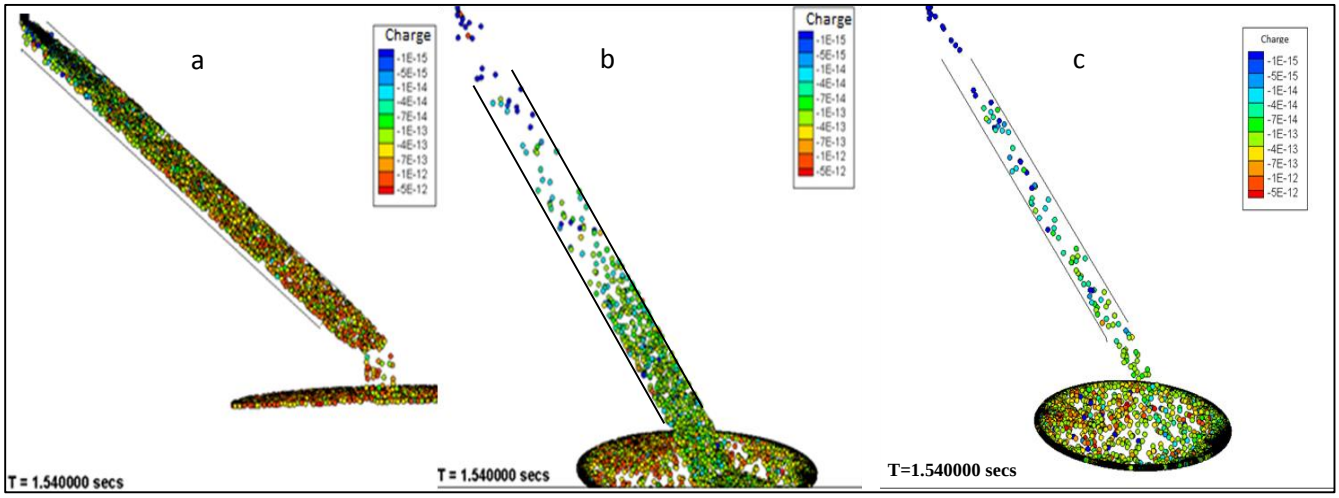

Figure 5: DEM snapshots of evolution of charge at different chute angle a) 30º b) 40º c) 50º

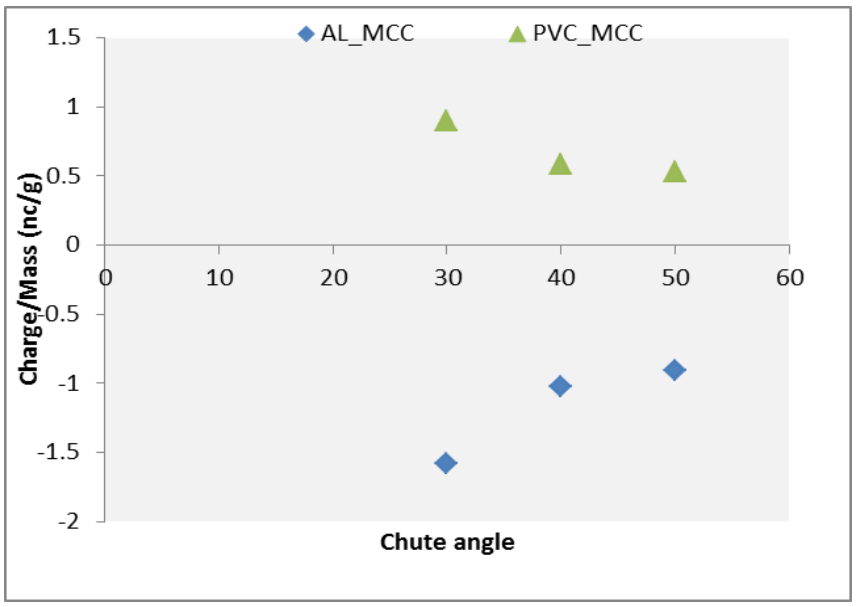

Figure 6: Effect of chute angle on triboelectrification of MCC non-pareils

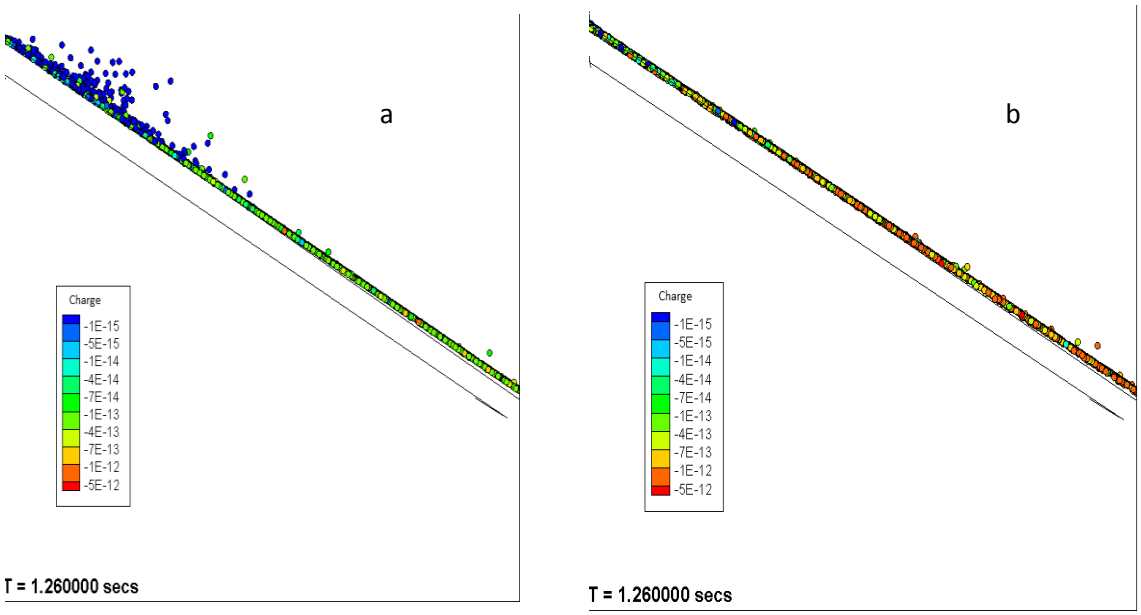

Figure 7: DEM snapshots of evolution of charge at different COR a) 0.9 b) 0.4

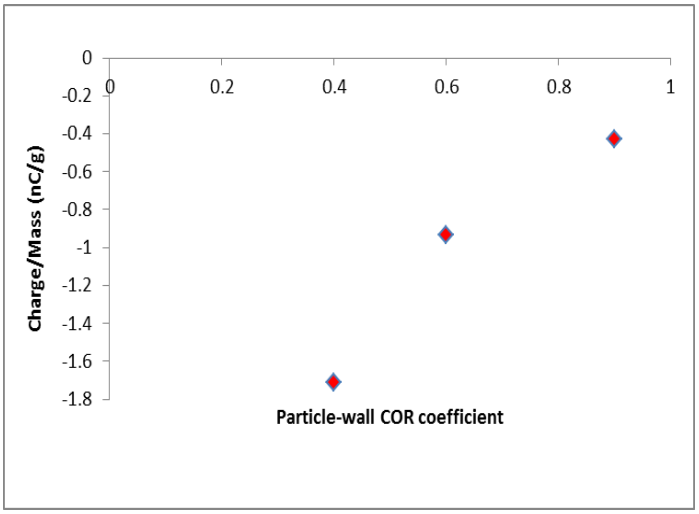

Figure 8a: Charge/mass ratio at different particle-wall COR

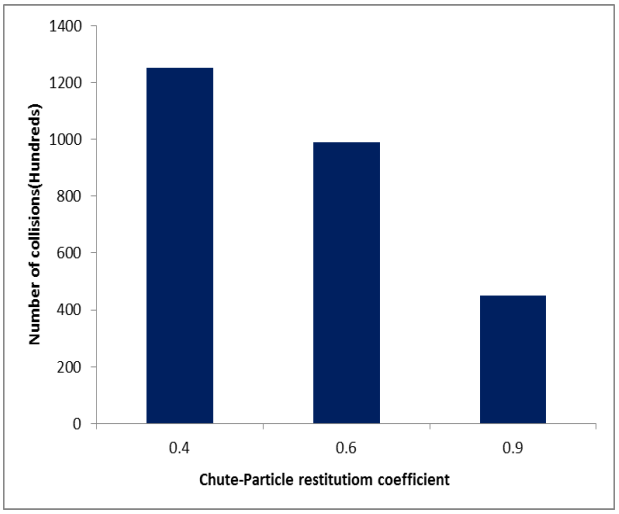

Figure 8b: Number of particle-wall collisions at different COR

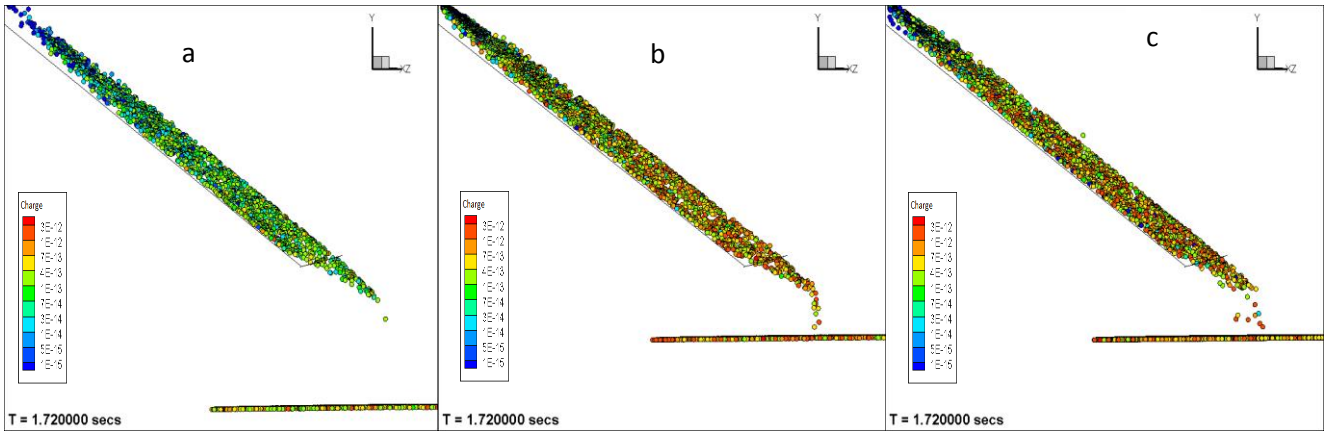

Figure 9: DEM snapshots of evolution of charge at different friction coefficients a) 0.1 b) 0.4 c) 0.7

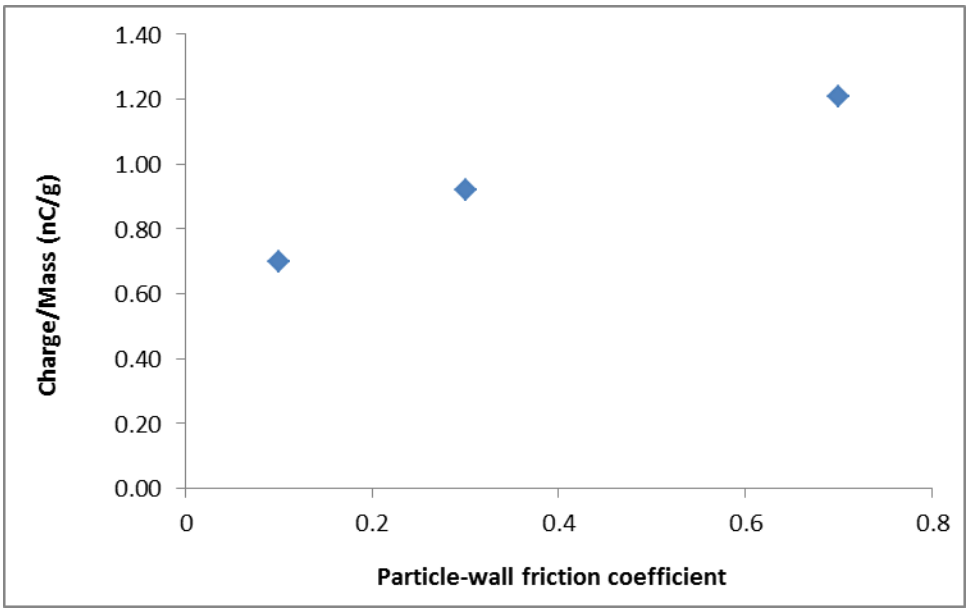

Figure 10: Charge/mass at different particle-wall friction

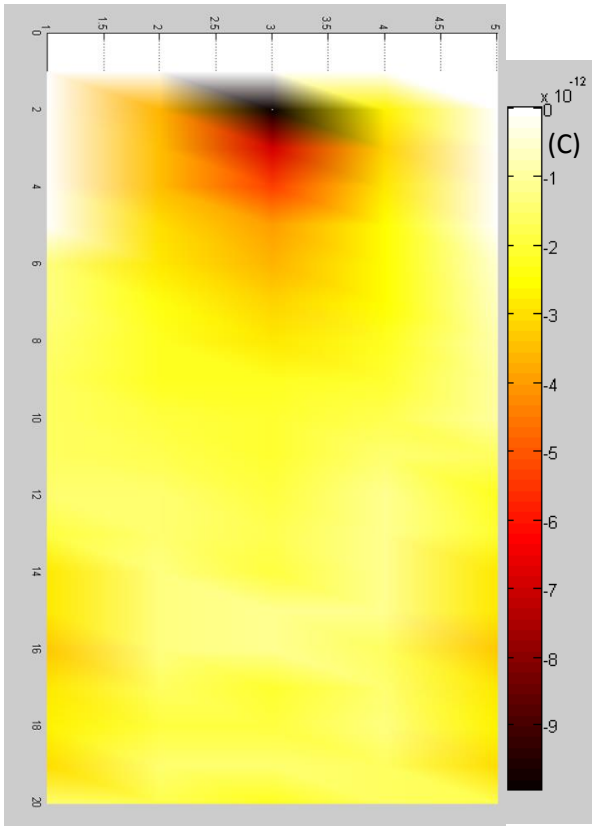

Figure 11a) Charge distribution on chute wall for particle wall friction 0.1

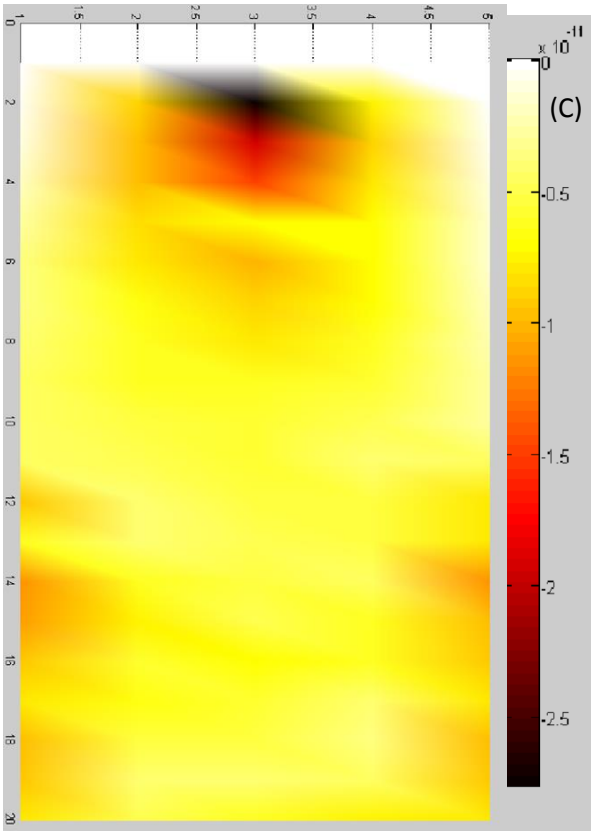

Figure 11b) Charge distribution on chute wall for particle wall friction 0.7

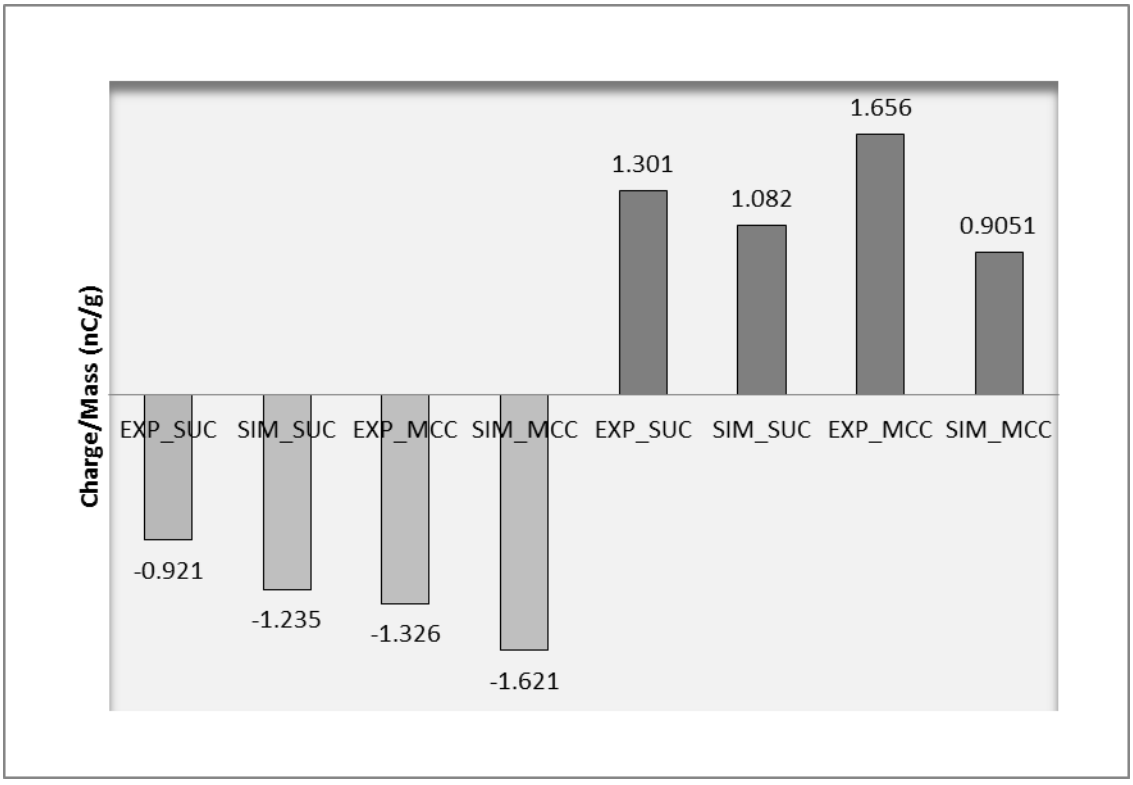

Figure 12: Experimental and DEM model comparison for MCC and sucrose

Chapter 4

Triboelectrification of pharmaceutical blenders in a V-blender: An experimental and model based study

Shivangi Naik[1], B.C. Hancock [2], Y. Abramov [2], Yu Weili [2], Bodhi Chaudhuri[1,3*]

[1]Department of Pharmaceutical Sciences,

University of Connecticut,

Storrs, CT, 06269, USA

[2] Pfizer Inc,

Groton CT 06340, USA

[3] Institute of Material Sciences,

University of Connecticut,

Storrs, CT, 06269, USA

*Corresponding Author

Email: bodhi.chaudhuri@uconn.edu

Abstract

Pharmaceutical powders are very prone to electrostatic charging by colliding and sliding contacts. In pharmaceutical formulation processes, particle charging is often a nuisance and can cause problems in the manufacture of products, such as affecting powder flow, fill and dose uniformity. For a fundamental understanding of powder triboelectrification, it is essential to study charge transfer under well-defined conditions. Hence all experiments in the current study were conducted in a V-blender located inside a glove box with a controlled humidity of 20%. To understand tribocharging, different contact surfaces viz. aluminum, Teflon, PMMA, Nylon were employed along with two pharmaceutical excipients and two drug substances. The work function values were estimated using MOPAC, a semi-empirical molecular orbital package which has been previously employed for the solid state studies and molecular structure predictions. For a mechanistic understanding of tribocharging a Discrete Element Model (DEM) incorporating charge transfer and electrostatic forces was developed. An, effort was made to correlate tribocharging of pharmaceutical powders to properties such as cohesive energy density (CED) and surface energy.

Keywords: V-blender, tribocharging, work function, DEM

1. Introduction

Tribo-electrification is traditionally defined as the generation of charges when two surfaces are brought into contact and then separated from each other (1). Most pharmaceutical operations provide ample opportunities for triboelectrification as they inevitably involve relative motion of particles against dissimilar solid surfaces. Consequently, processes such as micronization, fluidization, sieving, conveying of powders through pipes and hoppers, transfer into silos, and spray drying invariably generate charges (2-4). Usually, higher the energy involved in a process the greater is the resultant charging. It has been reported that flow of granular material in a typical unit operation can generate 10^{-7} to 10^{-4} C/kg of static charges (5). As pharmaceutical powders are organic materials with high resistivities ($> 10^{13}$ Ωm) and slower relaxation times (6-7), they have a high tendency to accumulate and retain these charges for a longer time. As a result of these static charges, the powders are quite prone to adhesion and agglomeration leading to processing difficulties such as poor flow, jamming, segregation and weight variation. In case of dry powder inhalers (DPI) such charge generation has also known to influence the release of the drug from the device and hence it's deposition into lungs. Moreover, considerable efforts have also been devoted in reducing electrification of powders, since it's a major safety hazard, especially in presence of flammable gases, solvent fumes and dust typically found in many chemical and pharmaceutical industries (8-9).

Electrostatic particle charging has inspired a number of industrial applications, such as electrostatic precipitator, xerography, electrostatic dry powder coating and powder separation. Depending on the contact materials involved triboelectrification can be can be classified into three categories viz. metal-metal, metal-insulator and insulator-insulator contact. Traditionally, electron transfer due to the difference in work function of materials has been well established for metal-metal contacts. When two metals with differing work functions / Fermi levels are placed in contact, electrons are transferred from one to the other until the Fermi levels align. Thus, the material with the higher work function acquires excess of electrons and a negative charge (10). Although ideal insulators are not expected to charge, mechanism of tribocharging for metal-insulator and insulator-insulator contacts is thought to be analogous to metals. This has been attributed to impurities and morphology defects present in insulators that produce additional energy levels into which charge can move and display contact charging (11). Some researchers

have also suggested that adsorbed water and electrolytic ions play an important role in the surface charging process. These theories have been fairly successful in elucidating the triboelectrification of polymers with mobile ions (12-14).

Theoretical relationships between work function and dielectric constant of polymers have been explored by Gallo and Lama (15). The electrostatic behavior was exemplified by generating a triboelectric series in which the materials followed the order of decreasing dielectric constants. Thus when two substances with different dielectric constants establish contact, the material with the higher dielectric constant (i.e. lower work function) would donate electrons to the other and thus become positively charged. These potential differences are mainly due to disparate electronic configurations of contact materials but may also be influenced by different particles sizes, surface roughness and impurities. As such for most materials the electron transfer model has provided a reasonable description of a charging process driven by a difference in work function.

Electrostatic charging in pharmaceutical systems is a complex process that depends on a number of factors viz. process or formulation factors along with electrical and mechanical properties of the powders and the contact surfaces involved. The atmospheric condition, e.g. relative humidity (RH) is also known to affect charge generation and dissipation. In some cases, the event may be further complicated by material transfer between the two surfaces. Thus, it is not easy to anticipate how the sign and magnitude of a charge in a system (16). In light of these potential effects, different approaches have been applied to the characterize tribocharging. As most processes that involve multiple contacts are often difficult to analyze, triboelectrification due to single contact has been investigated by Watanabe *et al*. (17). In these studies, triboelectrification of different powders including α lactose monohydrate, aspirin, sugar granules and ethyl cellulose has been explored against a stainless steel target. The authors concluded that the impact velocity was found to influence charge accumulation and the amount of charge was found to be a function of the area of contact and the impact velocity. Moreover, the equilibrium charge was also found to vary linearly with the contact potential difference of the sample powders. In a similar manner, electrification of pharmaceutical excipients has been investigated in a cyclone charger with detachable walls of different materials to generate an overall triboelectric series inclusive of α-lactose monohydrate and dextrose monohydrate that charged negatively against steel and

positively against PVC and polypropylene (18). Zhu *et al.* (19) has investigated the effect of particle size and mixer type on triboelectrification. Their studies concluded that the charge/mass ratio of particles was found to be inversely proportional to particle size. With respect to blender type, it was observed that particles charged more by the sliding motion than by direct impact. A similar study using mannitol was performed in a turbula mixer by Karner *et al.* (20). Their study indicated that the amount of charge accumulated on powder is a directly proportional to the container size and the fines fraction. It was also shown that charge dissipation to the atmosphere is negligible indicating that charge relaxation for insulators is very slow. These studies underscore the importance of mechanical events during triboelectrification that can influence the overall charge accumulated on these powders (21). It is quite challenging to experimentally quantify the contact mechanics involved i.e. contact force, frequency or contact time and to establish relation with theoretical predictions or experimental data. Considering the prevalence of electrostatics in process operations, this paper aims at modeling the triboelectrification of pharmaceutical powders in a V-blender. In order to simulate such a dynamic system, a comprehensive model should be exploited that considers both charge transfer between dissimilar surfaces as well as the mechanical interactions that occur upon particle-wall or particle-particle collisions. This necessitates the coupling of a charge transfer model with a well-established numerical scheme for computing the motion of deformable particles. The charge transfer model used in this study is based on a condenser model which is suitable for charge accumulation due to repeat impacts (22) whereas DEM has been used to model flow of granular material. The in house DEM code has been previously validated to model granular flow during heat transfer, milling and mixing (23-25).

2. Materials and Methods

2.1. Materials

For a comprehensive understanding of tribo-electrification a series inclusive of four pharmaceutical powders and five different surfaces was employed. Ibuprofen and theophylline powders were purchased from BASF, lactose monohydrate from Foremost Farms and microcrystalline cellulose Avicel (PH-101) from Sigma Aldrich. All powders were dispensed from bulk as received from the vendor. All contact surfaces viz. Aluminium, PMMA, Nylon, PVC and Teflon were obtained from McMaster-Carr to be fabricated into a V-blender

2.2. Material Characterization

2.2.1. Sample Purity:

The purity of the all powder samples has been determined using XPS (ESCALAB MKII) with a focused monochromatic Al Kα source (hν = 1486.4 eV) at a background pressure of 10^{-9} mbar and a pass energy of 100 eV (Table 1).

2.2.2. Particle Size, Surface Area, X-ray Diffraction and Moisture Content:

Particle size determination for all materials was determined using Malvern Mastersizer 2000E using the Scirocco unit for dry powder measurements. Characterization of specific surface area of materials was done using BET methodology in a NOVA Quantachrome 1000 analyzer with 5 point determination. The moisture content of these materials was determined using Karl Fischer titrimetry after equilibrating at 20% RH at 25°C. (Table 2). Powder diffraction patterns (Fig 1) were recorded with Bruker D2 Phaser-Desktop X-ray diffractometer. Samples were scanned in continuous mode using *CuKα* (λ = 1.54 Å), tube voltage of 30 kV and tube current of 10 mA. The intensities were measured at 2-theta values from 10 º to 60 º at continuous rate of 5 º/min.

2.2.3. Surface Energy:

IGC–SEA was employed to examine the surface energy of the as received powders. Decane, nonane, octane, hexane, and heptane were used as nonpolar probes; dichloromethane and ethyl acetate were used as polar probes. Adsorption measurements were performed at 32°C and 25% RH. Probes were carried into the column by helium with a gas flow rate of 10 sccm (standard cubic centimeter per minute), and the retention time was detected by a flame ionization detector (FID). The dead volume was calculated based on the elution time of methane. The surface energy (Table 3) of all the powders was measured at very low probe coverage of 0.5%.

2.2.4. Work function:

The triboelectric series is a list of materials established according to the tendency of a material to acquire positive or negative charges upon contact. The series can rank materials according to their work function and hence enable predictions of net charge. Secondly, the relationship between charge and work function could also facilitate the choice of materials for storage and

packaging of powders as well as for the components of dry powder inhaler (DPI) devices (26-27). It has been previously demonstrated that the work function of a material can be modified by altering its chemical structure i.e. by introducing functional groups that can decrease (electron donor groups such as NH_4) or increase (electron acceptor groups such as halogens) the contact potential difference (28). Consequently, for organic compounds, the charging tendency can be determined by the energy level of HOMO and LUMO since they depend on the functional groups present in the chemical structure. Hence, in this study, the work functions (Table 3) of all materials have been estimated using semi-empirical quantum calculations i.e. restricted Hartree Fock (RHF) with PM7 methodology. Calculations were performed using MOPAC 2012, a molecular orbital package, that makes approximations to the Hartree Fock formalism in treatment of Schrodinger's equation and calculates the band gap (E_g) and ionization potential (χ) of the molecule under consideration. The work function (Φ) can be then calculated (29-30) as

$$\Phi = \chi - 0.5E_g \qquad (1)$$

2.3. Experimental Method

The pharmaceutical materials along with the V-blender assembly were equilibrated at 20% RH for 24-48 hours inside a humidity controlled glove box (Fig. 1). The materials were spread in thin layers onto Aluminium foils to condition them at 20% RH. At the beginning of each experiment the initial charge on the material was measured in a Faraday's cup connected to a nano- Coulomb-meter (Monroe Electronics, NJ, Model 284). The particles were then loaded into the blender (5 %), which was then rotated at a prescribed speed. At end of a run, the powder is collected directly into the Faraday cup and the charge is measured. Following each experimental run, the blender assembly was thoroughly cleaned using isopropyl alcohol (Fischer Scientific, MA) and then dried with industrial grade air. All experiments were done in triplicate at ambient temperature (25 ± 2 ˚C) and humidity (20 ± 2% RH).

3. Simulation Method

Discrete Element Method (DEM), originally developed by Cundall and Strack (31) has been successfully used to simulate powder flow in different particulate systems (32-35). In contrast to CFD and FEM models, DEM is a Lagrangian model and, as such, tracks the positions, velocities, and accelerations of each particle individually. This soft-particle model relies on force–

displacement relations to determine the interaction forces for both particle–particle and particle–wall contacts. In a typical simulation cycle, the system geometry (such as drum dimensions, etc.) and properties of the particles (such as diameter, volume, density, etc.) are first defined and the particles are then placed randomly into the simulation volume. In the current DEM model, the normal forces (F_N) and tangential forces (F_T) for inter-particle and particle-wall collision have been calculated using the "latching spring model and "incrementally slipping model" respectively, developed by Walton and Braun (36-37).

3.1. Modeling charge transfer

The introduction of tribocharging effects into the DEM algorithm requires the determination of charge on particles/wall as well the calculation of electrostatic forces that works in conjunction with the existing contact mechanics models. It has been widely recognized that contact electrification between conductors is primarily due to electron transfer from one material surface to another (12, 38). This concept has also been extended to insulator-insulator and insulator-metal contacts. For these systems besides electrons, charge transfer has been attributed to ions particularly for polymers with mobile ions (39). In this study considering electrons as the charge carrier agents (40, 41), a DEM based electrostatic model has been employed that determines the charge exchanged between colliding species and estimates the final charge of the system under consideration. Similar to the concept of charge transfer between conductors, the driving force considered is the work function difference between different materials.

$$\Delta q = \frac{s\varepsilon_0}{ze}\left[\varphi_i - \varphi_j\right] \qquad (2)$$

In Eq.2, Φ_i and Φ_j represent the work function of the two materials i and j, ε_o is the relative permittivity, z is the cutoff distance for charge transfer (250 nm), e is the charge on electron, s is the contact area between the surfaces (42). In case of metal surfaces, these charges dissipate very fast unlike insulators for which charges are retained on surfaces for quite some time. Moreover, experimental observations indicate that triboelectrification follows an exponential increase in time followed by a saturation limit (43-45). Consequently, besides the work function difference between the surfaces, the potential difference is determined by the charge accumulated on the

materials during contacts/collisions. These induced potentials (46) produce localized electric fields as a result of which the materials will reach their saturation (Eq 3).

$$\Delta q = \frac{s\varepsilon_0}{Ze}\left[\varphi_i - \varphi_j - \left(E_{ii}.\frac{d_{ij}}{||d_{ij}||}\right)ze\right] \quad (3)$$

The electric field at the center of a particle (E_{ii}) is obtained by the Coulomb law, using the superposition principle whereas d_{ij} represents the position vector between the particle and wall (47).

3.2. Modeling electrostatic forces

The aim of the Discrete Element Method (DEM) is to compute the contact forces acting on each particle within the system. Since the system involves charged particles, besides contact forces, electrostatic forces also need to be calculated. The introduction of electrostatic forces into the current scheme requires the addition of a long-range coulombic force that works in conjunction with the existing Walton and Braun calculations. The long-range force model (48) is based on Coulomb's law and incorporates a screening term to account for the presence of other charged particles. For these long ranged forces (Eq. 4.1 & Eq. 4.2), q_e is the charge of the electron (1.602×10^{-19} C), ε is the relative permittivity of the medium, ε_o is the permittivity of the free space (8.85410^{-12} F/m), T is the temperature in Kelvin, K_B is the Boltzmann's constant (1.38×10^{-23} JK^{-1}), and n_i is the number of particles with charge z_i in the near vicinity.

$$F_{sc} = \frac{q_1 q_2}{4\pi\varepsilon_o}\left(\frac{\tau}{r} + \frac{1}{r^2}\right)e^{-\tau r} \quad (4.1) \qquad \tau = q_e\sqrt{\left(\frac{1}{K_B T\varepsilon\epsilon_0}\sum_i n_i z_i^2\right)} \quad (4.2)$$

Besides the repulsive electrostatic forces, tribocharging also generates attractive electrostatic forces between particles and boundary. The electrostatic force on a charged particle q_i located near a wall can be calculated as $f_{ew,i} = E.q_i$, where E represents electric field due to continuous charge distribution on the boundary wall (49).

4. Results and Discussion

4.1. Experimental

4.1.1. Material Characterization

The XPS data for elemental composition (Table 1) revealed that all pharmaceutical powders received from vendor had minimal contamination. The median particle size obtained from Mastersizer for Ibuprofen particles was around 17 µm whereas the median particle size for theophylline, MCC and lactose monohydrate was found to be quite close viz. 63 µm, 51 µm and 52 µm respectively. The specific surface areas for Ibuprofen, theophylline, lactose monohydrate and MCC were found to be around 0.9202, 0.373, 0.412 $m^2 g^{-1}$, and 1.07 $m^2 g^{-1}$ respectively. The dispersive and polar surface energy results from SEA (at a surface coverage of 5%) are shown in Table 3. In case of MCC, a higher total surface energy is suspected to be due to partial amorphous nature as indicated by XRD diffractogram (Fig. 1d). In silico computation estimated a triboelectric series (Table 4) from which the tendency of a material getting charged positively or negatively in contact with another material can be evaluated. Therefore, PMMA, Nylon, Aluminum are expected to release electrons in contact with materials such as theophylline, whereas PVC and Teflon can remove electrons when in contact. Consequently, materials positioned higher in the table are expected to charge positively following contact with a material in the lower end of series (16, 38).

4.1.2. Effect of contact time

To study the effect of contact time on electrification, a measured quantity of powder (100g) was loaded into the V-blender. The blenders were rotated at 13 rpm for some time and then discharged from the blender directly into the Faraday cup. The weight of particles inside the Faraday cup was measured and the specific charge (nC/g) was then calculated. As illustrated in Fig.3a, the charge profile displayed an initial rise followed by a plateau for all powders. Under similar conditions of impact, Ibuprofen (IBU) was found to charge the most compared to the other powders. Secondly, Ibuprofen also required longer time to be charged to the saturated value. The difference in the charging kinetics of Ibuprofen can be due to its smaller particle size (Table 2) and a greater triboelectrification that results in substantial adhesion of particles to the wall and hence can effectively reduce the available surface for charge transfer. With respect to

other powders, the triboelectrification of theophylline was found to be least around -0.624 ±0.23 nC/g, whereas for MCC and lactose monohydrate the charge was found to be around -1.26±0.13 nC/g and -2.32 ±0.56 nC/g respectively. Similar charging profile was obtained against Teflon with charges of opposite polarity (Fig. 3b).

4.1.3. Effect of blender speed

To evaluate the effect of blender speed, the charge accumulated for each of the material was determined at the end of 20 and 80 blender revolutions at a speed of 13 rpm, 40 rpm and 80 rpm. After a prescribed time, the powders were directly discharged from the blender into the Faraday cup. As observed from Fig. 4a-4c, the triboelectrification of Ibuprofen was found to much higher than the other powders in the Aluminium blender. A similar observation was obtained for PVC blenders (Fig. 5a-5c) with a change in charge polarity. The difference in the specific charge for all the powders was found to be practically insignificant upon changing the blender revolution for a given speed of 13 rpm and 40 rpm. Nonetheless, there was a steep decrease in charge value upon increasing the blender speed to 80rpm. Thus, the saturation charge does not seem to be influenced by the blender speed or the energy of contact as long as the powder can effectively contact the blender surface for charge transfer.

4.1.4. Effect of Contact Surface

The total charge of all powders was determined against all contact surfaces at the end of 20 blender rotations since the powders particles were charged to saturated values under these conditions. As observed from Fig.6 Ibuprofen, theophylline, lactose and MCC charged negatively against PMMA, Nylon whereas these powders charged positively against Teflon and PVC. For all cases considered, electrification of Ibuprofen particles was highest. In case of theophylline, the magnitude of charge accumulated on the surface seems to build up with increase in surface potential difference between the two surfaces with largest charge accumulation against Teflon. Lactose monohydrate and MCC also showed a similar trend but for Ibuprofen the magnitude of charge remained almost same against all surfaces. Even so, the powders seem to follow the triboelectric series established in table 4.

4.2. Simulations

The DEM model described in section 3 implements the electrostatics algorithm by first determining the contact between particles and the blender wall. Once a contact has been established, charge transfer occurs according to Eq (3), considering work function difference to be the driving force for charge transfer. The charges are considered to be homogenously distributed on the surface of particles. Traditionally, in a DEM model, the contact forces are calculated numerically by employing force-displacement schemes that divide the computational time into small time steps; normally micro-seconds. As a result, the contact force goes from zero at the beginning of a collision to a maximum value and then back to nearly zero at the end of a collision. The consequence is that a contact between two particles can last for several time steps. Hence, the charge transfer can occur over multiple time steps resulting in excess charging. Accordingly, in these simulations the maximum contact force was first determined which is then followed by charge transfer. As the transferred charge on highly insulating particles can be retained for several hours, charge relaxation has been ignored in this study (46).

The basic assumptions used in this model can be summarized as

1) Charge transfer occurs only due to work function difference between two surfaces
2) With respect to contact detection, charge transfer occurs only for the maximum contact force between two colliding surfaces.
3) Charge is assumed homogeneously distributed.
4) Charge relaxation or charge dissipation has not been considered in this study.

Prediction of charge in V-blender system

To investigate tribocharging, particles were deposited in a V-blender of same dimensions as that of the experiment. The particles were assumed to be mono-disperse spheres with the number of particles set according to the fill level in experiments (5 %). Simulations were performed by varying blender speeds from 13 to 80 revolutions per minute. Initially (t=0), all particles have been considered to have no charge. As triboelectrification proceeds charge transfer occurs in accordance to the algorithm described in section 3. The DEM parameters for the system investigated have been provided in Tables 5

4.2.1. Effect of contact time

The effect of contact time on triboelectrification was determined by calculating the total charge accumulated by the powders. The snapshots (Fig.7) display the evolution of charge with time for Ibuprofen and MCC against PMMA blender. All particles at initial time t =0 secs are uncharged and are represented by dark blue color. It can be observed from the DEM snapshots; the extent of tribocharging is higher in case of Ibuprofen (Fig. 7a) as compared to the other particles and is suspected to be due to smaller particle size of Ibuprofen. Moreover, the number of particles charging in the range of 7e-12 to 5e-11C (orange to red) is much greater for Ibuprofen than for theophylline. Additionally, the superior tribocharging of Ibuprofen also results in greater adhesion to the blender wall. The initial evolution of charge with time (Fig 8) illustrates that there is first an increase in tribocharging followed by some plateau effect. Consequently, the induced potential generated by the charged particle could ultimately lead to equilibrium charge on these powders. Thus, the charge kinetics is simulated by the DEM model as it incorporates the effect of the increasing potential of a charged particle in terms of its electric field (E_{ii}) as depicted in Eq.3.

4.2.2. Effect of Blender speed

The effect of blender rotational speed on tribocharging was studied at 40 rpm and 80 rpm. Experimentally, these studies did not reveal considerable differences in specific charge observed at 13 rpm and 40 rpm for a given number of revolutions. However at 80 rpm there was a steep decrease in charge. To investigate this behavior, a simulation study was performed at different blender speeds. The snapshots in Fig. 9 illustrate the evolution of charge at 40 and 80 rpm respectively. From these snapshots, it can be qualitatively observed that charging reduced when blender speed was increased to 80 rpm. At a blender speed of 80 rpm, the powder bed seemed to remain stagnant resulting in decrease in particle-wall contacts and hence decreases charge transfer. The larger centrifugal forces generated at 80 rpm seem to be responsible for this decline in charge (Fig 10a). This effect is further validated by decrease in particle wall collisions (Fig. 10b) at 80 rpm as compared to 40 rpm.

4.2.3. Model verification

The graph in Fig. 11 illustrates the comparison of charge accumulation obtained from experiments and from the simulation model. The simulation data was obtained at 30 seconds at 40rpm (Fig 12) where the materials are expected to reach their saturation levels. As observed from the graph, the results obtained from simulation model lie within the expected experimental range for all powders. Moreover, similar to the experimental results, the triboelectrification of theophylline was found to be the least. However, there are discrepancies between the experimental and simulation data which are quite evident especially for Ibuprofen particles. These inconsistencies could be due to greater deformation of the particles resulting in higher charge accumulation during impact or might be due presence of surface defects generated during processes such as micronization which may serve as electron trapping sites and hence result in greater triboelectrification. Some association seems to exist between the polar surface energy of powders (Table 3) and the accumulated charge, since polar interactions are associated with electron transfer (50), and can contribute to tribocharging. Besides surface defects, greater deformation of particles might also result in significant tribocharging of the powders. A comparison of cohesive energy density (CED) of the pharmaceutical powders suggests (Table 6) that Ibuprofen has the least CED. The CED of a material can be related to its Young's Modulus and hence its extent of deformation (51). As Ibuprofen has the least CED of all the materials it is suspected to deform the most and hence tribocharge to a greater extent. All these factors in addition to the small particle size can contribute to the greater electrification of Ibuprofen. Nonetheless, the DEM model could capture the dynamics and difference in charging behavior of the powders, as the general trends obtained from experiments and simulations were quite similar. Thus, the prediction of models can complement and improve the understanding of tribocharging of pharmaceutical powders thereby filling the gaps in our knowledge of processes.

5. Conclusions

The current investigation has revealed the effects of some operating parameters on tribocharging of pharmaceutical powders in a simple V-blender and Faraday cup assembly. For all powders considered, triboelectrification displayed an initial rise followed by a constant equilibrium charge. Particle charging was found to be collisional and increased with blender speed as long as the powder could effectively contact the blender. Triboelectrification of Ibuprofen was found to

be highest as compared to other powders against all surfaces that resulted in significant adhesion to the processing equipment, a common problem encountered in solid–dosage manufacturing. Additionally, electrostatic process has been modeled by employing discrete element method incorporating electrostatic forces. The developed model captures the collisional nature of tribocharging and agrees well with experimental data for most of powders. In case of Ibuprofen, the discrepancy between experimental and simulation data is quite evident and an attempt has been made to understand this difference based on some material properties of these powders like CED and surface energy. Efforts are now being directed to investigate tribocharging of powders with different CED and incorporate these effects into the DEM model. Thus, process modeling based approach provides a mechanistic understanding of different factors involved, which are otherwise difficult to be quantified experimentally.

Acknowledgements

The authors would like to thank Dr. Dave and Zhonghui huang for their help in surface energy calculations

Nomenclature

Φ	Work Function
z	Cut off distance for charge transfer
ε_o	permittivity of the free space
E	Electric field
E_g	Band gap
χ	Ionization potential
s	Contact area
e	Charge of an electron
q	Charge of particle
T	Temperature
K_B	Boltzmann Constant
d	Position vector
F_N	Normal Force
F_T	Tangential Force
F_{sc}	Electrostatic force between particles
$F_{ew,i}$	Electrostatic forces between particle and wall

Abbreviations

MCC Microcrystalline cellulose

LAC Lactose Monohydrate

THEO Theophylline

IBU Ibuprofen

CED Cohesive energy Density

XPS X-ray Photoelectron spectroscopy

XRD X-ray diffraction

6. References

1) C.D. Hendricks. *Charging macroscopic particles*. In Moore AD, editor Electrostatics and its Applications. New York, NY: John Wiley & Sons. 57-85 (1973).

2) A.G. Bailey. Electrostatic phenomena during powder handling. *Powder Technology* **37**:71-85 (1984).

3) M. Murtomaa, E. Räsänen, J. Rantanen, A. Bailey, E. Laine, J-P. Mannermaa and J. Yliruusi. Electrostatic measurements on a miniaturized fluidized bed. Journal of Electrostatics **57**:91-106. (2003)

4) M. Murtomaa, M. Savolainen, L. Christiansen, J. Rantanen, E. Laine and J. Yliruusi. Static electrification of powders during spray drying. *Journal of Electrostatics* **62**:63-72 (2004).

5) A.G. Bailey. Charging of solids and powders. *Journal of Electrostatics* **30**:167-180 (1993)

6) J. Peart. Powder electrostatics: Theory, techniques, and applications. *Kona* **19**:34-45 (2001).

7) M.P. Grosvenor and J.N. Staniforth. The influence of water on electrostatic charge retention and dissipation in pharmaceutical compacts for powder coating. *Pharmaceutical Research* **13:**1725-1729 (1996).

8) K.C. Pingali, S.V. Hammond, F.J. Muzzio and T. Shinbrot. Use of a static charge eliminator to improve powder flow. *International Journal of Pharmaceutics* **369** :2–4 (2009).

9) K.N. Palmer. *Dust Explosions and Fires*, Chapman and Hall Ltd., London, 1973

10) I. I. Inculet. *Electrostatics and its applications* (ed. Moore, A. C.) John Wiley & Sons, New York, 86-114 (1973).

11) M. Murtomaa, P. Harjunen, V. Mellin , V. P Lehto, and E. Laine. Effect of amorphicity on the triboelectrification of lactose powder. *Journal of Electrostatics* **56**:103-110 (2002).

12) W. R Harper. *Contact and frictional electrification* (Oxford University Press, London, 1967).

13) A. F. Diaz and D. Fenzel-Alexander. An ion transfer model for contact charging. *Langmuir*, 9:1009–1015(1993).

14) L.S. McCarty and G.M. Whitesides. Electrostatic charge due to separation of ions at interfaces: contact electrification of ionic electrets. *Angewandte Chemie: International Edition in English* **47**: 2188–2207 (2008).

15) C.F. Gallo and W.L. Lama. Some charge exchange phenomena explained by a classical model of the work function. *Journal of Electrostatics* **2**:145-150 (1976).

16) S. Karner and N.A. Urbanetz. The impact of electrostatic charge in pharmaceutical powders with specific focus on inhalation-powders, Journal of Aerosol Science **42** 428–445(2011)

17) H. Watanabe, M. Ghadiri, T. Matsuyama, Y.L. Ding, K.G. Pitt, H. Maruyama, S. Matsusaka, and H. Masuda,. Triboelectrification of pharmaceutical powders by particle impact. *International Journal of Pharmaceutics* **334**: 149–155 (2007a).

18) L.A. Mackin, G. Rowley, E.J. Fletcher and R. Marriott. An investigation of the role of moisture on the charging tendencies of pharmaceutical excipients, Proceedings of the 12th Pharmaceutical Technical Conference **2**: 300–317 (1993).

19) K. Zhu, R.B.H. Tan, F. Chen, K.H. Ong, P.W.S. Heng, Influence of particle wall adhesion on particle electrification in mixers, *International Journal of Pharmaceutics* **328**: 22–34 (2007).

20) S. Karner and N.A. Urbanetz .Triboelectric characteristics of mannitol based formulations for the application in dry powder inhalers. *Powder Technol*. **235:**349–358 (2013).

21) G. Rowley. Quantifying electrostatic interactions in pharmaceutical solid systems. *International Journal of Pharmaceutics* **227:** 47–55 (2001).

22) T. Matsuyama and H. Yamamoto. Charge transfer between a polymer particle and a metal plate due to impact. *IEEE Transactions on Industry Applications* **30**:602–607 (1994).

23) S. Manickam, R. Shah, J. Tomei, T. Bergman and B. Chaudhuri. Investigating Mixing in a Multi-dimensional Rotary Mixer: Experiments and Simulations, *Powder Technology* **201**: 83-92, (2010).

24) E. Sahni and B. Chaudhuri, Numerical Simulations of Contact drying in Agitated Filter-dryer, Chemical Engineering Science **97**: 34-49 (2013).

25) S. Naik, R. Malla, M. Shaw and B. Chaudhuri. Investigation of Comminution in a Wiley Mill: Experiment and DEM Simulations, *Powder Technology* **237**: 338-354 (2013).

26) P.R. Byron, J. Peart and J.N. Staniforth. Aerosol electrostatics I: properties of fine powders before and after aerosolization by dry powder inhalers. *Pharm. Res*. **14:**698–705 (1997)

27) M.J. Telko, J. Kujanpää and A.J. Hickey. Investigation of triboelectric charging in dry powder inhalers using Electrical Low Pressure Impactor (ELPI). *Int. J. Pharm*. **336**: 352–360 (2007).

28) C.U. Yurteri, M.K. Mazumder, N. Grable, G. Ahuja, S. Trigwell, A.S. Biris, R. Sharma and R.A. Rims. Electrostatic effects on dispersion, transport, and deposition of fine pharmaceutical powders: development of an experimental method for quantitative analysis.*Part.Sci.Technol.***20**: 59–79. (2002)

29) S. Trigwell, N. Grable, C.U. Yurteri, R. Sharma and M.K Mazumder. Effect of surface properties on the tribocharging characteristics of the polymer powder as applied to industrial processes. *IEEE Transactions in Industry Applications* **39**:79–86 (2003).

30) S. Sarkar, J. Cho and B. Chaudhuri. Mechanisms of electrostatic charge reduction of granular media with additives on different surfaces.Chem.Eng.Process.**62**: 168–175 (2012).

31) P.A. Cundall and O.D.L. Strack. A discrete numerical model for granular assemblies. *Geotechique* **29**: 47–55(1979).

32) R.Y. Yang, A.B. Yu, L. McElroy and J. Bao. Numerical simulation of particle dynamics in different flow regimes in a rotating drum. *Powder Technology* **188**: 170–177 (2008).

33) Nan Gui, Jie Yan, Wenkai Xu, Liang Ge, Daling Wu, Zhongli Ji, Jinsen Gao, Shengyao Jiang, and Xingtuan Yang. DEM simulation and analysis of particle mixing and heat conduction in a rotating drum. *Chemical Engineering Science* **97:** 225–234 (2013).

34) W.R. Ketterhagen. Modeling the motion and orientation of various pharmaceutical tablet shapes in a film coating pan using DEM. *International Journal of Pharmaceutics* **409**:137–149 (2011).

35) Daniele Suzzi, Gregor Toschkoff, Stefan Radl, Daniel Machold, Simon D. Fraser, Benjamin J. Glasser and Johannes G. Khinast. DEM simulation of continuous tablet coating: Effects of tablet shape and fill level on inter-tablet coating variability. *Chemical Engineering Science* **69**:107–121(2012).

36) O. Walton and R. Braun. Viscosity, granular-temperature and stress calculations for shearing assemblies of inelastic, frictional disks. *J. Rheol*. **30**:949–980 (1986).

37) O. Walton. Numerical simulation of inclined chute flows of mono-disperse, inelastic, frictional spheres. *Mech. Mater*. **16:** 239–247 (1993).

38) S. Matsusaka. Control of particle tribocharging. *Kona Powder Part.J* .**29**:27–38 (2011)

39) A.F Diaz and D. Fenzel-Alexander. An ion transfer model for contact charging. *Langmuir* **9**:1009–1015 (1993).

40) N. Duff and D.J. Lacks. Particle dynamics simulations of triboelectric charging in granular insulator systems. *J. Electrostat*. **66**: 51–57 (2008).

41) C. Liu and A.J Bard. Electrostatic electrochemistry at insulators. *Nat.Mater*.**7**:505–509 (2008).

42) J. Lowell and A.C Rose-Innes. Contact electrification. *Advances in Physics* 29:947–1023. (1980)

43) H. Watanabe, A. Samimi, Y.L. Ding, M. Ghadiri, T. Matsuyama and K.G. Pitt, Measurement of charge transfer due to single particle impact, *Part. Part. Syst. Charact.* **23**: 133–137 (2006).

44) W.D. Greason. Investigation of a test methodology for triboelectrification. *J. Electrost*. **49**: 245–256 (2000).

45) J.W. Peterson. Contact charging between nonconductors and metal, *J. Appl. Phys*. **25**:907–915 (1954).

46) C. Pei, C.-Y. Wu, D. England, S. Byard, H. Berchtold and M. Adams. Numerical analysis of contact electrification using DEM–CFD. *Powder Technol*. **248**: 34–43 (2013)

47) J.C. Laurentie, P. Traoré, L. Dascalescu. Discrete element modeling of triboelectric charging of insulating materials in vibrated granular beds. *Journal of Electrostatics* **71**: 951-957 (2013).

48) M.D. Hogue, C.I. Calle, D.R. Curry, and P.S. Weitzman. Calculating the trajectories of triboelectrically charged particles using Discrete Element Modeling (DEM). *Journal of Electrostatics* **66**: 32–38. (2008).

49) S. Watano, S. Saito and T. Suzuki Numerical simulation of electrostatic charge in powder pneumatic conveying process. *Powder Technology* **135–136**:112–117 (2003).

50) N.M. Ahfat, G. Buckton, R. Burrows and M.D. Ticehurst. An exploration of interrelationships between contact angle, inverse phase gas chromatography and triboelectric charging data. *Eur. J. Pharm. Sci*. **9**: 271–276 (2000).

51) Bruno C. Hancock, Peter York and Raymond C. Rowe The use of solubility parameters in pharmaceutical dosage form design. *International Journal of Pharmaceutics* **148**: 1-21(1997).

52) R.J. Roberts R.C Rowe and P. York. The relationship between Young's modulus of elasticity of organic solids and their molecular structure. *Powder Technol.*, **65**: 139-146 (1991)

Tables

Table 1: XPS data showing normalized elemental percentage compositions of different materials

Material	C	O	N	Si
Ibuprofen	76.82	23.18	---	---
Theophylline	59.12	14.77	26.12	---
MCC	58.93	41.07	---	---
Lactose Monohydrate	59.48	40.41	---	0.11

Table 2: Some material properties of pharmaceutical powders

Material	d_{50} (µm)	Surface Area (m^2/g)	Moisture content (%w/w)
Ibuprofen	17.02	0.920	0.056
Theophylline	63.12	0.373	0.027
MCC	51.47	1.071	4.812
Lactose Monohydrate	52.34	0.412	0.012

Table 3: Surface energy of all as received pharmaceutical powders obtained at 0.5% surface area coverage (SAC),n=2

Material	Dispersive (mJ/m^2)	Polar (mJ/m^2)	Total (mJ/m^2)
Ibuprofen	46.64	13.18	59.82
Theophylline	53.21	7.82	61.03
MCC	59.08	10.91	69.99
Lactose Monohydrate	43.21	6.93	50.14

Table 4: Work function of all powders and contact surfaces from molecular orbital calculation (MOPAC)

Material	SEMI-EMPIRICAL CALCULATION (eV)
Aluminium	4.33
Nylon	4.43
PMMA	4.51
Ibuprofen	4.77
Theophylline	4.90
MCC	5.11
Lactose monohydrate	5.18
PVC	5.33
PFTE	6.01

Table 5: DEM parameters for tribocharging in V-blenders

	Values		
DEM Parameters	THEO	MCC	IBU
Total number of particles	20,000	20,000	90,000
Size of the particles	800 µm	800 µm	400 µm
Coefficient of restitution Particle/particle	0.4	0.4	0.4
Coefficient of restitution Particle/wall	0.6	0.6	0.6
Friction coefficient: particle/particle	0.5	0.5	0.5
Work function: Surface (PMMA)	4.51 eV	4.51 eV	4.51 eV
Work function particle	4.90 eV	5.11 eV	4.77 eV
Friction coefficient particle/wall	0.5	0.5	0.7
Blender speed	13 rpm		

Table 6: CED of pharmaceutical powders using group contribution method [51]

Powder	CED (MPa)
Ibuprofen	376.3
Theophylline	763.4
MCC	1013.1
Lactose Monohydrate	912.3

Figures

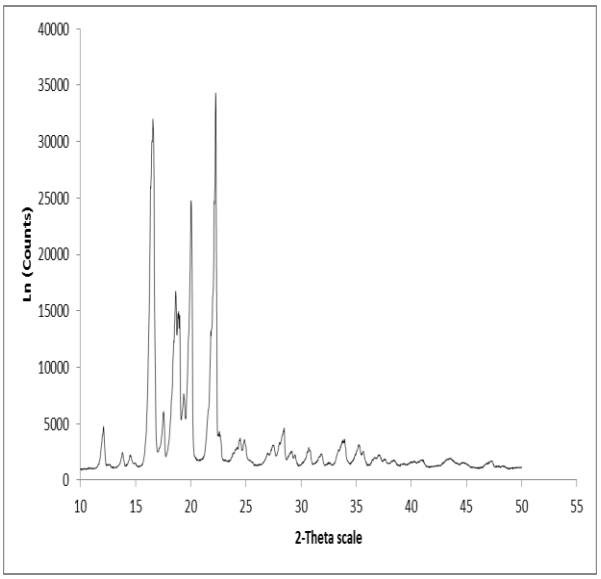

Fig 1a: XRD diffractogram for Ibuprofen

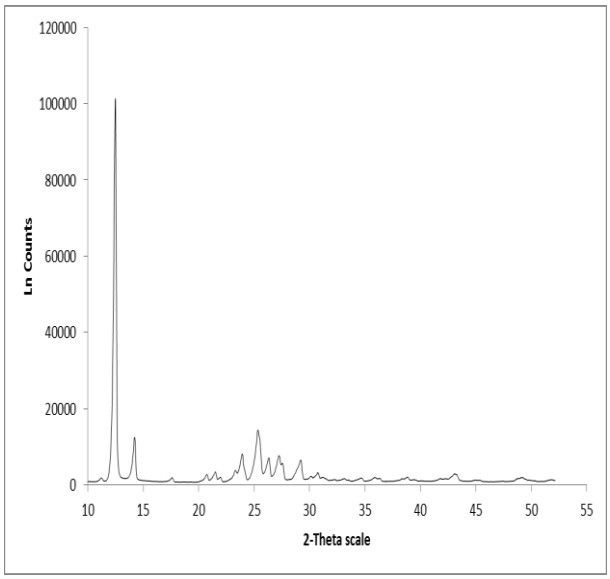

Fig 1b: XRD diffractogram for Theophylline

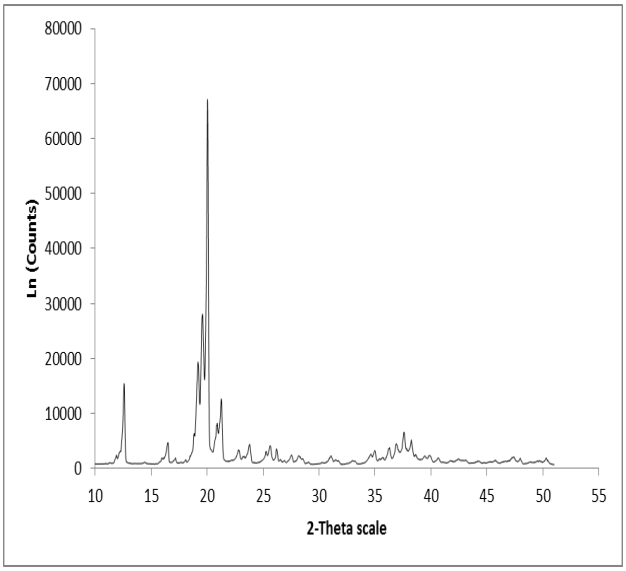

Fig 1c: XRD diffractogram for Lactose monohydrate

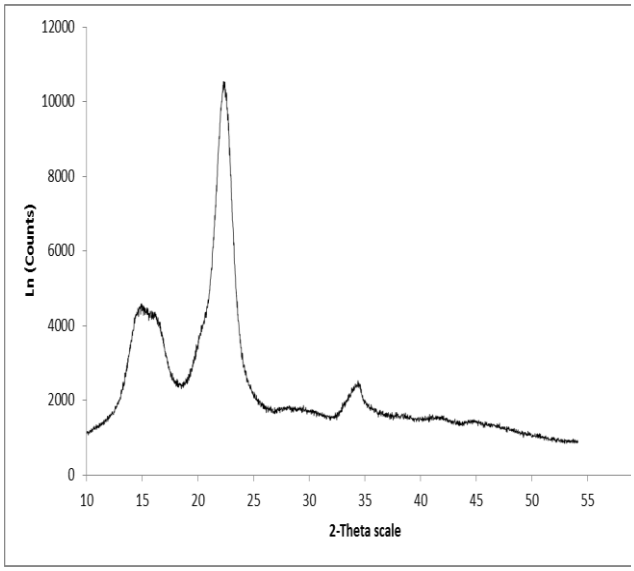

Fig 1d: XRD diffractogram for MCC

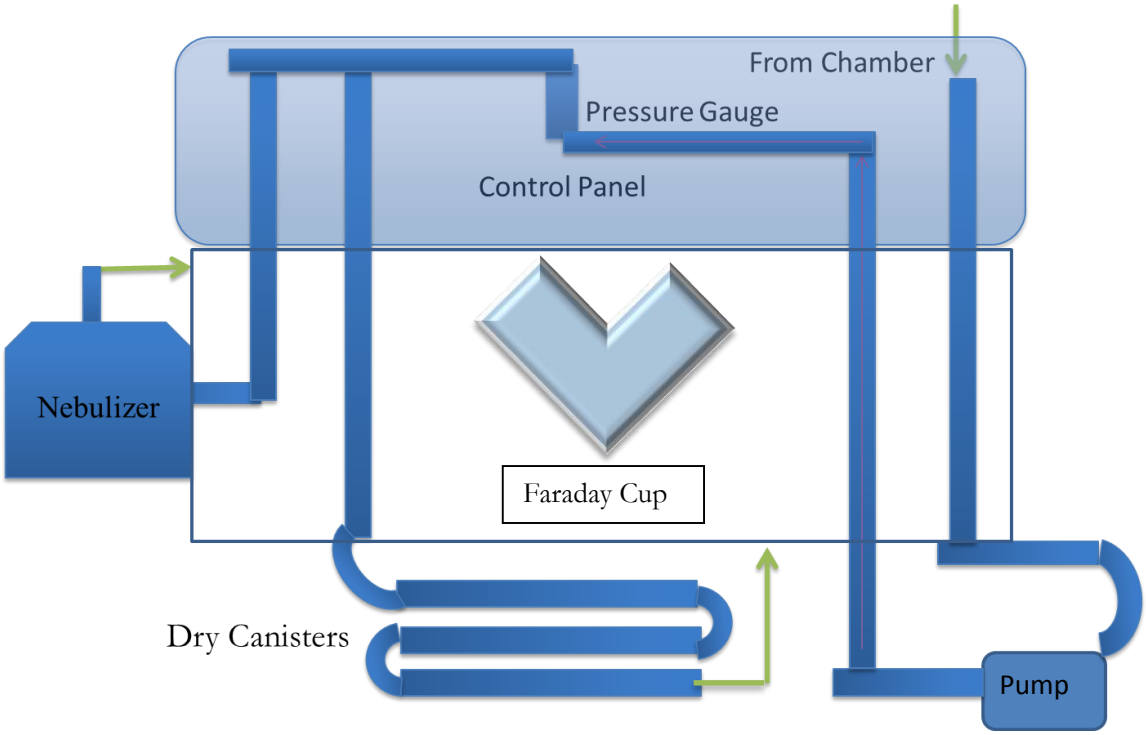
From Chamber
Pressure Gauge
Control Panel
Nebulizer
Faraday Cup
Dry Canisters
Pump

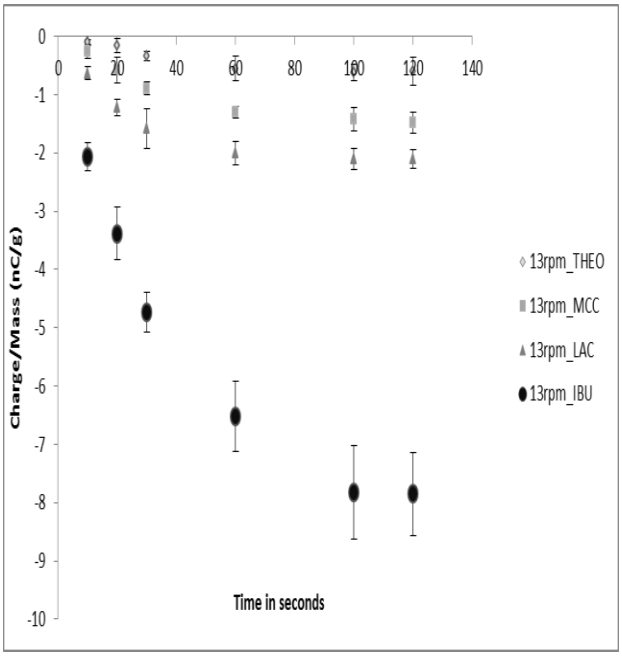

Figure 3a: The accumulation of electrostatic charge as a function of time against PMMA surface

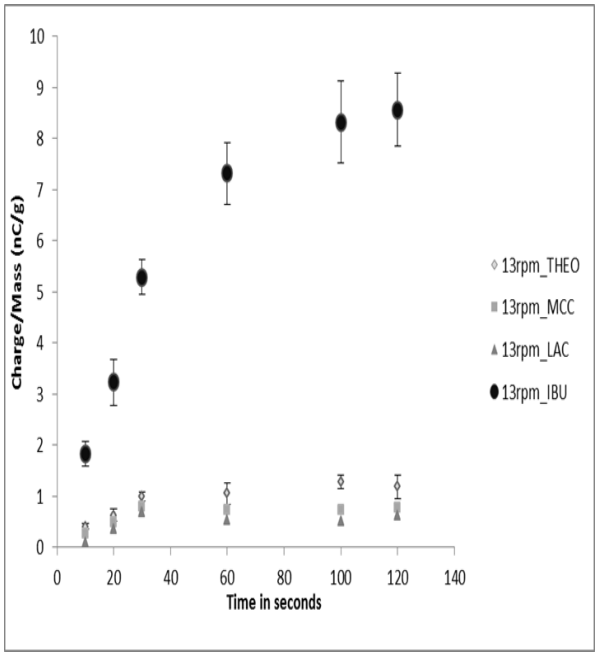

Figure 3b: The accumulation of electrostatic charge as a function of time against Teflon surface

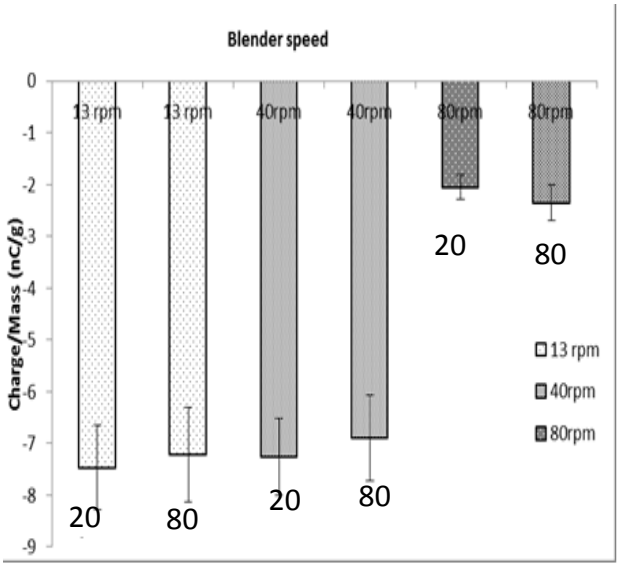

Figure 4a: Charge/mass of Ibuprofen against Aluminum surface

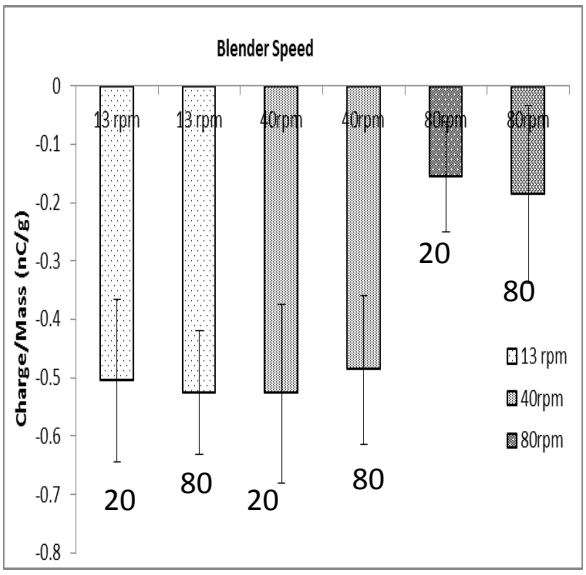

Figure 4b: Charge/mass of Theophylline against Aluminum surface

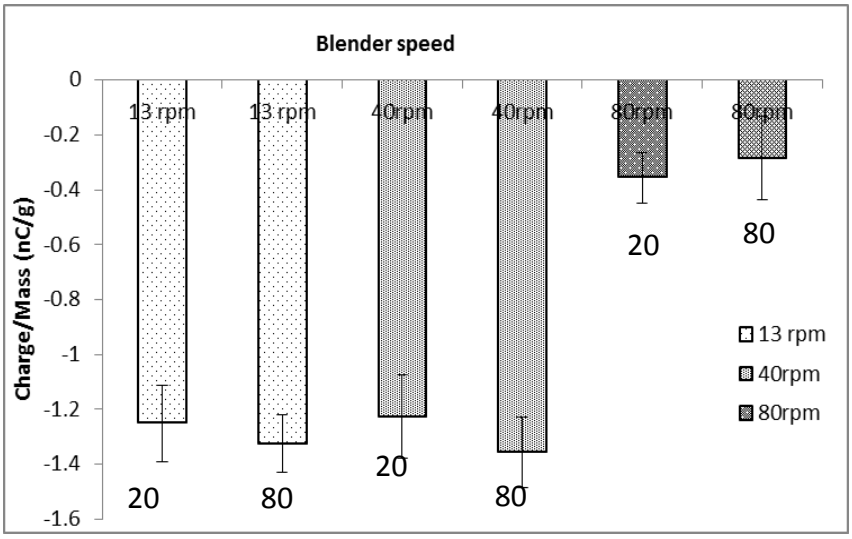

Figure 4c: Charge/mass of MCC against Aluminum surface

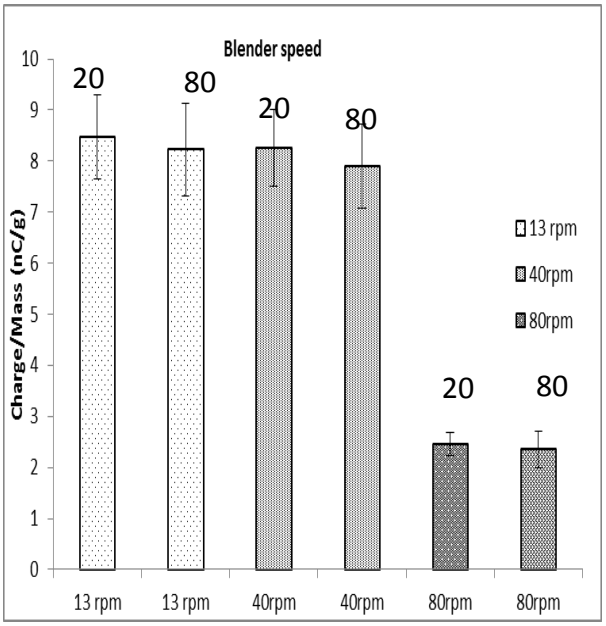

Figure 5a: Charge/mass of Ibuprofen against PVC surface

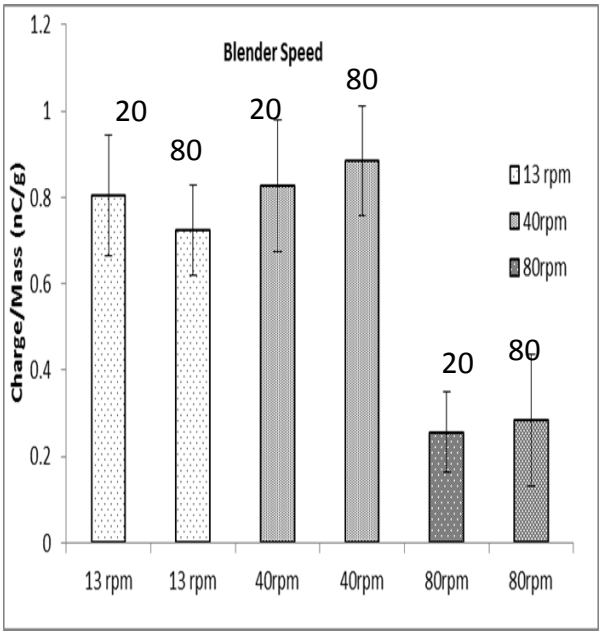

Figure 5b: Charge/mass of Theophylline against PVC surface

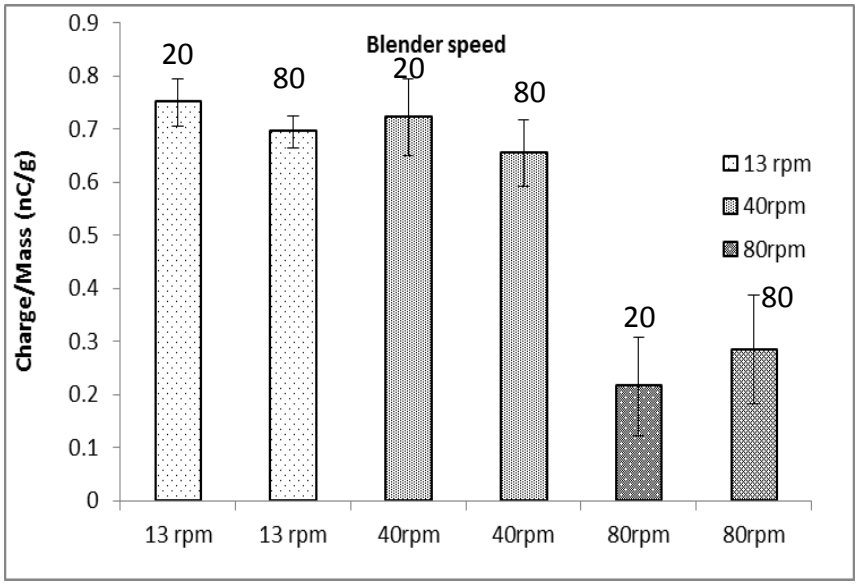

Figure 5c: Charge/mass of MCC against PVC surface

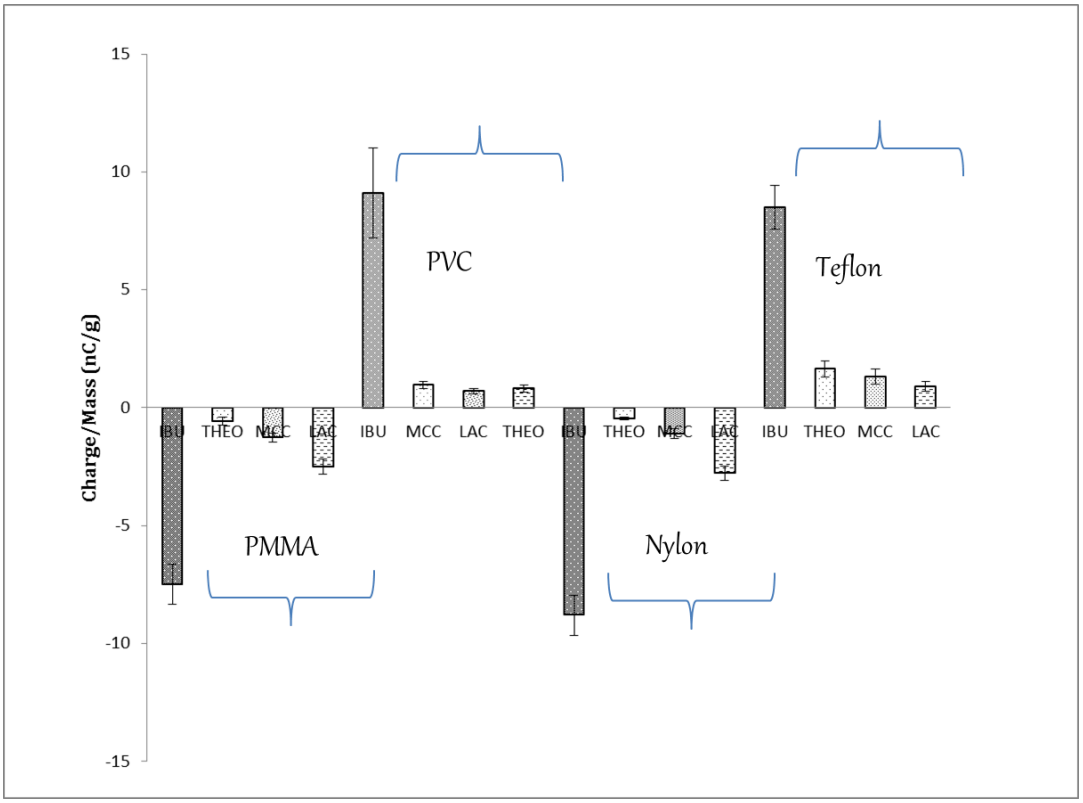

Figure 6: Charge/Mass for all powders against PMMA, Nylon, PVC and Teflon surface

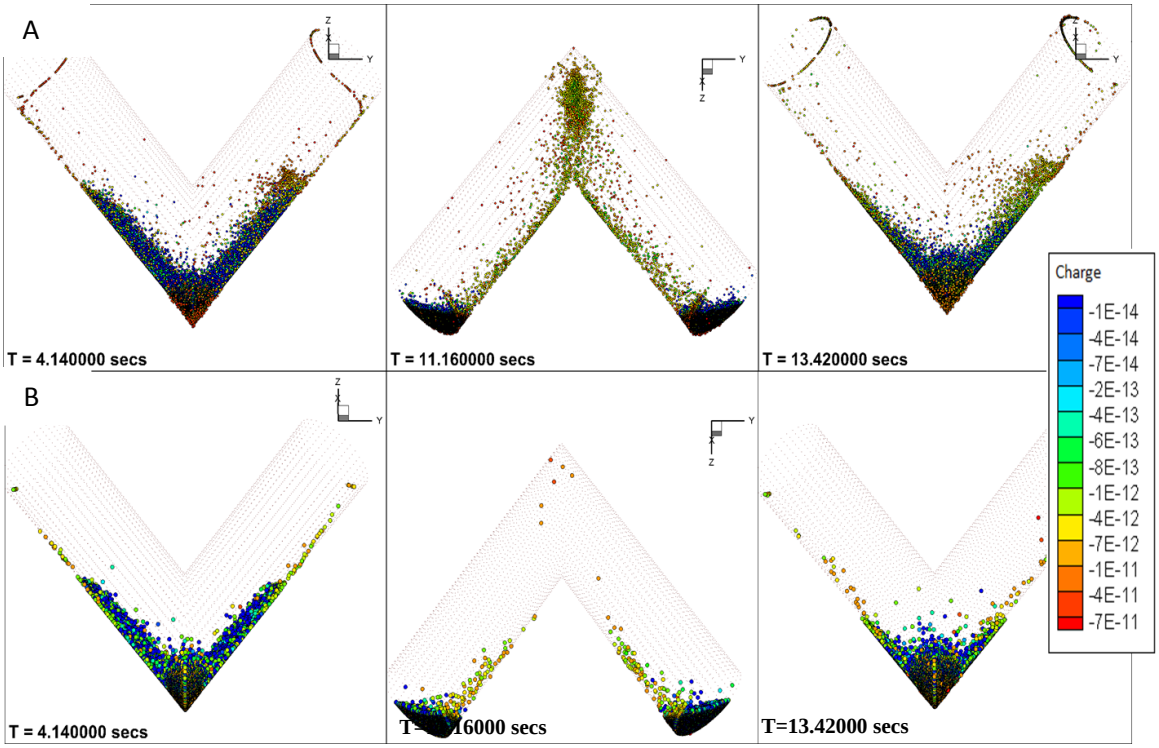

Figure 7: DEM snapshots of Evolution of charge with time at 13rpm A) Ibuprofen B) Theophylline

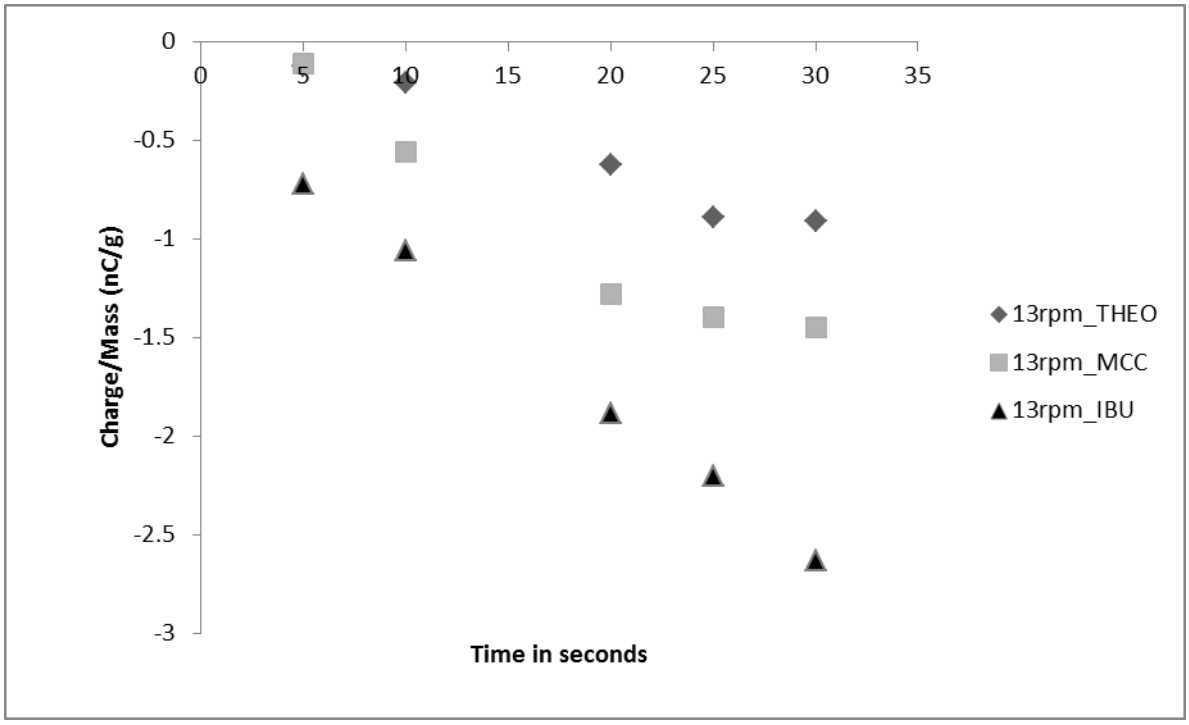

Figure 8: The accumulation of electrostatic charge as a function of time.

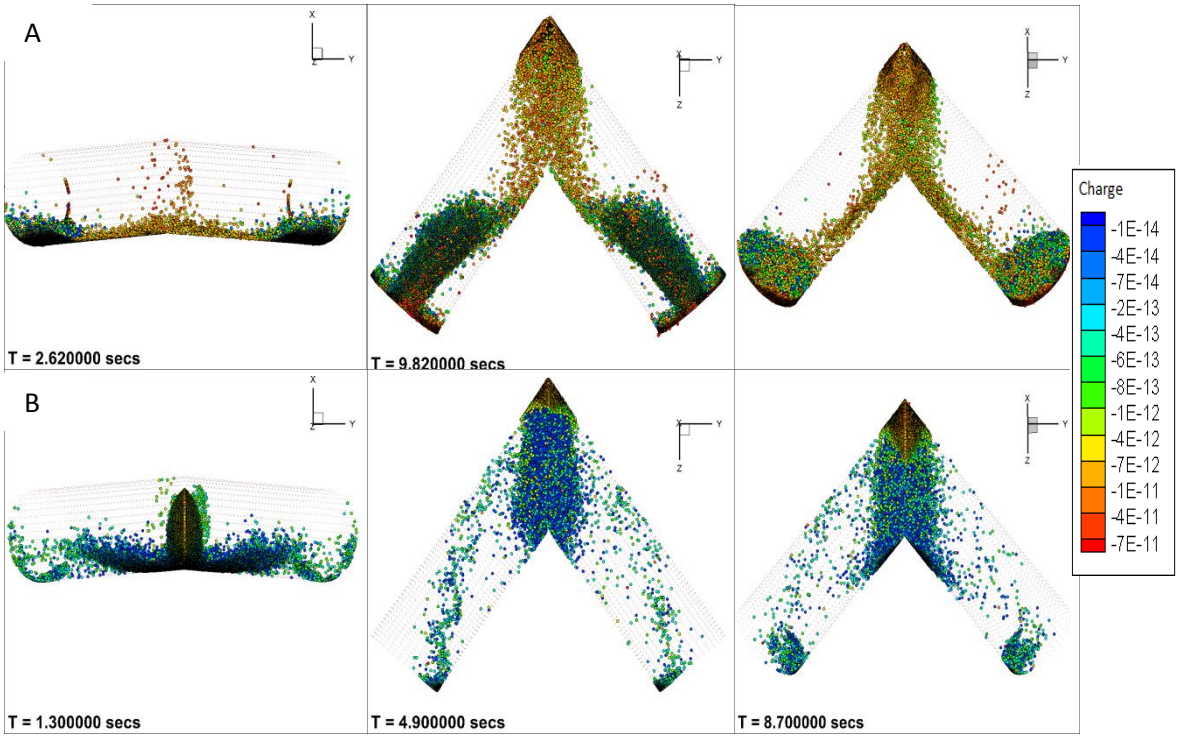

Figure 9: DEM snapshots of evolution of charge with number of revolutions A) 40 rpm B) 80 rpm

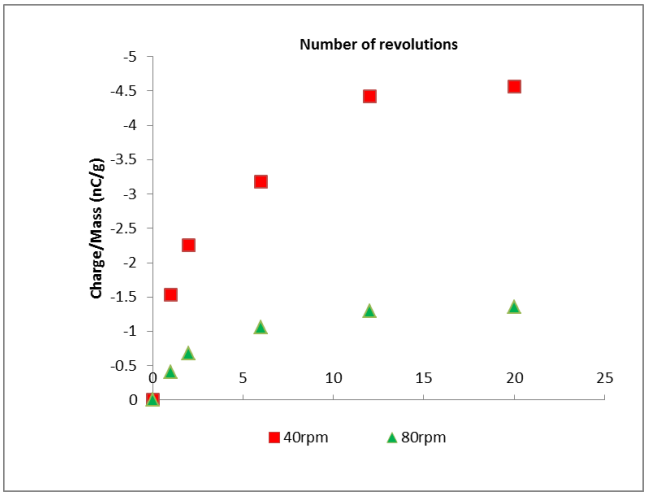

Figure 10a: Charge accumulation at different blender speeds

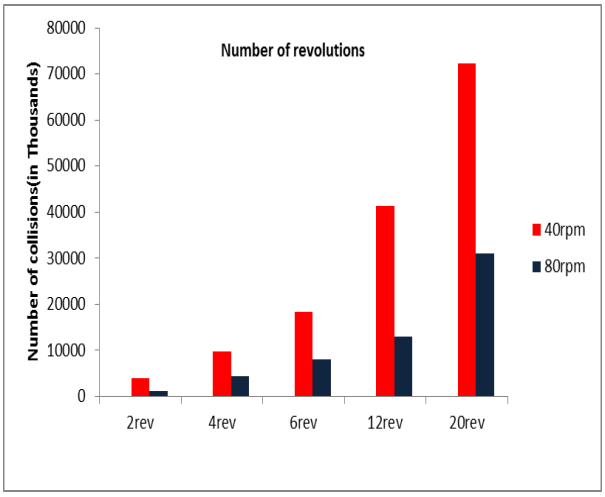

Figure 10b: Particle-wall collisions at different blender speeds

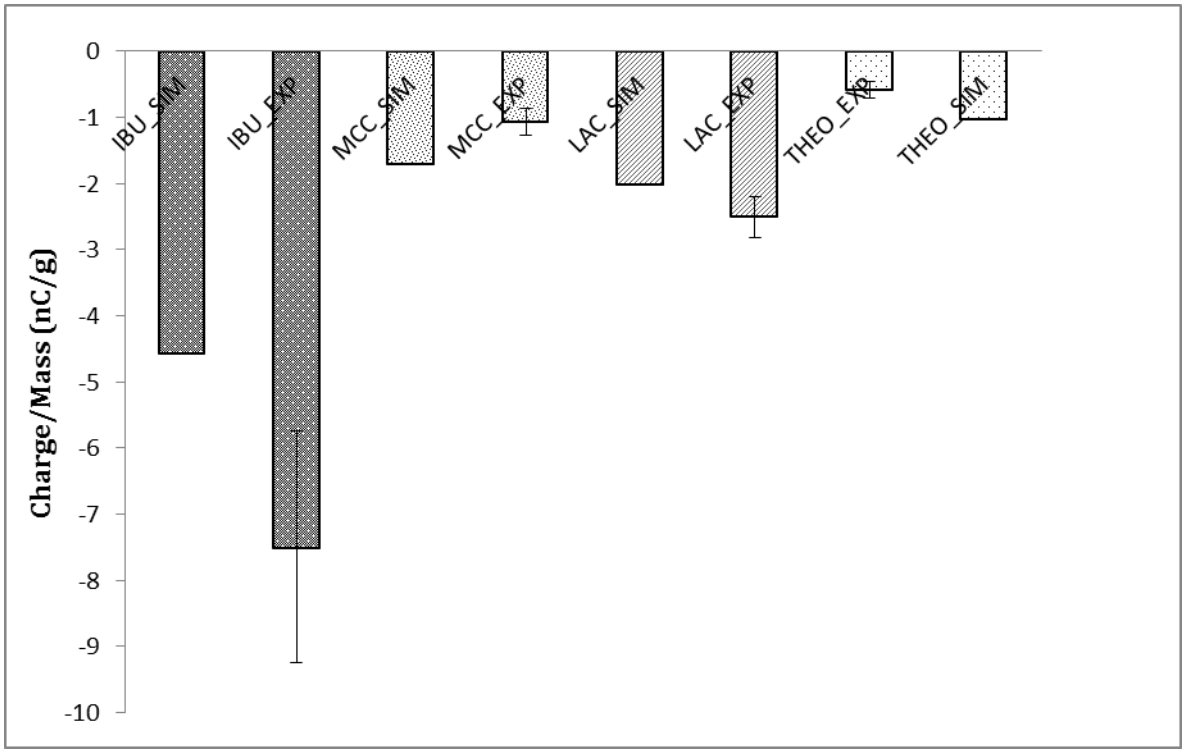

Fig. 11 Charge/Mass prediction by DEM-electrostatic model against PMMA surface

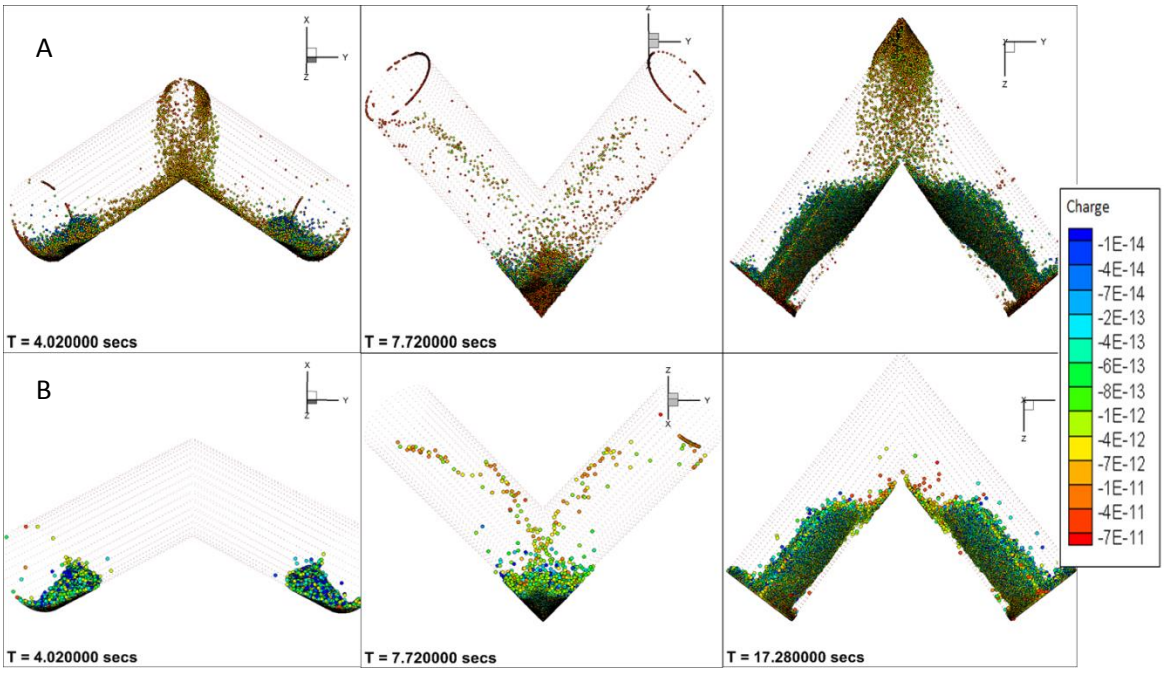

Figure 12: DEM snapshots of evolution of charge with time at 40rpm A) Ibuprofen B) MCC

Chapter 5

An experimental and numerical based study of tribocharging of pharmaceutical mixtures

Shivangi Naik[1], B.C. Hancock [2], Y. Abramov [2], Yu Weili [2], Bodhi Chaudhuri[1,3*]

[1]Department of Pharmaceutical Sciences,

University of Connecticut,

Storrs, CT, 06269, USA

[2] Pfizer Inc,

Groton CT 06340, USA

[3] Institute of Material Sciences,

University of Connecticut,

Storrs, CT, 06269, USA

*Corresponding Author

Email: bodhi.chaudhuri@uconn.edu

Abstract

Most pharmaceutical powders are dielectric materials that often accumulate charge during manufacturing process. In this study, triboelectrification of binary mixtures of drug and excipient has been investigated. Powder samples for charge measurement were mixed using a V- blender and dispensed directly into a Faraday cup. The mixtures at intermediate concentration exhibited significant charge mitigation. These unanticipated trends previously reported have been explored using process modeling approaches. Additionally, in silico computations have been performed to estimate the work function of the all contact materials. DEM simulations suggest that the drug particles (Ibuprofen) charge positively whereas the excipient (MCC) charges negatively when particle-particle collisions become substantial. This charge transfer is suspected to actually enhance electrostatic interaction between the drug and excipient and decrease the overall charge transfer between particle and wall.

Keywords: mixtures, charge mitigation, DEM

1. Introduction

Triboelectrification can be described as a charge transfer process which occurs during powder handling when sliding and frictional forces are involved. Since pharmaceutical powders are insulators, they are unable to dissipate these charges and therefore accumulate them during different manufacturing processes. Due to it's the inherent multi-variate nature, static electrification generated during powder handling operations is inadequately understood and difficult to predict. [1, 2] There are many factors that can affect tribocharging including particle size shape, surface roughness [3-5], impurities, contact material and relative humidity [6-9]. Another parameter that can affect tribocharging is the mixing ratio of two or more different materials. Such systems are inherently known to be complicated as it becomes more difficult to predict in which way the sign and magnitude of the charge can change [10]. To investigate this phenomenon, Engers *et al.* studied the tribocharging of pharmaceutical mixtures in a stainless steel bin blender. The effect of binary mixtures of drug and excipients on tribocharging was studied with the API pseudoephedrine hydrochloride, acetaminophen and excipients dicalcium phosphate dihydrate, microcrystalline cellulose, and lactose monohydrate. Binary mixtures were prepared at two levels, 10 and 90 %w/w, and blended at 12 rpm for 40 rotations in a stainless steel bin blender. For these binary systems, the charge of the mixtures was found to be lower that the individual components. Thus the surface charge density was found to be effectively dampened with respect to the values of the pure components. In case of acetaminophen, charge reversal was also observed along with charge mitigation. In a subsequent study the authors suggested that charge mitigation for dicalcium phosphate and MCC mixtures occurs due to relatively high dielectric constants of these excipients. The higher dielectric constant of these materials has been attributed to their greater moisture adsorption. The excipients with higher dielectric constants are expected to charge more electropositive than the API and hence enable charge mitigation. However, given the low concentration of the higher dielectric material, the resultant excess positive charge is somewhat unanticipated [11-12]. In a similar manner, Murtomaa and Laine experimentally studied the tribocharging of mixtures of lactose and glucose through a glass pipe. They observed that the pure excipients charged positively. However, a charge reversal was observed for the mixtures when the amount of lactose was between 20 and 40 % wt [13]. They suggested that the work function of glucose could be higher than that of lactose which could be responsible for suppression of charge at intermediate concentrations. Elajnaf et al. also investigated the interactions between micronized salbutamol sulphate and ipratropium bromide with lactose

mixtures in different mixing vessels. It was shown that the micronized API strongly altered the charging characteristics of lactose powder resulting in charge reversal and some mitigation effects [8]. It was not clearly explained why this phenomenon arises and was considered to be possibly due some dynamic charge transfer effects. It is evident from this short literature review that the current knowledge on triboelectric charging of mixtures is quite limited. Hence, in this study an effort was made to understand the effect of binary mixtures on triboelectrification in a V-blender and faraday cup assembly. Previous studies have employed process modeling approaches to examine and understand the triboelectrification of single component systems. For instance, Supuk et al.[14] performed DEM simulations for triboelectrification of particles in a container agitated at different frequencies. The triboelectrification model used in this investigation was based on an experimentally developed empirical equation linking the extent of charge transfer to contact time and saturation charge. The model included the effects of electrostatic forces on particle flow but was limited to a few numbers of particles. Pie *et al*. developed a 2D-DEM model for particle-wall electrification based on contact potential difference for dissimilar surfaces. Although their model did not include the effect of any electrostatic forces it lacked the empiricism from the previous models for triboelectrification [15]. In this study, the condenser model has been extended to incorporate both particle-particle and particle-wall charge transfer due to effect of collision. An in-house Discrete Element Model (DEM) [16-17] has been employed incorporating all relevant physical factors, charge transfer and the electrostatic forces.

2. Materials and Methods

2.1. Materials

The materials used in this study were Ibuprofen and theophylline purchased from BASF, lactose monohydrate from Foremost Farms and microcrystalline cellulose Avicel (PH-101) from Sigma Aldrich. All powders were dispensed from the bulk as received from the vendor. Mixing studies have been performed in PMMA and Aluminium V- blenders. The material were characterized for their particles size (Table 1) using the dry dispersion unit of Malvern Mastersizer. In silico computations for work function were done using MOPAC 2013 from structures imported with Avogadro 1.0.3. This method was adopted from the work done by Mazumder *et al*. who

computed the work function from band gap calculations i.e. the energy gap between HOMO and LUMO orbitals [18]. The calculated work functions are tabulated in Table 2.

2.2. Experimental Method

The individual powders are spread in thin layers onto the Aluminum foils in form of trays to condition them. These containers have been earthed to reduce the initial charges and equilibrated at 20% RH along with the blender for 24 hrs. The fill level for these experiments has been kept constant at 7 %. Following equilibration, the initial charge was measured in the Faraday cup. After transferring each powder from the cup into the blender; the blender was rotated at 13 rpm for 20 mins. Thereafter the powder is collected directly into the faraday cup and the charge is measured. Each experiment is repeated at least four times. The V-blender is then thoroughly cleaned first by dry air then by IPA. After cleaning with IPA, the blender is then purged with dry air to facilitate removal of any residual alcohol.

3. Discrete Element Method.

The charge transfer model used in this study is based on a condenser model that accounts for charging of powders whereas the DEM has been used to model flow of granular material. Owing to charge transfer between particles, one surface gains electrons and gets negatively charged whereas the other surface loses electrons and acquires a positive charge. As charge transfer continues, the actual potential between the particles begins to decline since the particles are getting charged. Therefore, the tendency of the particles to charge gradually declines and hence the ability of a negatively charged particle to accept more charge also diminishes. This effect needs to be considered for any tribocharging model as it ensures that particle charging is not a continuous process and can proceed to saturation. Hence in this model the effect of charged particles has been considered by determining the intensity of the local electric field of particles from super-position principles [19]. Considering these effects, the charge on a particle due to particle-particle charging can be then determined from Eq (1)

$$\Delta q = \frac{s\varepsilon_0}{Ze}\left[\varphi_i - \varphi_j - \left(E_{ij}.\frac{d_{ij}}{||d_{ij}||}\right)ze\right] \quad (1)$$

In Eq (1), Φ represents the work function of two dissimilar surfaces, in this case the drug and excipient, *z* is the cutoff distance for charge transfer and has been estimated to be around 250 nm. [20] E_{ij} represents the electric field at the point of impact of the two particles calculated from the linear interpolation of the individual electric fields of particles *i* and *j*. Using a similar approach, Eq (2) has been used for particle-wall charge transfer where the effect of induced potential of charged particle (E_{ii}) has been incorporated into the model.

$$\Delta q = \frac{s\varepsilon_0}{ze}\left[\varphi_i - \varphi_j - \left(E_{ii}.\frac{d_{ij}}{||d_{ij}||}\right)ze\right] \quad (2)$$

In DEM, the trajectories of all particles are estimated from the sum of forces acting on each particle that primarily include the collisional and gravitational forces. Besides these contact mechanical forces that determine the particle trajectories, the presence of charged particles in a system necessitates the incorporation of electrostatic forces into the DEM model. A screened electrostatic force described by Hogue *et al*. has been incorporated into this DEM model [21-22].

4. Results and Discussion

4.1. Experimental

In these mixing studies, the powders viz. API (Ibuprofen/Theophylline) and excipient have been added separately (unmixed) into the blender. After prescribed time i.e after 20 mins the powders have been discharged and the final charge has been measured in the faraday cup. This procedure was performed for all mixing ratios of the drug to excipient of viz. 3:1, 1:1, 1:3. Additionally, the individual powders have also been tribocharged under the similar conditions. It can be observed from Figure (1a-1d), that all intermediate combinations of Ibuprofen charged much lower than the individual powders. This implies that both powders are having a synergistic effect on overall charge behavior of the powders resulting in a parabolic charging behavior. Such an effect although demonstrated has not been well explained. For instance, these effects have been attributed to geometrical arrangements of particles within a mixture that affect the overall charge behavior [11-13]. If we observe the snapshots of MCC and IBU blends (Fig. 3); pure IBU charges a lot and also adheres significantly to the blender. Upon addition of MCC to IBU there is a decline in charging of ibuprofen as well as adhesion of drug. Thus charge mitigation can be due to a

decrease in particle wall contacts of pure API. A similar effect may be involved in IBU-lactose mixtures since these mixtures also illustrate plateau effects at intermediate concentrations. In case of these IBU-LAC mixtures some charge reversal is also observed which is quite evident at higher excipient concentration. It seems in drug-excipient mixtures, the extent of charge transfer between the drug and excipient becomes as important as charge transfer between the drug/excipient and the blender wall. Thus when IBU drug particles (Φ = 4.77 eV) interact with MCC (Φ = 5.11 eV) or with lactose (Φ = 5.18 eV), electrons will transfer from the drug particles to excipients. On the other hand interaction of the two powders with blender wall (Φ = 4.51 eV) will result in the powders charging negatively. As a result, the drug particles can also acquire a positive charge whereas the excipient particles will acquire a negative charge. Moreover, as charge mitigation was observed to be to similar extent against a Aluminium and PMMA surface suggests a substantial involvement of particle-particle charge transfer. In case of Ibuprofen, an additional study has been performed at 90 % w/w which did not show much charge mitigation effect. A similar plateau effect was observed in THEO-excipient (2a-2d) mixtures. However, charge mitigation was not as high as Ibuprofen since theophylline itself charges low.

4.2. Simulations

The DEM model described in section 3 takes into account charge transfer due to particle-wall as well as due to particle-particle contact. As DEM is an explicit numerical method the contact between particles or particle-wall can last for more than a few time steps. This can result in overflow of charge and hence can overcharge the system under consideration. To avoid charge transfer for all time steps in a given collision, the DEM algorithm was modified such that charge transfer occurs on when the contact force between particles or between particle and wall is highest. Thus in this model charge transfer occurs only due a difference in work function between two surfaces for the largest contact force. Moreover charge distribution is considered to be uniform on the surfaces of particles. Being insulators, charge relaxation or dissipation has not been considered in this study [15]. After incorporating the electrostatic forces into DEM algorithm, simulations were performed for mixtures in a V-blender. No tribocharging was considered during deposition of particles in the blender. Particles of two different sizes (Table 3) were deposited into the blender with the number of particles set according to the fill level of experiments (7 %). DEM simulation have been performed at a blender speed of 13 rpm for

particles of two different sizes where the larger particle size represents the excipient (1000 μm) and the smaller particle size the API (500 μm). Initially all particles have been considered to have no charge. As triboelectrification proceeds, charge transfer occurs in accordance to the algorithm described in section 3 for both particle-wall and particle-particle contacts. To quantify triboelectrification, the evolution of charge with time has been documented. The coordination number (CRN) i.e. the average number of contacts per particle (Eq.3) as has also been determined for a the mixtures

CRN = Sum (CRN * Number of particles with the given CRN)/ Total particles (3)

The DEM snapshots in Fig 4A-Fig.4D illustrate the tribocharging of DEM mixtures at different ratios. Color coding was done to visually track the evolution of particle charge. From the snapshots it can be observed qualitatively that for higher excipient concentrations, the charge of the system begins to decrease. As tribocharging occurs, the particles acquire a charge depending whether it's a particle-particle or a particle-wall collision. The positively charged particles are represented by different shades of blue whereas the color of negatively charged particles varies from yellow to dark red. Specifically, particles in the range of 7e-13 C to 7e-12 C are colored dark blue, 4e-13 to 1e-14 C are light blue, -1e-14 to -1e-12 are yellow to pale orange -3e-12 to -7e-11 C are red in color. The uncharged particles are white in color. At 90 %w/w of drug, the charge on the system is dominated by the drug particles (Fig 5A) and most of the drug particles charge in the range of -7e-13 to -4e-11. At 75% w/w of drug, there was a considerable decline in the charge with few particles now charging in the range of -7e-13 to -1e-11. Moreover, as the concentration was further decreased towards 25% w/w, the drug particles acquired a positive charge (Fig 5C, 5D) in range of 1e-13 to 7e-12. In these simulations, charge mitigation occurs primarily because of charge transfer between drug and excipient. As a result, the drug particles charge positively and excipients charge negatively due to particle-particle charge transfer. Hence, the charge on the particles depends upon the extent of particle-wall and particle-particle collisions. At lower excipient concentrations <10%w/w, the charge transfer between particles and wall dominate resulting in majority of particles acquiring a negative charge (red color). However as the concentration of excipient is increased > 30% w/w the particle-particle collisions exceed the particle wall collision by almost 4 times. Hence, the negative charge on the particle decreases and there are few particles which charge in the range of -4e-11 to -7e-11 (Fig. 6). This

charge transfer is suspected to actually reduce the overall charge on the particles and also decrease the adhesion of the particles to the blender.

As this study was focused on binary mixtures, an attempt has been made to investigate the effect of triboelectrification on mixing. Coordination number (CRN) has been determined to assess the extent of interaction between the drug and the excipient particles. CRN in this case has been defined as the number of particles of a given size attached to a sphere of another given size. Thus, if two dissimilar particles of a given size are in contact with each other and form an adhesive mixture one can count and identify them. In these simulations, since the drug and the excipient particles have opposite charges the electrostatic interaction between the particles are likely to increase. Hence, the coordination number Eq. (3) has been determined for each of the mixtures. As illustrated in Fig (7), the number average coordination number for a 90 % drug and 75% drug was quite low. In case of 90% drug mixture, the drug particles as well as excipient particles charge negatively. Hence, the coordination number for such a system is low due to repulsive forces between the particles. As the amount of excipient is increased, the average coordination number also increased suggesting a better interaction between the drug and excipient and a hence better mixing [23].

5. Conclusion

The underlying mechanism for charge mitigation of powder mixtures is still unknown although such behavior has been previously reported. The current investigation employed both experimental and process modeling approaches to explore triboelectrification of powder mixtures. In these mixture studies, charge obtained for powder mixtures was found to be more electropositive than the charge obtained for the individual components. It was hypothesized that this behavior is due to considerable charge transfer between drug and the excipient particle. This mechansim should be reinforced by employing dynamic charge measurements that can actually measure the charge of individual particles. In this study, an attempt was made to verify this hypothesis by employing a 3D DEM model incorporating charge transfer for powder mixing. DEM simulations do suggest that a decline in charge with increasing excipient concentrations. The drug particles were found to charge positively at higher excipient concentrations due to more particle-particle collisions. Such interactions could also be involved in DPI formulations were charge reversal has been reported. Consequently, formulations may be optimized to produce a

larger difference in charge magnitude / polarity to encourage fine particles to adhere to larger carrier particles and reduce segregation during mixing.

Nomenclature

Φ	Work Function
z	Cut off distance for charge transfer
ε_o	permittivity of the free space
E	Electric field
s	Contact area
e	Charge of an electron
q	Charge of particle
d	Position vector

Abbreviations

API	Active product ingredient
DPI	Dry Powder Inhalers
CRN	Coordination number
IBU	Ibuprofen
LAC	Lactose Monohydrate
MCC	Microcrystalline cellulose
THEO	Theophylline

6. References

1. Carter P.A., Rowley G., Fletcher E.J., Hill E.A., 1992. An experimental investigation of triboelectrification in cohesive and non-cohesive pharmaceutical powders. Drug Dev.Ind.Pharm.18, 1505–1526.

2. Rowley G. 2001. Quantifying electrostatic interactions in pharmaceutical solid systems.Int.J.Pharm.227, 47–55.

3. Carter P.A., Cassidy O.E., Rowley G., Merrifield D.R., 1998. Triboelectrification of fractionated crystalline and spray-dried lactose.Pharm.Pharmacol.Commun.4, 111–115.

4. Kwek J.W., Heng D., Lee S.H., Ng W.K., Chan H.K., Adi S., Heng J., Tan R.B.H., 2013. High speed imaging with electrostatic charge monitoring to track powder de-agglomeration upon impact.J.AerosolSci.65,77–87

5. Stefan Karner, Eva Maria Littringer, Nora Anne Urbanetz .Triboelectric: The influence of particle surface roughness and shape on charge acquisition during aerosolization and the DPI performance. Powder Technology 262 (2014) 22–29

6. Eilbeck J., Rowley G., Carter P.A., Fletcher E.J (1999). The effect of materials of construction of pharmaceutical processing equipment and drug delivery devices on the triboelectrification of size fractionated lactose. Pharmacy and Pharmacology Communications, 5, 429–433

7. Eilbeck J., Rowley G., Carter P.A., Fletcher E.J (2000). Effect of contamination of pharmaceutical equipment on powder triboelectrification. International Journal of Pharmaceutics, 195, 7–11.

8. Elajnaf A., Carter P., Rowley G. (2006). Electrostatic characterization of inhaled powders: effect of contact surface and relative humidity. European Journal of Pharmaceutical Sciences, 29, 375–384.

9. Rowley, Mackin L.A. (2003).The effect of moisture sorption on electrostatic charging of selected pharmaceutical excipient powders. Powder Technology, 135&136, 50–58.

10. S. Karner, N. Anne Urbanetz,. The impact of electrostatic charge in pharmaceutical powders with specific focus on inhalation-powders, J. Aerosol Sci. 42 (2011) 428–445.

11. Engers D.A., Fricke M.N., Storey R.P., Newman A.W., Morris K.R. (2006). Triboelectrification of pharmaceutical relevant powders during low-shear tumble blending. Journal of Electrostatics, 64, 826–835

12. Engers D.A., Fricke M.N., Storey R.P., Newman A.W., Morris K.R. (2007).Triboelectric charging and dielectric properties of pharmaceutically mixtures. Journal of Electrostatics, 65, 571–581.

13. Murtomaa M., Laine E. (2001). Effect of surface coverage of a glass pipe by small particles on the triboelectrification of glucose powder. Journal of Electrostatics, 54, 311–320.

14. Šupuk E., Seiler C., Ghadiri, M., 2009. Analysis of a simple test device for triboelectric charging of bulk powders. Part.Part.Syst.Charact.26, 7–16.

15. Pei C., Wu C.-Y., England D., Byard S., Berchtold H., Adams M., 2013. Numerical analysis of contact electrification using DEM–CFD. Powder Technol.248, 34–43.

16. Walton O., Braun R., 1986. Viscosity, granular-temperature and stress calculations for shearing assemblies of inelastic, frictional disks.J.Rheol.30, 949–980.

17. Walton, O.R. 1993.Numerical simulation of inclined chute flows of monodisperse, inelastic, frictionalspheres.Mech.Mater.16,239–247

18. Trigwell S., Grable N., Yurteri C.U., Sharma R., Mazumder M.K., 2003. Effect of surface properties on the tribocharging characteristics of the polymer powder as applied to industrial processes, IEEE Transactions in Industry Applications 39, 79–86.

19. Laurentie J.C., Traoré P., Dascalescu L., 2013. Discrete element modeling of triboelectric charging of insulating materials in vibrated granular beds. Journal of Electrostatics 71, 951-957

20. Lowell J., Rose-Innes A.C., 1980. Contact electrification. Advances in Physics 29, 947–1023.

21. Hogue M.D., Calle C.I., Curry D.R., Weitzman, P.S. (2008). Calculating the trajectories of triboelectrically charged particles using Discrete Element Modeling (DEM). Journal of Electrostatics 66, 32–38

22. Hogue M.D., Calle C.I., Curry D.R., Weitzman, P.S. (2009). Discrete element modeling of triboelectrically charged particles: Revised Experiments. Journal of Electrostatics, 67(4), 691-694

23. Staniforth J.N., Rees J.E., 1981. Powder mixing by triboelectrification. Powder Technol.30, 255–256.

Tables

Table 1: Particle size distribution of powders

Material	d_{10} (μm)	d_{50} (μm)	d_{90} (μm)
Ibuprofen	5.07	17.02	53.12
Theophylline	14.23	63.12	200.13
MCC	15.10	51.47	130.21
Lactose Monohydrate	22.18	52.34	140.16

Table 2: Work function of powders and contact surfaces from molecular orbital calculation (MOPAC)

Material	SEMI-EMPIRICAL CALCULATION (eV)
Aluminium	4.33
PMMA	4.51
Ibuprofen	4.77
Theophylline	4.90
MCC	5.11
Lactose monohydrate	5.18

Table 3: DEM simulation parameters for binary mixtures in PMMA blender

DEM Parameters	Values			
DRUG (500 µm): EXC (1000 µm)	(4:1)	(3:1)	(1:1)	(1:3)
Coefficient of restitution: Particle/particle	0.4			
Coefficient of restitution: Particle/wall	0.6			
Friction coefficient: particle/particle	0.5			
Friction coefficient: particle/wall	0.5			
Work function: Surface	4.51 eV			
Work function: DRUG (IBU)	4.77 eV			
Work function: EXC (MCC)	5.11 eV			

Figures

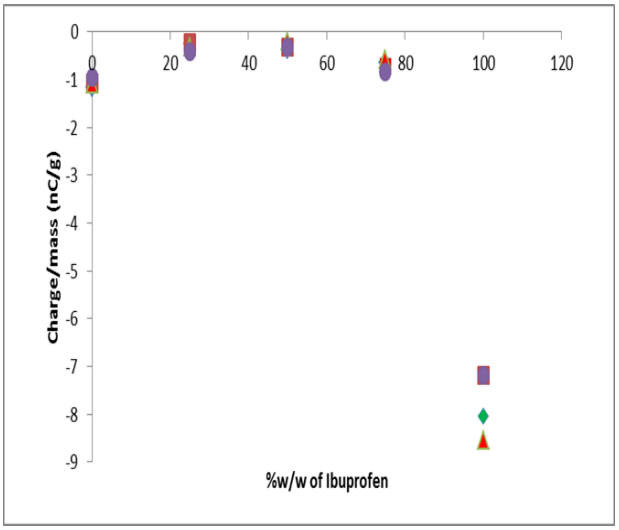

Figure 1a: Charge/mass of Ibuprofen-MCC mixtures against Al surface, (n=4)

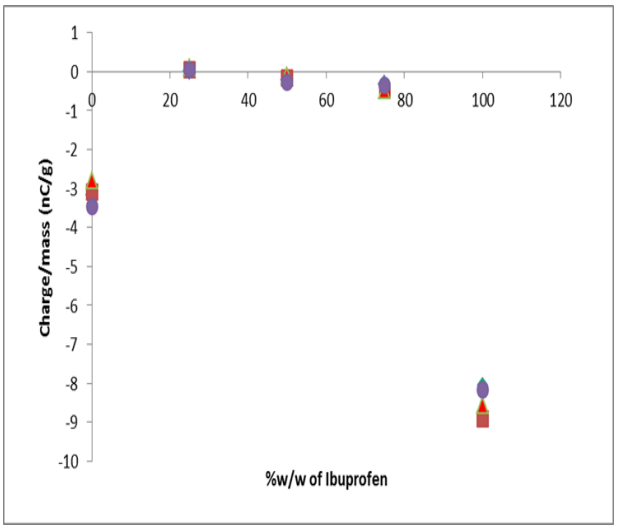

Figure 1b: Charge/mass of Ibuprofen-LAC mixtures against Al surface, (n=4)

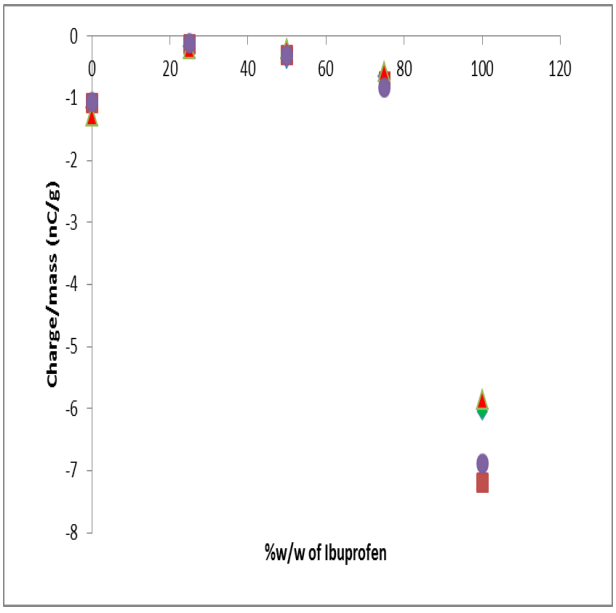

Figure 1c: Charge/mass of Ibuprofen-MCC mixtures against PMMA surface, (n=4)

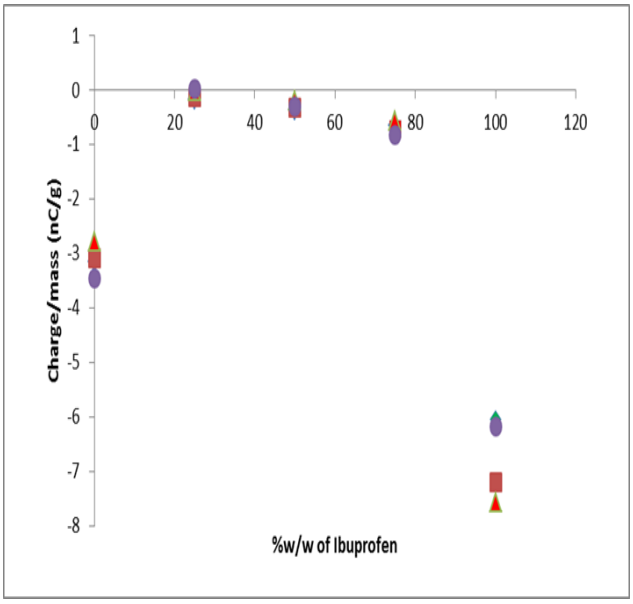

Figure 1d: Charge/mass of Ibuprofen-LAC mixtures against PMMA surface, (n=4)

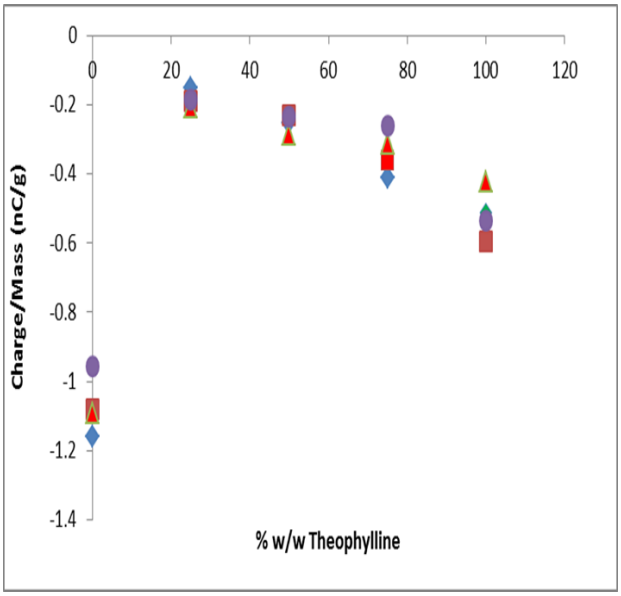

Figure 2a: Charge/mass of Theophylline-MCC mixtures against Al surface, (n=4)

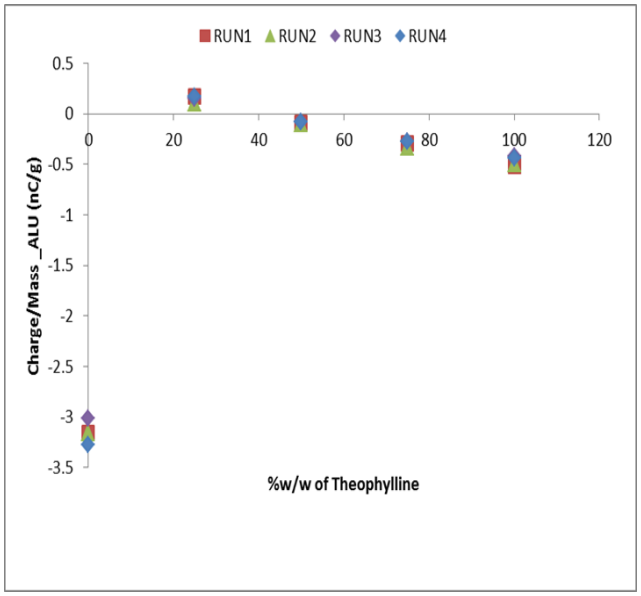

Figure 2b: Charge/mass of Theophylline-LAC mixtures against Al surface, (n=4)

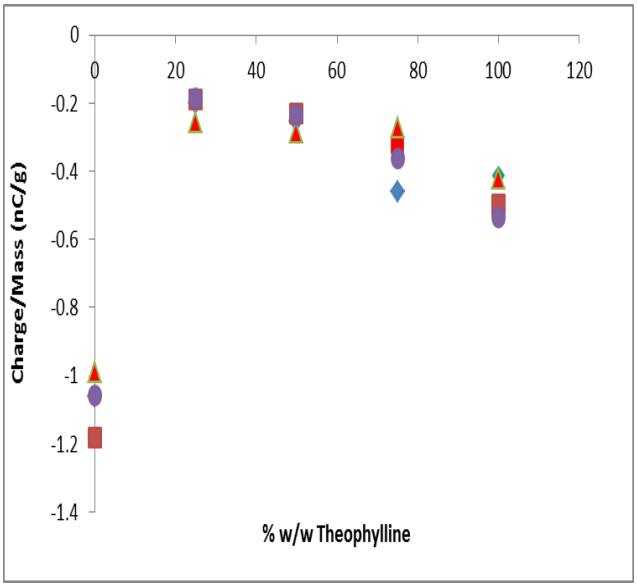

Figure 2c: Charge/mass of Theophylline-MCC mixtures against PMMA surface, (n=4)

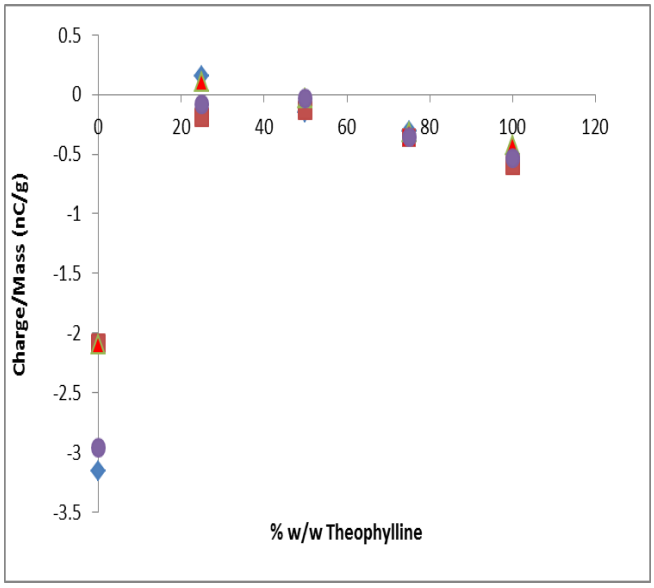

Figure 2d: Charge/mass of Theophylline-LAC mixtures against PMMA surface, (n=4)

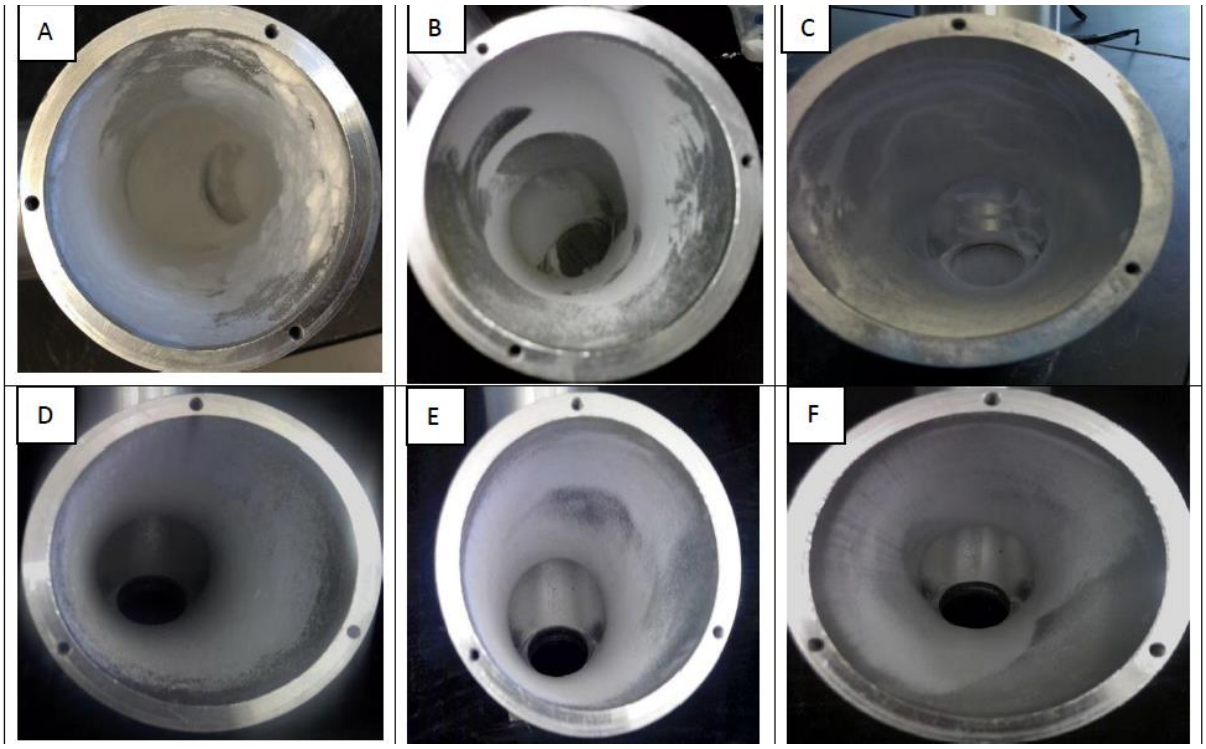

Figure 3: Snapshots of mixtures after blending (A) Pure IBU (B) 75% IBU (C) 50% IBU (D)PURE THEO (E) 75% THEO (F) 50% THEO

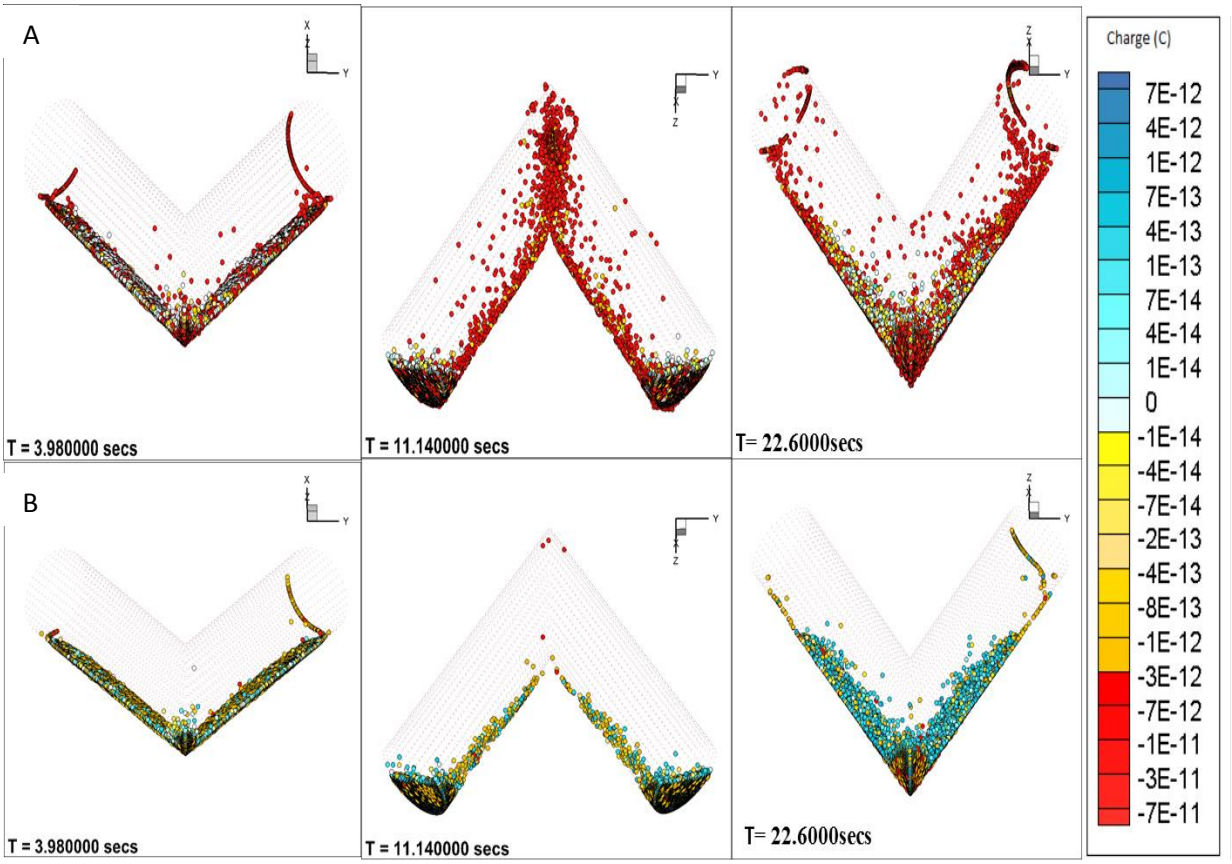

Figure 4: DEM snapshots of evolution of charge at different drug to excipient ratios A) 90%w/w of drug B) 75%w/w of drug

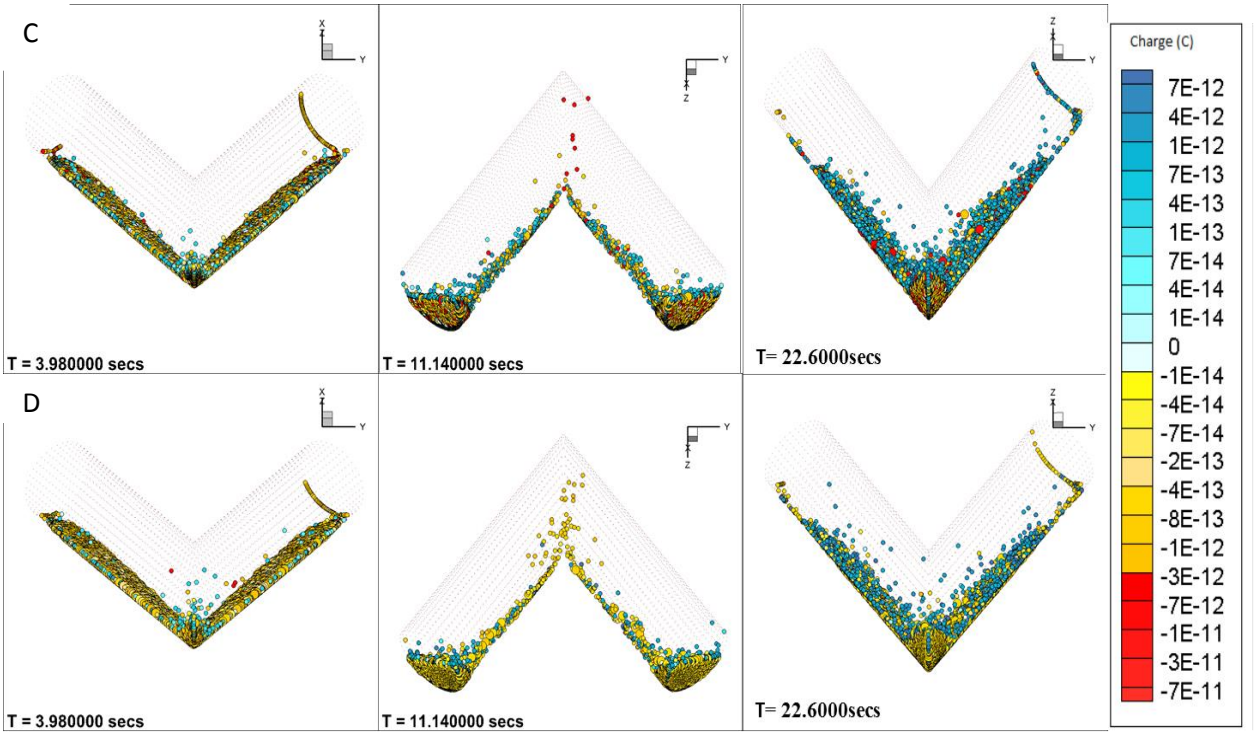

Figure 4: DEM snapshots of evolution of charge at different drug to excipient ratios C) 50%w/w of drug D) 25%w/w of drug

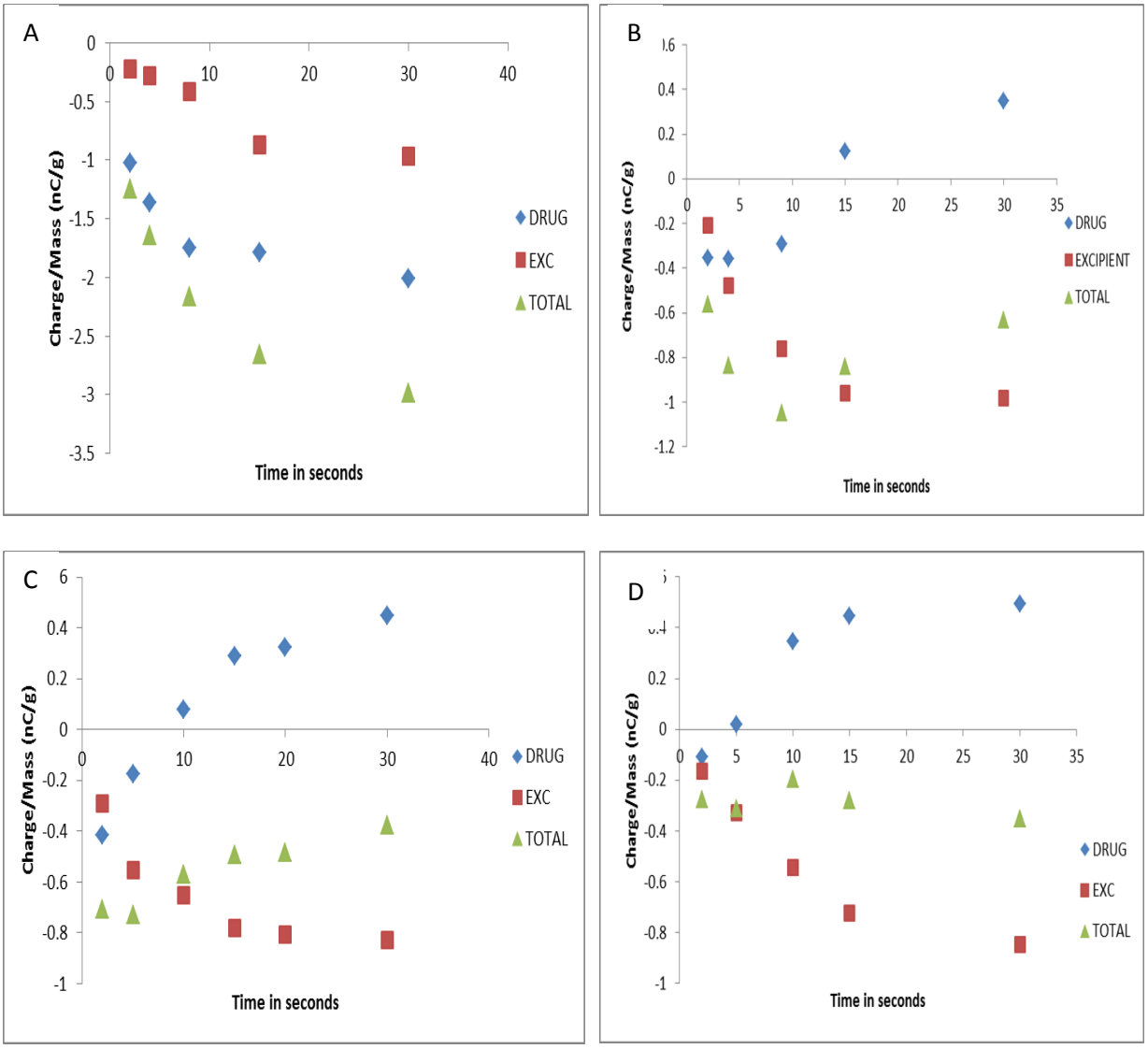

Figure 5: Evolution of charge for binary mixtures A) 90% w/w/ B) 75% w/w C) 50% w/w D) 25% w/w

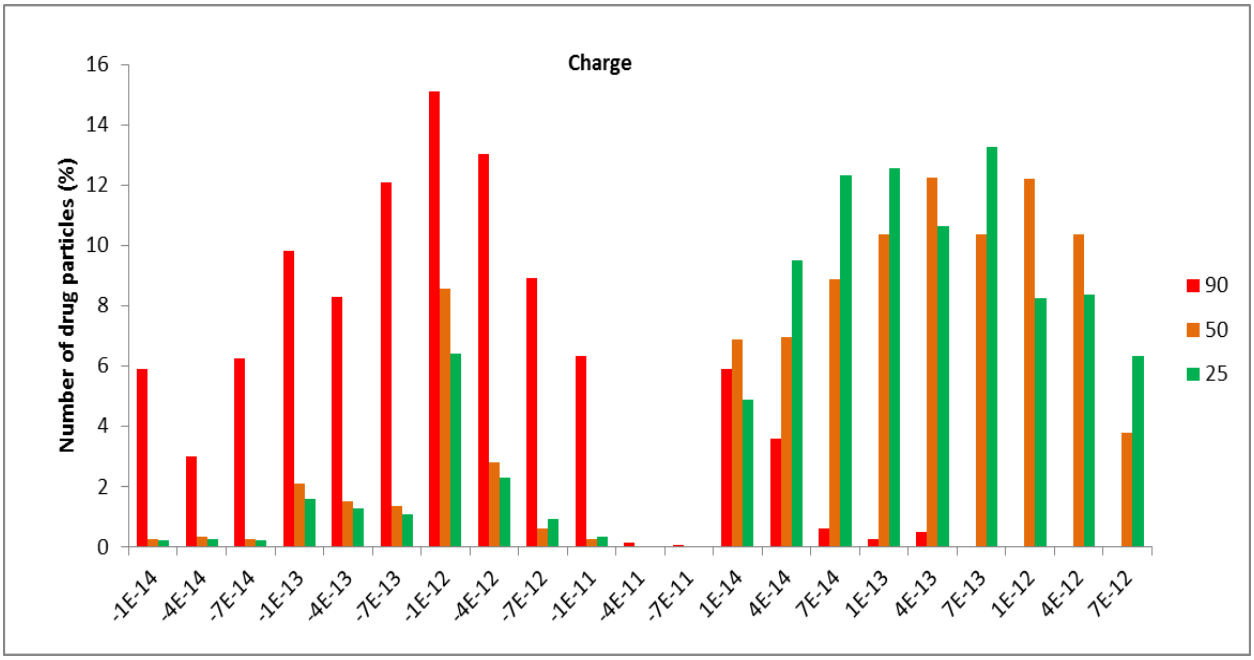

Figure 6: charge on the drug particles for a given drug: excipient ratio

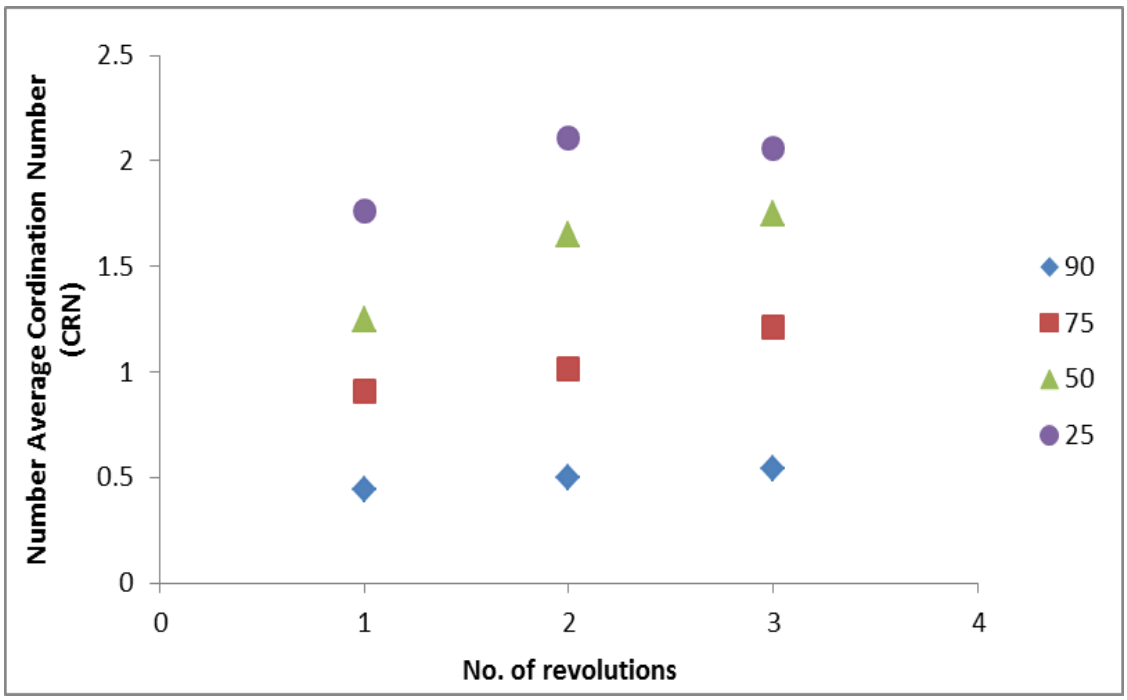

Figure 7: CRN for different binary mixtures

Chapter 6

Quantifying dry milling in pharmaceutical processing: A review on experimental and modeling approaches

Shivangi Naik[1], Bodhisattwa Chaudhuri[1,2*]

[1]Department of Pharmaceutical Sciences,
University of Connecticut,
Storrs, CT, 06269, USA.
[2] Institute of Material Sciences,
University of Connecticut,
Storrs, CT, 06269, USA.

*Corresponding Author,

Email: bodhi.chaudhuri@uconn.edu

Abstract:

Particle size reduction by mechanical means is an important unit operation in the pharmaceutical industry, used to improve flow, solubility and in amorphization of drugs. It is usually achieved by fracturing of particles under the action of applied energy. Despite being pervasive in pharmaceutical field it is one of the least understood processes owing to the complexity of material and process variables involved during milling. To comprehend the process efforts should be focused on techniques that measure the particle size as well as the control the process. With the ongoing initiative of FDA to encourage design in quality the review is focused on some process analytical tools to characterize particle size distribution as well process modeling tools to simulate particle size reduction. Additionally, an overview of some fundamental aspects relating to milling is provided. To this end, the review is limited, mainly concentrating on some of experimental and modeling approaches used to quantify and understand the physics behind the process of dry milling.

KeyWords*:* Milling, Particle Size, Fracture, PAT, Process modeling,

1.Introduction

Particle size reduction or milling is an imperative unit operation employed in different manufacturing fields such as ceramics, mining, food, agriculture, paper and pharmaceutical industry. Various terms such as crushing, disintegration, dispersion, grinding and pulverization have been used synonymously with milling. [1-2] Briefly, the process is related to the internal structure of the material and consists of two steps, first opening up of any small fissures (or fractures) which are already present, and secondly forming new surfaces through fragmentation with the application of any external forces.[3-4] In pharmaceutical solid dosage form manufacturing, milling process (Fig. 1) occurs following the API synthesis/filtration and following granulation process.[5-6] The desired particle size distribution required for any of these operations can be achieved by dry or wet milling. The choice of dry or wet milling depends on the end use of the product. One of the most important applications of particle size reduction is improving the solubility of Biopharmaceutics Classification System (BCS) II drugs. This is because a decrease in particle size from a few microns to nano-size range can significantly increase the rate and extent of solubility of poorly soluble drugs. In dry milling, the focus of this article, the selection of the mill (as shown in Table 1) depends upon the extent of fineness required and the hardness of the materials under consideration. Since a much greater increase in surface results from crushing fines as opposed to coarse material, fine grinding requires more power. Moreover, the limit of fineness may be restricted in the region of 100 microns due to material caking unless flow aids such as talc are used. Wet grinding is more appropriate when further reduction in size is required. Besides improving solubility, dry milling is often exploited during tablet and capsule manufacturing to improve powder flow, compressibility, tablet hardness, and uniformity of content.[2,7-10] In all these processes, milling essentially involves size reduction and size separation combined together to obtain a desired particle size distribution to avoid any over-processing of the product. Consequently, to comprehend the process, efforts should be directed towards techniques that measure the particle size as well as control the process. In this context, aspects of milling are reviewed briefly based on process analytical technology and recent modeling approaches. In the current review, the authors do not intend to discuss elaborately any core fundamentals of milling process and are focused on existing experimental and modeling methodologies used to quantify and understand the process of dry milling.

2.Background

Particle size distribution (PSD) and the effect of machine parameters are vital attributes that need to be quantified to achieve a quality product during milling. Depending on the nature and scope of the experimental investigation, the techniques employed to measure PSD often diverge. With respect to particle size measurement, the approaches employed can be partitioned into two chief categories: stream-scanning and field-scanning techniques. In stream scanning particles are examined one at a time and then classified into corresponding size intervals. In field scanning, the PSD is inferred from the interaction between the assembly and measurement probe i.e. PSD is derived from integral field response. These field-scanning methods are more robust, faster and hence better suited for Process analytical technology (PAT) applications.[11]

In pharmaceutical industry, laser diffraction (LD) and sieve analysis have been frequently employed to measure particle size with sieving being common for coarser materials and laser diffraction common for finer materials. Particle size analysis by sieving involves physically subdividing a large quantity of material into different classes. The process largely comprises of mechanical vibration of a sample through a series of successively smaller sieve apertures. The portion retained on each sieve is then weighed and a particle size based on mass distribution is obtained. The most important advantage of sieve analysis is that it is relatively simple and is the least expensive of all methods. However this method is not suitable for cohesive powders as they can easily clog the sieve apertures. In some cases wet sieving may be a beneficial option when the cohesion between the materials is very high. A combination of wet and dry sieving becomes a choice for very wide particle size distribution i.e. with fine and coarse powder. Some of the drawbacks of this method include standardization of the sieving procedure that necessitates use of large amount of sample and is often time consuming. For the same purpose LD has found to much more convenient in measuring PSD owing to relatively rapid particle size measurement and a smaller sample size. [2, 12,13]

In LD, a series of detectors positioned at different angles measure the scattering pattern of a monochromatic laser light by an assembly of particles. The spatial distribution of scattered light intensities is found to be contingent on the particle size, shape and optical properties. Depending on the ratio of particle size to wavelength of incident light, the scattering pattern can either follow Fraunhofer approximation or Mie's theory. The Fraunhofer theory considers the particles

as two dimensional opaque disks and hence measures the interaction of light at contour of particle. It takes into account scattering only in the near forward direction i.e. when the scattering angle is very small. As larger particles scatter light of low intensity and at larger angles, Fraunhofer theory is suitable for very opaque particles greater than 50 µm. All smaller particles can be measured using Mie's theory where it then becomes necessary to know the optical properties i.e the refractive index of materials. These optical properties can be estimated from an iterative approach based upon the goodness of fit between the modeled data and the actual data collected for the sample. In these methods, the scattered intensities are deconvoluted to a volume based particle size distribution using a system of linear equations. The most significant drawback of this method is that it always assumes the particles to be spherical. For micronized particles, deviation from sphericity is negligible and the shape factor should be taken into account in order to obtain an accurate measurement. [12,14]

The primary disadvantage of these off line methods is that they are intrusive i.e. they determine the outcome of a milling operation by stopping at preset times and in case of continuous processing operations may also resume, at risk, to the subsequent process.[15] Hence there has been an amplified concern to incorporate particle size analysis into process monitoring. The ongoing PAT implementation emphasizes on the need to understand and control the manufacturing process and therefore facilitates "Quality by Design", or QbD. Building quality within the product entails the determination of product and process attributes along with measuring relevant properties of raw and in-processed materials. The efforts to move towards such a risk based and science focused approach for pharmaceutical processing are now recognized by the development of process analyzers such as NIR, Raman spectroscopy and FBRM. [16-18] Besides various in/on line process analyzers; process modeling tools such as Discrete Element Method (DEM), Computational fluid dynamics (CFD) have gained momentum since they offer a fundamental approach to improve process understanding, efficiency, scale-up and equipment design. Moreover, using simulations, process effects can be much easily anticipated thereby reducing any effortful or expensive experiments. Consequently, these modeling tools also facilitate process economics by trimming down any developmental and manufacturing costs as well as any production delays. Thus these PAT techniques serve as predictive and diagnostic tools for a manufacturing process thereby providing valuable

information regarding the process methodology. However, each of these techniques has their own inadequacies in terms of computational or operational speed, ease and accuracy. [19-21]

3. Characterization of milling performance

3.1 Non-intrusive methods

The eventual goal of PAT is to initiate and develop a progressive fundamental understanding of manufacturing processes. During the last decade non-intrusive PAT tools such as focused beam reflectance measurement (FBRM), Dynamic Image Analysis (DIV), spatial filtering technique (SFT) have been introduced to measure PSD. As these are non-intrusive techniques, they have the advantage of not interfering with the process in progress and allow real-time process monitoring and control. Moreover these techniques also eliminate any sample preparation required for conventional off-line methods. However, in these systems often a side stream of particles needs to be isolated since the traditional process streams are highly concentrated with flow rates that can cause fouling of the detectors. [13,16]

3.1.1.Dynamic image analysis (DIA)

Automated image analysis instrumentations are capable of capturing two dimensional images of particles when presented in front of the detector. In a DIA system, dry powder particles are first placed on a vibratory chute and then accelerated to high speeds by a Venturi tube located in the sample dispersion line. As the particles pass through a detecting zone, the xenon flash light illuminates the particles and the camera acquires images of the fast moving particles. This image analysis system is capable of measuring particle sizes in the range from 1 to 3000 µm. Using DIA Nalluri *et al.* [23] have compared different modes i.e. on-line, in-line and at-line for monitoring size reduction in a conical mill. The results from the on-line, in-line and the at-line measurement modes showed similar size distributions for the various materials studied with some differences that were mainly attributed to sampling and dispersion techniques. In addition to PSD, time evolving size and shape analysis (TESSA) was applied for determining changes in particle shape as well as to detect when the process reaches or falls out of equilibrium. For this purpose the mill was run continuously for 10 mins and data was collected for every 20 secs. To determine equilibrium of process the changes in standard deviations over time in terms of size and shape were monitored by a sigma box in a two-dimensional graph. The process was found to

arrive at the equilibrium within 4 min and was found to fall out of equilibrium towards the end. Thus the evolution of particle size and shape determined by TESSA was found to be helpful in monitoring the process changes in the conical mil. A main advantage of this sensor system is that it can provide digital images of the particles and hence allows a quick assessment of shape information. The TESSA concept can be particularly beneficial in collecting information regarding equilibrium milling conditions for a specific material and thus achieve uniform particle characteristics. A feedback control system for the conical mill can also be set-up with a DIA sensor that would enable enhanced understanding and control of the pharmaceutical dry milling process. [22, 23]

3.1.2.Focussed Beam Reflectance Microscopy(FBRM)

The FBRM system uses a rotating laser optics design that can determine particle chord lengths by detecting reflected light from the particle. The FBRM instrument (Fig 2) is composed of three parts: a measurement probe, an electronic measurement unit, and a computer for acquiring and analyzing data. Briefly in an FBRM measurement a laser beam is projected through a sapphire window onto a stream of particles. The optics is then rotated so that the beam traces out a circular path. Until the beam reaches the opposite end of particle, light gets reflected and propagated as the particle passes near the window. The chord length of the particle is then obtained by multiplying the speed of the laser focused beam with duration of reflection. The chord length is measured several times over few seconds and then grouped into size intervals providing a probability density function. The chord length distribution (CLD) obtained from FBRM measurement depend on both the PSD and the particle shape. The probability of the measured chord length is independent of the particle orientation in case of spherical particles. However the probability density function of irregular particles will be influenced by both shape and size. Different sample particle size distributions, dispersion concentrations and flow rates can be accommodated by adjusting the scan speed from 2 to 8 m/s. For measuring the chord length the FBRM probe is typically immersed in a flowing suspension of particles and thus it is necessary for particles to flow over the sapphire window. Consequently the placement of the FBRM probe becomes imperative as particles positioned a few hundred micrometers away from probe will be less likely measured. [13,24]

Li *et al*.[25] compared FBRM technique with three different sizing techniques, including laser diffraction ultrasonic attenuation, and image analysis for glass beads and silica particles. They concluded that FBRM measurements can under predict particle size in case of transparent particles as the signal amplitude does not possess a sufficient pulse strength. For non-spherical particles CLD measurement by FBRM was found to be complex as the measured chord length distribution tends to be misleading in terms of the actual particle size and hence a calibration specific to the concerned system of relevance is required. With respect to calibration, Heath *et al.* [26] concluded that a mean of square-weighted chord lengths, for objects in the size range of 50–400 μm, compared well with the actual mean diameter obtained using traditional sizing techniques. Length and cube weightings were found to be appropriate for particles smaller (< 50 μm) and larger (> 400 μm) respectively. Ai Tee Tok *et al*. [27] used a similar approach to monitor particle size distribution during fluidized bed granulation. By inserting FBRM and near-infra red spectroscopy (NIR) probes into the fluidized bed real-time measurements could be performed. Additionally, by attaching piezoelectric sensors on the external wall of the fluidized bed acoustic emission measurements (AE) were performed. Owing to higher sensitivity, FBRM probe was found to be more resistant to fouling in comparison to an NIR probe. Moreover, any fouling problem could be easily diminished by raising the focal point of the measurement from the normal setting of +20 to +100 μm. FBRM was also found to be more robust than AE since the latter is more sensitive to fluidizing air flows and external intrusions. Thus from an operational point, FBRM was found to effective in monitoring particle size in a pilot-scale fluidized bed granulator. In an analogous approach FBRM has also been employed for particle size analysis in a Continuous Granulation–Drying–Milling process. A self-cleaning spinning disc assembly was employed in this study to minimize small particles adhering to the probe window. The study also revealed a significant relationship ($p<0.0001$) between D_{20}, D_{50}, and D_{80} chord length and sieve particle size. The authors suggested that by establishing a meaningful relationship with sieve data, a real-time feedback control loops within the continuous process can be created. This PAT control loop could assist the generation of uniform and optimized cycle for different manufacturing processes or runs thereby reducing the effect of variability due to changes in raw material or other factors. [24]

3.1.3.Spatial filtering velocimetry(SFV)

SFV technique involves determining the velocity of an object by observing it through a spatial filter in front of a receiver. In SFV measurements, particles pass through a laser beam and cast shadows onto a linear array of optical fibers. As the particles pass through the beam, a secondary pulse is generated by a single optical fiber and from the time of the pulse and the velocity of the moving particles, the chord length can be calculated. The measurement cell (Fig.3) of the SFV probe is constructed from stainless steel and has sapphire windows. This probe system is suitable for size measurements in the range 50–6000 μm with an uncertainty of 1% and for velocity measurements between 0.01 m/s and 50 m/s with a standard deviation of 0.5%. The probe can be installed directly into the process line to provide real-time analysis. The optical windows can be clear by passing compressed air or other gases. If the particle loading is too high an in-line disperser can also be used to dilute or disperse the sample flow. SFV has been recommended for particle size monitoring in mixing and coating, fluidized bed processes, dry granulation, high shear wet granulation, and spray-drying. [13],[28-29]. Närvänen et al. compared three different particle size measurement techniques: sieve analysis, laser diffraction and SFV and found the latter to be the most consistent among the three studied techniques. The in-line SFV probe provided information every 10 s about the process that allowed better understanding of different process variables, which was not possible using the off-line LD data. Another study by the same group showed that the in-line particle size data measured via SFV could be used to monitor different process phenomena and process failure.

Spatial filter velocimetry (SFV) is similar to FBRM i.e. both the techniques provide a chord length distribution but FBRM uses the backscattered light and converts it to size measurement, while SFV relies on the particle shadow. Moreover the placement of the FBRM probe is of extreme importance since it is necessary for particles to flow over the sapphire window. [13,28,30-31]

4. Modeling approaches for milling processes

In a grinding process, machine and material parameters interact in a complex way thereby making it difficult to comprehend the entire process. Hence extensive tests are often required to operate any new milling equipment in order to establish correlations between operation parameters and product properties. Hence the consideration of different components contributing

to comminution is necessary for a profound understanding of the whole process. Besides, this understanding has to be quantified in order to develop a predictive model.[32] Besides monitoring particle size during milling a considerable effort has been made to model the particle breakdown in c systems. Different approaches (table 2) based on energy distribution, fracture mechanics, population balance modeling or a combination of these methods have been developed for modelling size reduction. In considering energy utilization, size reduction is a very inefficient process, only 0.1- 2.0 per cent of the energy supplied to the machine appears as increased surface energy in the solids. Such poor energy utilization primarily occurs when the applied forces do not exceed the elastic limit of the particle. As a result it gets reversibly deformed or stressed and when the load is removed, the particle returns to its original condition without doing useful work. Consequently, energy appears as heat and no size reduction is affected. Hence initial efforts were aimed at elucidating energy consumption in mill that led to the development of empirical rules for size reduction to quantify particle size reduction [2, 33-35]. Application of principles of fracture mechanics to particle size reduction resulted in a more fundamental approach towards modeling comminution and led to a development of models based on material and machine parameters. In essence in these models, an energy balance is applied to the process of crack extension by equating the loss of energy from the strain field within the particle to the increase in surface energy when the crack propagates. [36] For the purpose of PAT applications a dynamic mechanistic model is an excellent tool for mapping process knowledge. The mechanistic models that have been increasingly applied to pharmaceutical production processes are Computational fluid dynamics (CFD) Population balance models (PBM), Discrete Element Method (DEM). Computational fluid dynamics is usually an Eulerian method and can be extremely accurate for systems consisting of fluids and hence restricted for continuum material. Population balance models (PBM) describe the change in number and properties for given system with time. A comprehensive model for size reduction based on PBM was proposed by Broadbent and Callcott. This model is based on the concept of selection and breakage functions where selection function represents the probability of breakage and the breakage function represents the size distribution of broken particles. Discrete element method (DEM) on the other hand is a Lagrangian model providing a high level of detail of the process by describing the dynamic behavior of the particles. Fundamentally, DEM solves Newton's equations of motion to resolve particle motion and uses contact laws to resolve inter-particle contact forces. It explicitly considers inter-particle

and particle-boundary interactions, providing an effective tool to model fragmentation. Moreover, it can be used to calculate many particle-scale quantities of interest such as local concentrations; particle stress as well as observe some particle-level phenomena. These mechanistic models are particularly beneficial as predictions can readily be made from simulations that would be difficult, and possibly expensive, to obtain experimentally. [21, 37]

4.1.Energy based Based Models

Damage'' or ''breakage'' is a general term referring to the reduction in mass of a mother particle due to external forces. The method of application of these external forces affects the breakage pattern of particles resulting in impact, shear or attrition. Stress conditions generated during milling depend upon the operational parameters and vary with the number of loading points, stressing rate and intensity. [32] As stresses created due to attrition or impact can be coupled to energy consumption, a quantitative relation can be established between size reduction and energy consumption. As mentioned earlier milling is an energy inefficient process and initial attempts to quantify milling have led to the development of empirical based energy models: Rittinger's model, Kick's model, and Bond's model. Rittinger's model is based on the assumption that all of the input energy is absorbed by the fractured particles and the energy required for size reduction is proportional to surface area generated per unit mass of the particle. Kick's model is based on the concept that fracture occurs when elastic limit is exceeded and the strain energy needed to fracture the particle is proportional to its volume. Thus the Kick's model neglects the energy absorbed by fractured particles whereas the Rittinger's model ignores energy absorbed in the elastic deformation. Bond's model is a compromise between Rittinger's and Kick's models [38-40]

Based on these energy models, the comminution behavior of lactose monohydrate in a single ball mill under different frequency and loading rates has been investigated.[41] The results suggest that Rittinger's model best describes the milling behavior for low mill loadings at high frequencies, whereas the data for high mill loading at low frequencies are well suited for Kick's model. Also from the initial size reduction rate it was observed that attrition and/or chipping was found to be the dominant mechanism for milling at low frequencies whereas fragmentation by impact seemed to be accountable for size reduction at high frequencies. Although these energy based models are phenomenological, they do not deliberate on material properties or fracture mechanics which are the fundamental factors involved in comminution. Secondly their

predictiveness is limited by the inherent complexity of milling process and hence the results from this study cannot be extended to other mills and are applicable only under limited operating conditions. [42.]

4.2.Fracture Mechanics based Models

The inherent inadequacies of the grinding laws led to the notion that milling is considered to be an art that can be learned from years of experience. From the perspective of process control this is an undesirable situation particularly for pharmaceutical field where product control is critical. With the advent of fracture mechanics and population balance modeling, the mathematical analysis of milling operations has been moderately successful. A more detailed understanding of fracture mechanics became possible only after the analysis of stress in spheres. Hertz considered contact between two homogenous bodies with ellipsoidal surfaces and determined the normal stresses in the contact area and also duration of contact.[43] This theory was further extended by Huber who described stresses in the vicinity of contact area. [44-45] Griffith proposed that all brittle materials contain a population of small cracks and flaws. Fracture will result upon application of stress when the theoretical yield stress is exceeded at the tip of one of these flaws. Owing to the practical difficulties of energy approach, Irwin reformulated the equation in terms of stress rather than energy. This resulted in new material property called stress-intensity factor which is now universally accepted as a defining term for fracture mechanics and a characteristic material property. [46] Thus a comprehensive study of the entire process requires an adequate knowledge of the stressing events, which are determined by the operational conditions, as well as the materials reaction to the applied stress. Consequently, from energy based models the focus shifted towards establishing models from the principles of fracture mechanics, being a combination of both material properties and machine effects [32,47]

Based on indentation fracture mechanics a model for attrition of particulates has been developed by Zhang *et al.* [48]. The fracture mechanics based model was developed from the analysis of propagation of the lateral cracks in single crystals of KCl, NaCl and MgO to provide an estimate on the rate of attrition. Damage during fracture can result in localized loading that can lead to significant deformation followed by the formation of radial cracks or subsurface lateral cracks. At low velocities these lateral cracks are considered to be responsible for the material removal and hence attrition whereas at sufficiently high velocities the propagation of the radial cracks

causes fragmentation. [49-50] Applying these principles of fracture mechanics, the fractional loss from a particle due to an attrition was found to be in (Eq. 1) where α is the proportionality factor, and the dimensionless group η is regarded as the attrition propensity parameter. This parameter includes all the relevant material properties, i.e. density (ρ), particle linear dimension (l), hardness (H), and fracture toughness (K_c), and the impact velocity (v). In order to determine the constant of proportionality single particle impact tests were conducted and the material loss due to attrition was quantified gravimetrically. The trends of the experimental results were found to agree with the predictions of the mechanistic model of attrition. Moreover, the dependence of attrition rate on material properties, impact velocity and particle size was validated. Although this model does not take into account the effect fatigue or defect accumulation it is one of the few mechanistic models that actually describe attrition. [51-52]

$$\xi = \alpha\eta = \alpha \frac{\rho v^2 l H}{{K_c}^2} \quad (1)$$

4.3.Population balance modelling

Population balance modeling consists of a set of integro-partial differential equations which describe the behavior of particles from the analysis of behavior of a single particle in local conditions.

$$\frac{dm_i(t)}{dt} = -S_i(t)m_i(t) + \sum_{j=1}^{i-1} b_{ij}S_j(t)m_j(t) \quad (2)$$

In a typical PBM system (Eq.2) t, m, S, and b represent time, mass density distribution function, selection function, and breakage distribution function respectively. The portion of particles which is damaged in an experiment is obtained from the breakage probability whereas the breakage function represents the size distribution of the fragments. Most researchers have modified traditional PBM functions by adding semi-empirical relationships that are fitted to measure the equipment response. These relationships modify the breakage rates, enabling the model to respond to changes in feed and operating conditions, thereby providing some predictive capability. The main drawback of this approach is that it can't be used for design purposes and for optimization.[53-55] Fracture mechanic principles have facilitated the incorporation of material

properties into the breakage probability functions of PBM. Starting from simplifying assumption of both geometrical similarity of particles undergoing size reduction and similarity of states of stress and strain Rumpf developed a relation between initial particle size and the elastic strain energy. Using dimensional analysis the similarity law was extended to include different materials with varying flaw distributions. The same correlation was obtained by applying Weibull statistics for flaw size distribution along with Hertz theory and mechanics of crack propagation. [56-58] Vogel and Peukert [32] used this approach to arrive at an impact model which exclusively deals with both material and mill function. They simplified both approaches i.e. similarity considerations by Rumpf and the fracture mechanical model based on the Weibull statistics and arrived at two new parameters namely f_{Mat} and $W_{m,minx}$.

$$S = 1 - \exp\{-f_{Mat}\ k\chi\ (W_{kin}\ - W_{m,min})\ \} \qquad (3)$$

In this impact model, f_{Mat} represents the resistance of particulate material against fracture, $W_{m,min}$ characterizes the specific energy which a particle can absorb without breakage, x being the particle size and k the number of impacts. Meir *et al.* [59] have used this impact model to describe the grinding behavior of pharmaceutical materials based on f_{mat} and $W_{m,min}$. These parameters were determined experimentally by particle impact tests. Single particle fracture studies have been used since the early 1960s and have now undergone significant improvement to study milling process and the material functions such as f_{Mat} and $W_{m,min}$. A variety of testing methods including single/double impact or slow compression have been used to measure the breakage characteristics of particles Particle impact tests can be performed by drop tests or by propelling particles against a target using a pneumatic gun. [60-62] In this study the particles are accelerated along a tube and hit an impact plate made of hardened steel. After the impact, the material is collected in bottom of the impact chamber. Several experiments were performed at different impact speeds to obtain a dependency of S over $W_{m,kin}$ that provided the parameter f_{Mat} and $W_{m,min}$. These material parameters allowed for a quantitative differentiation between various materials and enabled a comparison between different materials such as lactose monohydrate, sucrose, glycine, ascorbic acid, acetylsalicylic acid and tartaric acid. The results clearly indicate the high friability of citric acid as compared to other compounds. Thus this method can be used to identify those compounds that break easily from the ones that require a higher input of energy for breakage. The method also permits a quantitative characterization of breakage behavior in a

size range down to about 25µm. Moreover, the method allows the characterization of grinding behavior of materials using smaller amounts of substance, thus reducing any developmental costs. Vogel and Peukert's impact model is however limited to describing breakage by repeated impacts of constant magnitude only. Moreover, when using more detailed breakage functions, additional parameters need to be introduced, that can differ from substance to substance. Therefore, care has to be taken when choosing a model for describing the breakage function in PBM.[59]

4.4. DEM modeling

The Discrete Element Method (DEM), proposed by Strack and Cundall[63] is a deterministic approach to investigate the particle dynamics. This method serves as predictive tool for granular behavior typically observed for pharmaceutical powders and treats each particle as a separate entity. It employs different numerical schemes to solve Newton's equations of motion and contact mechanics to predict the time history response of material and corresponding particle trajectories.[64-67] This mechanistic model has now become been widely accepted as an effective method of addressing engineering problems and has been successfully used to simulate chute flow, [68] hopper discharge, [69] flows in rotating drums, [70-71] and tablet coating. [72-73] .

The earliest DEM model of a ball mill was by Mishra and Rajamani [74,75] . A 2D model was developed to analyze the motion of balls and particles during flow. To experimentally verify the results obtained from DEM, the mill was computationally divided into slices such that percentage of area occupied by the discs, along with the void area is equal to the proportion of charge filling of the actual mill. As the torque of the experimental mill is the product of resultant value for the slice and the quantity of slices, power consumption was compared between the experimental mill and the DEM model. Although overall agreement was found to be satisfactory, the 2D model does not account for the torque component in the axial direction and hence should be used cautiously when analyzing slices at the feed or discharge end of mill where axial component dominates. This two-dimensional DEM for the ball mill was further extended by Cleary [76, 77] by incorporating particles of different size and shape. Detailed comparison of charge profiles in a mill predicted by the model with high speed photographs demonstrated a very close agreement. Segregation within the mill was also studied by computing the coefficient of variation of particle size distribution. The largest amount of radial segregation in a mill was

found to be at 50% fill where the balls were confined to the center of mill. Under these conditions the balls cannot enter the cataracting stream and therefore do not break particles by high energy impacts. Additionally, particles were found to collide with neighbors of similar size and hence reduce the overall breakage opportunities. Following validation on flow and power consumption it was observed that increasing the angularity of charge can lead to higher dynamic angles of repose for the cascading free surface and hence higher power consumption. As the particles become rounder the shear strength of the charge was found to decline leading to lower power consumption. Thus the predictive ability of DEM can reinforce the effect of operational and feed parameters on the performance of mills and hence improve the sensitivity of predictions to various modeling assumptions. [74-77]

Besides the charge flow and power consumption, DEM has been extensively used to study energy distribution in mills [78-81]. Since the fundamental phenomenon for particle breakage occurs due to collision of particles with the grinding media, most studies have sought to relate the impact energy distribution obtained from DEM simulations to the breakage rate. In these models, the collision energy spectrum is calculated from the energy loss within the mill due to contact damping and friction rather than the kinetic energy of the collision. Damping energy is calculated during contact for both normal and shear components. Consequently, these techniques based on energy logging elaborate the various contributions to the overall energy dissipation within the mill and quantify the amount the energy actually utilized by the particles. Such efforts can enhance energy utilization of mills since it's well-known that they are highly inefficient. [82] This method of energy logging has been extensively used to determine the energy spectrum for tumbling mills. The frequency distributions for these mills indicate that majority of the particle impacts occur at low energy and hence are more likely to result in attrition than fragmentation. Therefore, high energy impact models may not be representative of the collision environment within these mills.[82-83] Besides determining the impact spectra, DEM simulations have been used to determine breakage rates of particles. Earlier approaches used by Datta and Rajamani [84] determined the breakage rate by DEM, based on energy and frequency of collision and compared to the impact energy determined experimentally. Similar to Datta and Rajamani, Concas et al.[85] established a breakage parameter in as the product of collision rate and the breakage probability by averaging the collision energy. Despite incorporating the effect of collision spectrum on milling these methods lacked the consideration of any fundamental properties of particles such as

fracture toughness on breakage rate. Moreover in these studies the impact energy distribution was obtained by assuming that all energies contribute to breakage, which may not be practical since minimum impact energy must be overcome to cause flaws and crack propagation for particle breakage to occur. An attempt was made by Capece *et al.* [86] to resolve these deficiencies in determining the specific breakage rate parameter by exploiting the particle scale interactions obtained from DEM and the impact model established by Vogel and Peukert [32] (Eq 3). The impact model had to be revised since in the original experiments of Vogel and Peukert preset collision energy was provided to particles by an impacting plate. This may not be similar to the environment inside a mill as the particles will undergo a several series of impacts with varied impact energies. To address this issue Capece *et al.* modified the equation to make it well-suited to the collisional environment within a mill and determine a specific breakage rate parameter (Eq.4) based on fracture mechanics.

$$k \equiv k_1 = f_{mat}\, x_1 \sum_{l=1}^{L} f_{coll,l}\ (E_{m,l} - E_{m,min}) \qquad (4)$$

The parameters $f_{coll,l}$ represents collision frequency with energy $E_{m,l,}$and x_1 is the particle diameter. DEM simulations parallel to the experimental conditions of ball milling of silica glass were performed for various feed and media sizes. The specific breakage rate parameter based on impact model determined from the DEM calculations was found to agree very well with the experiment, which suggests that impact spectra obtained from DEM are accurate. Such comparisons demonstrate the capability of DEM based models to simulate an intrinsically dynamic milling environment and hence a more fundamental analysis of the process.[86] However the validity of the model with respect to shear-based milling processes is still undetermined. Additionally this model involves no parameter that explicitly accounts for the material amenability to weakening by repeated impacts and hence cannot simulate conditions of low-energy stressing or any defect accumulation.

A model that exploits these principles from damage mechanics and Hertzian contact theory has been developed by Tavares *et al.* [87] to describe fracture of particle by damage accumulation. This model takes into account the distribution of collision energies in a mill obtained from DEM calculations along with distribution of fracture energies from impact tests to describe breakage by repeated stressing. From the particle impact tests the amount of damage "D" sustained (Eq.5) in the n^{th} loading cycle was estimated as the damage accumulation constant, and was used for

force-displacement calculations in DEM. By incorporating the contact mechanics of load-deformation of a sphere during compression the reduced stiffness of material was calculated based on the damage variable D thereby taking into account the weakening of material by repeated impacts.

$$D_n = \left[\frac{2\gamma}{(2\gamma - 5D_n + 5)} \frac{E_{k,n}}{E_{n-1}}\right]^{\frac{2\gamma}{5}} \quad (5)$$

In this model, $E_{k,n}$ and E_{n-1} represents the impact energy of the striker and the fracture energy of particle respectively. Although, the model was capable of describing breakage rate of coarse particles, it predicted a significant departure from experiments for finer particles (<= 0.075 mm), probably due to the assumption that the energy is evenly split among particles. Despite these limitations an important the model could determine the optimum impact energy for breakage of all particles. Moreover, the model requires fitting of only one parameter i.e. the damage coefficient (γ); a material dependent parameter from experimental data of repeated-impact tests. [88,89]

Simulation centered only on the collision energy spectra provide the opportunity to understand the various contributions to the energy dissipation within the mill and also predict the amount of energy consumed by particles. Hence these are appropriate for the simulations of the flow of materials where intensity of breakage can be deduced from the energy spectrum. Although these methods demonstrate the method's validity they do not involve any breakage of the particles and hence are mostly concerned with qualitative comparisons between simulated and experimentally observed granular motion in a mill. [90-93] To simulate actual size reduction of the particles, breakage and its controlling mechanisms need to be included in the DEM simulations. Recent progress in computing power and coding efficiency for numerical models are paving the way for simulations of particle breakage facilitating better equipment design and process operating conditions. The earlier models for simulating fracture are based on agglomerate structure where particles are glued to each other. This method is called Bonded Particle Method (BPM), suitable for non-porous particles. BPM simulates the mechanical behavior of a collection of particles that are bonded together at their contact points. The particles interact only at the soft contacts, which possess finite normal and shear stiffness. The mechanical behavior of such a system is described

by a force–displacement behavior at each contact defined by the normal and shear stiffness, k_n and k_s; and the friction coefficient, μ; of the two contacting particles. In these systems the breakage of particles is considered to be an elastic–brittle model with Griffith energy criterion for crack propagation. [94,95] Based on this approach simulations of fracture due to normal impact against a solid wall have been reported by Potapov and Campbell [96]. In these simulations it was observed that the macroscopic load generated during impact was found to generate heterogeneous force transmission and induce several sites of tension or compression. It is these micro-forces and micro-moments that consequently induce a global force and stress redistribution. If the stress redistribution results in a maximum tensile or shear stress that exceeds the tensile strength or shear strength of the bond, breakage occurs due to formation of rupture zones. Unlike Finite Element Method (FEM) that idealize material behavior as an elastic continuum with elliptical cracks; BPM does not impose any theoretical assumptions and limitations on material behavior. Consequently in BPM, cracks form, interact and coalesce resulting in macroscopic fractures. [82,95] In a similar approach Thornton *et al.* [97-99] presented numerical simulations of spherical, crystalline face centred cubic agglomerate impacting a target wall. In this approach, agglomerates were created with arbitrarily arranged spherical particles and glued together with surface adhesive forces. Agglomerates with different inter-particle bond strengths were created by attributing each particle a different surface energy (Γ). Simulations were performed to evaluate the effect of impact velocity and bond strength on the evolution of the wall force, kinetic energy of agglomerate and the proportion of broken bonds. The initial specific energy required to break a given number of bonds was found to scale with Γ^3. As consequence of the large forces being transmitted vertically upwards upon impact with wall, the primary particles in this region of agglomerate were found to decelerate whereas those in the lower side of the agglomerate did not experience any slowdown. Subsequently a heterogeneous velocity field was created due to a velocity discontinuity producing a relative shear motion between the agglomerate planes; ensuing breakage of contacts and fragmentation. Geometry and orientation of the agglomerate at wall interface were found to dictate the pattern of weakened planes and hence mechanism of damage. Based on this approach Ghadhiri *et al.* [100] has shown that weakly agglomerated lactose particles tend to deform plastically rather than fracture. Thus the different stages encountered during fracturing of the materials during agglomerate breakage can be envisioned through these simulations and force analysis, which is almost impossible by

experiments. Although the bonded/glued particle method can be used to study agglomerate breakage it is challenging to extend this method to an ensemble of particles due to the computational cost required to model sub-particles elements and glued/bonded particles [94-95,98]. To circumvent this drawback, Cleary et al. [101] introduced a replacement strategy in which the parent particle is replaced by an assembly of progeny when the breakage criteria are exceeded. Based on this approach Naik *et al.* [102] has explored the breakage of lactose in an impact mill. The simulations illustrate the effect of feed rate and impeller speed on milling where choke feed conditions has been observed at high feed rates and low impeller speeds. Although simulations agree with experimental trends the fragmentation model cannot be extended to accommodate effects of damage accumulation and hence are restricted to brittle materials. Additionally these models do not account for other modes of breakage such as attrition or chipping of particles.[102,103] New micro-scale population balance models have been now developed providing a comprehensive model that simulates flow and breakage of particles. These models keep track of the mass balance of particles and their fracture energy within a mill. In traditional PBM, size dependent empirical functions are chosen to describe the specific breakage rate parameter and the breakage distribution parameter for all particle sizes under consideration. This drawback can be overcome by these micro-scale population models that predict breakage and product size distribution based on energy distribution in mills. Consequently, in these models the selection and breakage function of the PBM are described in terms of collisional energy and material properties obtained from DEM calculations and impact tests respectively. The most common selection function that has been explored for these models is based on the fracture mechanics model described by Vogel and Peukert whereas the breakage function employed are either Napier Munn or Broadbent and Callcott. [104-107] Micro-scale population models have been used to describe breakage due to incremental impacts for spherical and non-spherical particles in ball mills. The simulation model estimates mass loss with particle size evolution based on cumulative damage. Based on the energy spectra it was concluded that many of the impacts that cause damage exceed the threshold breakage energy only by a small margin and a large amount of energy is lost in elastic deformation. While the DEM model gave good predictions for the size evolution it significantly over predicted the size of finer particles probably as the simulations were truncated at a minimum progeny size to limit the number of particles that can reasonably be modeled. Thus one of the key challenges still remaining for these mechanistic DEM models is

the need to adequately take account of the fine particles in milling applications. However in principle these are complete particle scale models lacking empiricism of population balance model and also benefit from the fact that design and process parameters are directly accounted by DEM simulations. In closing, the energy spectra from DEM along with population balance models are providing an essential contribution to advance the study of comminution process to an engineering science based on the mechanics of the processes.[82,108]

5. Conclusion

Particle size reduction is simply the result of a series of mechanical interactions between the feed material and vessel geometry. These interactions result in an intricate granular flow and particle rupture at the macro-scale, which are difficult to resolve. Consequently, like other particulate processes, it is difficult to design and control it partly due to the absence of any constitutive equations to describe particle breakage. Hence there is a need for established and consistent methods or models to quantify and predict this process. Traditional experimental methods are limited in providing a mechanistic model to illustrate the effects of particle properties and operational parameters on the process. Recently, studies have shown the emergence of micro-scale process modeling approaches as a promising tool for analyzing complex system geometries, parametric effects and energy efficiency in milling processes. However substantial testing of these techniques is still required to prove their predictive capabilities. Moreover validation is still inadequate especially in realistic environments as well against controlled pilot experiments. Experimental verification based on non-intrusive methods such as FBRM, SFT could facilitate model validation since they allow real time process monitoring. Thus, application of PAT tools along with process modelling could formulate dynamic mechanistic models in a structured way that facilitates development of predictive tools and knowledge transfer.

6. References

1) Snow RH, Allen T, Ennis BJ, Litster JD. 1997. Size reduction and size enlargement. In: Perry RH, Green DW, editors, Perry's Chemical Engineers' Handbook, 7th edition, Chap. 20, McGraw Hill, New York, New York.
2) Parrott EL. 1974. Milling of pharmaceutical solids. J. Pharm. Sci 63(6):813–829
3) HEYWOOD, H. 1952. Some notes on grinding research. J. Imp. Coll. Chem. Eng. Soc. 6 (26)
4) Piret, E. L. 1953. g. Chem. Eng. Prog. 49 (56).
5) Rohrs BR, Amidon GE, Meury RH, Secreast PJ, King HM, Skoug CJ. 1996. Particle size limits to meet USP content uniformity criteria for tablets and capsules. J. Pharm. Sci 95 (5):1049–1059.
6) Rogers Amanda J., Hashemi Amir and Ierapetritou Marianthi G. 2013. Modeling of Particulate Processes for the Continuous Manufacture of Solid-Based Pharmaceutical Dosage Forms. Processes 1(2):67-127
7) Mills L.A., Sinka I.C. 2013. Effect of particle size and density on the die fill of powders. European Journal of Pharmaceutics and Biopharmaceutics 84(3): 642–652
8) Vogt M., Kunath K., Dressman J.B. 2008. Dissolution enhancement of fenofibrate by micronization, co-grinding and spray-drying: Comparison with commercial preparations. European Journal of Pharmaceutics and Biopharmaceutics 68(2): 283-288.
9) Liversidge G.G., Cundy K.C. 1995. Particle size reduction for improvement of oral bioavailability of hydrophobic drugs: I. Absolute oral bioavailability of nanocrystalline danazol in beagle dogs. International Journal of Pharmaceutics 125(1): 91-97
10) Mullarney Matthew P., Leyva Norma. 2009. Modeling Pharmaceutical Powder-flow Performance Using Particle-Size Distribution Data. Pharmaceutical Technology 33(3): 126-134.
11) Shekunov, B.Y., Chattopadhyay, P., Tong, H.H.Y., Chow, A.H.L., 2007. Particle size analysis in pharmaceutics: principles, methods and applications. Pharm. Res. 24(2): 203–227.
12) Henk G. Merkus. 2009 Particle Size Measurements: Fundamentals, Practice, Quality. 1st ed. Springer

13) Silva Ana F.T., Burggraeve Anneleen , Denon Quenten, Meeren Paul Van der, Sandler Niklas, Kerkhof Tom Van Den, Hellings Mario, Vervaet Chris, Remon Jean Paul, Lopes João Almeida,Thomas De Beer. 2013. Particle sizing measurements in pharmaceutical applications: Comparison of in-process methods versus off-line methods European Journal of Pharmaceutics and Biopharmaceutics 85: 1006–1018.

14) Marriott, C; MacRitchie, H B; Zeng, X-M; Martin, G P 2006. Development of a laser diffraction method for the determination of the particle size of aerosolised powder formulations. International Journal of Pharmaceutics 326 :39–49

15) Sahni Ekneet, Chaudhuri Bodhisattwa. 2012. Contact drying: A review of experimental and mechanistic modeling approaches. International Journal of Pharmaceutics 434: 334– 348.

16) Beer T. De, Burggraeve A., Fonteyne Saerens M., Remon L., J.P., Vervaet C. 2011. Near infrared and Raman spectroscopy for the in-process monitoring of pharmaceutical production processes. International Journal of Pharmaceutics 417 : 32– 47

17) Hui, T.L., Wah, C.L., Heng, P.W.S., 2008. Rapid and convenient microsphere sizing: using a PAT instrument and pilot-scale spray dryer can provide real-time information regarding process and product size. Pharm. Technol., Asia Pacific 2 (3): 25–29.

18) Lehr-Schmidt S., Moritz. H.U., Juergens K.C., 2007. On-line control of particle size during fluidized bed granulation. Pharm. Ind. 69: 478–484.

19) Gernaey K.V., Gani R. 2010. A model-based systems approach to pharmaceutical product-process design and analysis. Chemical Engineering Science 65(21): 5757–5769.

20) Wassgren C, Curtis JS. 2006. The application of computational modeling to pharmaceutical materials science. MRS Bull 31(11):900–904.

21) Ketterhagen William, Am Ende T. Mary, Hancock Bruno C. 2009. Process modeling in the Pharmaceutical Industry using the Discrete Element Method. Journal of Pharmaceutical Sciences. 98(2) : 442:470

22) Weili Yu, Bruno C. Hancock. 2008. Evaluation of dynamic image analysis for characterizing pharmaceutical excipient particles. International Journal of Pharmaceutics 361 150–157

23) Venkateshwar Rao Nalluri, , Schirg Peter, Gao Xin, Virdis Antoine, Imanidis Georgios, Kuentza Martin 2010. Different modes of dynamic image analysis in monitoring of pharmaceutical dry milling process. International Journal of Pharmaceutics 391: 107–114

24) Kumar V, Taylor MK, Mehrotra A, Stagner WC. 2013 Real-Time Particle Size Analysis Using Focused Beam Reflectance Measurement as a Process Analytical Technology Tool for a Continuous Granulation–Drying–Milling Process. AAPS PharmSciTech, 14(2) 2:523-530

25) Lie, M., Wilkinson D., Patchigolla K. 2005. Comparison of particle size distributions measured using different techniques. Particle and Particle Systems Characterization 23(3):265–284

26) Heath A.R.,Fawell,P.D.,Bahri,P.A.,Swift,J.D.,2002.Average particle size by focused beam reflectance measurement(FBRM).Particle and Particle Systems Characterization 19(2):84–95

27) Ai Tee Tok, Xueping Goh, Wai Kiong Ng, and Reginald B. H. Tan.. 2008. Monitoring Granulation Rate Processes Using Three PAT Tools in a Pilot-Scale Fluidized Bed. AAPS PharmSciTech. 9(4):1083-1091.

28) Burggraeve A, Van Den Kerkhof T, Hellings M, Remon JP, Vervaet C, De Beer T. 2010. Evaluation of in-line spatial filter velocimetry as PAT monitoring tool for particle growth during fluid bed granulation. European Journal of Pharmaceutics and Biopharmaceutics 76 (1) :138–146

29) Petrak D., Dietrich S., Eckardt G., Köhler M. 2011. In-line particle sizing for real-time process control by fibre-optical spatial filtering technique (SFT). Adv. Powder Technol. 22(2):203–208

30) Narvanen T., Lipsanen T., Antikainen O., Raikkonen H., Yliruusi J. 2008. Controlling granule size by granulation liquid feed pulsing. Int. J. Pharm. 357 (1-2): 132–138.

31) Naervaenen, T., Lipsanen, T., Antikainen, O., Raeikkoenen, H., Heinaemaeki, J., Yliruusi, J., 2009. Gaining fluid bed process understanding by in-line particle size analysis. J. Pharm. Sci. 98(3):1110–1117

32) Vogel L., Peukert W. 2003. Breakage behavior of different materials—construction of a mastercurve for the breakage probability. Powder Technology 129: 101–110

33) Prasher, C. L. 1987. Energy for Size reduction. 1st ed. Crushing and Grinding Process Handbook. p 178-208.

34) Austin L.G., Klimpel R.R. 1964. Theory of grinding operations. Ing.Eng.Chem, 56:18-29

35) Owens, J. S. 1933. Notes on power used in crushing ore, with special reference to rolls and their behaviour. Trans. Inst. Min. Met. 42: 407-425.

36) SCHO¨NERT, K. 1972. Role of fracture physics in understanding comminution phenomena. *Trans. Soc. Mining Engineers AIME* 252**:** 21–26.

37) Broadbent S. R. & Callcott T. G. 1956. A matrix analysis of processes involving particle assemblies. Philosophical Transactions of the Royal Society of London A, 249:99-123.

38) Ramanan Pitchumani. 2003. Breakage behaviour of enzyme granules in a repeated impact test, Powder Technology 130 : 421– 427

39) Cho K. 1987. Breakage mechanism in size reduction. PhD Thesis. Department of Metallurgical Engineering, University of Utah.

40) Austin LG. 1973. A commentary on the Kick, Bond and Rittinger Laws of grinding. Powder Technol 7:315–318.

41) Chen Y., ding Y., Papadopoulos D.G., Ghadiri M. 2004. Energy-Based Analysis of Milling a-Lactose Monohydrate. Journal of pharmaceutical sciences 93 (4):886-895.

42) Vegt Onno de, Vromans Herman, Faassen Fried, Maarschalk Kees van der Voort. 2006. Milling of Organic Solids in a Jet Mill. Part 1: Determination of the Selection Function and Related Mechanical Material Properties Part. Part.Systems Charact. 22 (2): 133–140.

43) Vogel L., Peukert W. 2002. Characterization of grinding-relevant particle properties by inverting a population balance model, Particle & Particle Systems Characterization 19 (3):149– 157.

44) Huber M.T. 1904. Zur Theorie der Beruhrung fester elasticher korper . Ann. Phys. 14: 103-151

45) S.P. Timoshenko, J.N. Goodier, Theory of Elasticity, 3rd edition, McGraw-Hill, 1973

46) T. L. Anderson 2005. Fracture Mechanics: Fundamentals and Applications. Third Edition. Taylor and Francis.

47) Salman A.D., Ghadiri M. and Hounslow M.J.2007. Breakage of Single Particles: Quasi-Static. Handbook of Powder Technology, Particle Breakage 12 : 3-30.

48) Ghadiri, M., Zhang, Z., 2002. Impact attrition of particulate solids. Part 1. A theoretical model of chipping. Chem. Eng. Sci. 57:3659–3669

49) Evans, A. G., & Wilshaw, T. R. 1976. Quasi-static solid particle damage in brittle solids: I. Observations, analysis and implications Acta Metallurgica 24(10):939-956

50) Evans, A. G., & Wilshaw, T. R. 1977. Dynamic solid particle damage in brittle materials: An appraisal. Journal of Material Science 12(1):97-116

51) Yuregir, K.R., Ghadiri, M., Clift, R., 1986. Observations on impact attrition of granular solids. Powder Technol. 49: 53–57.

52) Ghadiri, M., Zhang, Z., 2002. Impact attrition of particulate solids. Part 1. Experimental work. Chem. Eng. Sci. 57: 3671–3686

53) Bilgili E., Scarlett B. 2005. Population balance modeling of non-linear effects in milling processes, Powder Technol. 153 : 59–71.

54) Bilgili E.2011. Quantitative analysis of multi-particle interactions during particle breakage: A discrete non-linear population balance framework. Powder Technology 213 :162–173.

55) Barrasso Dana , Oka Sarang , Muliadi Ariel , Litster James D. ,Wassgren Carl 2013. Population Balance Model Validation and Prediction of CQAs for Continuous Milling processes: toward QbD in Pharmaceutical Drug Product Manufacturing. J Pharm Innov 8:147–162.

56) Rumpf H. 1973. Physical aspects of comminution and a new formulation of a law of comminution, Powder Technology 7: 145– 159

57) Weichert R., 1992. Anwendung von Fehlstellenstatistik und Bruchmechanik zur Beschreibung von Zerkleinerungsvorga¨ngen. Zement-Kalk-Gips 45 (1) :1 –8.

58) Weibull W. 1951. A statistical distribution function of wide applicability, Journal of Applied Mechanics 9: 293–297.

59) Meier Matthias, Edgar John, Wieckhusen Dierk, Wolfgang Wirth, Wolfgang Peukert. 2008 Characterization of the grinding behavior in a single particle impact device: Studies on pharmaceutical powders. European journal of pharmaceutical sciences 34:45–55.

60) Sergiy Antonyuk, Jürgen Tomas, Heinrich Stefan, Mörl Lothar. 2005. Breakage behavior of spherical granulates by compression. Chemical Engineering Science 60: 4031 – 4044.

61) Maxim R.E., Salman A.D., Hounslow M.J. 2006. Predicting dynamic failure of dense granules from static compression tests. Int. J. Miner. Process. 79 (3): 188–197.

62) Kwan, C.C., Chen, Y.Q., Ding, Y.L., Papadopoulos, D.G., Bentham, A.C., Ghadiri, M., 2004. Development of a novel approach towards predicting the milling behaviour of pharmaceutical powders. Eur. J. Pharm. Sci. 23: 327–336.

63) Cundall P.A., Strack O. D. L. 1979. A discrete numerical model for granular assemblies. Geotechnique 29 (1): 47-65.

64) Renzo A. Di, Maio F.P. Di. 2004. Comparison of contact-force models for the simulation of collisions in DEM-based granular flow codes. Chemical Engineering Science 59 (3):525–541.

65) Thornton C., Cummins S.J., Cleary P.W. 2011. An investigation of the comparative behavior of alternative contact force models during elastic collisions, Powder Technology 210(3):189–197.

66) Thornton C., Cummins S.J., Cleary P.W. 2013. An investigation of the comparative behavior of alternative contact force models during inelastic collisions, Powder Technology 233: 30–46.

67) Zhu H.P., Zhou Z.Y., Yang R.Y., Yu A.B. 2007. Discrete particle simulation of particulate systems: theoretical developments. Chemical Engineering Science 62: 3378–3396.

68) Jiayuan Zhang Ziguo Hu, Wei Ge, Yongjie Zhang, Tinghua Li, and Jinghai Li. 2004. Application of the Discrete Approach to the Simulation of Size Segregation in Granular Chute Flow. Ind. Eng. Chem. Res. 43: 5521-5528

69) Ketterhagen William R, Curtis Jennifer S., Wassgren Carl R., Hancock Bruno C. 2009. Predicting the flow mode from hoppers using the discrete element method, Powder Technology 195(1):1–10

70) Yang R.Y., Yu A.B., McElroy L., Bao J. 2008. Numerical simulation of particle dynamics in different flow regimes in a rotating drum. Powder Technology 188(2):170–177.

71) Nan Gui , Jie Yan, Wenkai Xu , Liang Ge , Daling Wu, , Zhongli Ji, Jinsen Gao, Shengyao Jianga, Xingtuan Yang. 2013. DEM simulation and analysis of particle mixing and heat conduction in a rotating drum. Chemical Engineering Science 97 (28):225–234.

72) Ketterhagen W.R. 2011. Modeling the motion and orientation of various pharmaceutical tablet shapes in a film coating pan using DEM. International Journal of Pharmaceutics 409(1-2) :137–149

73) Suzzia Daniele, Toschkoff Gregor, Radl Stefan, Machold Daniel, Fraser Simon D., Glasser Benjamin J., Khinast Johannes G. 2012. DEM simulation of continuous tablet coating: Effects of tablet shape and fill level on inter-tablet coating variability. Chemical Engineering Science 69 (1): 107–121

74) Mishra B.K., Rajamani R.K. 1992. The discrete element method for the simulation of ball mills, Applied Mathematical Modelling 16 (11): 598–604.

75) Mishra B.K., Rajamani R.K. 1994. Simulation of charge motion in ball mills. Part 1: experimental verifications. International Journal of Mineral Processing 40 (3-4): 171–186.

76) Cleary P.W. 1998. Predicting charge motion, power draw, segregation and wear in ball mills using Discrete Element Methods, Minerals Engineering 11 (1):1061–1080.

77) Cleary P.W. 2001 Charge behavior and power consumption in ball mills: sensitivity to mill operating conditions, liner geometry and charge composition. International Journal of Mineral Processing 63(2):79-114.

78) Cunha E.R., Carvalho R.M., Tavares L.M. 2013.Simulation of solids flow and energy transfer in a vertical shaft impact crusher using DEM. Minerals Engineering 43–44 : 85–90

79) M. Sinnott, P.W. Cleary, R. Morrison. 2006. Analysis of stirred mill performance using DEM simulation: Part 1 — media motion, energy consumption and collisional environment, Minerals Engineering 19: 1537–1550.

80) Cleary P.W., Sinnott M.D., Morrison R.D. 2008. DEM prediction of particle flows in grinding processes. International Journal for Numerical Methods in Fluids 58: 319-353

81) Morrison R.D., Cleary P.W., Sinnott M.D., Using DEM to compare the energy efficiency of pilot scale ball and tower mills, Minerals Engineering 22 (2009) 665–672

82) Weerasekara N.S., Powell M.S., Cleary P.W., L.M. Tavares, Evertsson M., Morrison R.D, Quist J., Carvalho R.M. 2013.The contribution of DEM to the science of comminution Powder Technology 248: 3–24

83) Weerasekara N.S., Powell M.S.2008. The New energy logging from the discrete element method, CSRP'08 2nd Annual Conference, Brisbane, Queensland, Australia.

84) Datta A, Rajamani R. 2002. A direct approach of modeling batch grinding in ball mills using population balance principles and impact energy distribution. Int J Miner Process. 64:181–200

85) Concas A, Lai N, Pisu M, Cao G 2006. Modelling of comminution processes in Spex mixer/mill. Chem Eng Sci. 61:3746–3760

86) Capece Maxx, Bilgili Ecevit, and Dave Rajesh N. 2014. Formulation of a Physically Motivated Specific Breakage Rate Parameter for Ball Milling via the Discrete Element Method. American Institute of Chemical Engineers. 60: 2404-2415

87) Tavares L.M., King R.P.2002. Modeling of particle fracture by repeated impacts using continuum damage mechanics. Powder Technology 123:138–146

88) Tavares Luis Marcelo. 2009 Analysis of particle fracture by repeated stressing as damage accumulation. Powder Technology 190 : 327–339

89) Tavares Luís Marcelo, Carvalho Rodrigo M. de. 2009. Modeling breakage rates of coarse particles in ball mills. Minerals Engineering 22: 650–659.

90) Yang R.Y., Jayasundara C.T., Yu A.B., Curry D. 2006 DEM simulation of the flow of grinding media in IsaMill, Minerals Engineering 19 : 984–994.

91) Jayasundara C.T., Yang R.Y., Yu A.B., Curry D. 2006. Discrete particle simulation of particle flow in IsaMill, Industrial and Engineering Chemistry Research 19 : 6349–6359.

92) Jayasundara C.T., Yang R.Y., Yu A.B., Rubenstein J. 2010. Effects of disc rotation speed and media loading on particle flow and grinding performance in a horizontal stirred mill. International Journal of Mineral Processing 96(1-4): 27–35.

93) Cleary P.W. 2009. Industrial particle flow modelling using DEM, Engineering Computations 26:698–743

94) Alexander V. Potapov, Charles S. Campbell 1994. Computer simulation of impact-induced particle breakage. Powder Technology 81:207-216

95) Herbst J.A., Potapov A.V. 2004. Making a Discrete Grain Breakage model practical for comminution equipment performance simulation. Powder Technology 25:144–150.

96) Potyondy D.O., Cundall P.A. 2004. A bonded-particle model for rock, International Journal of Rock Mechanics and Mining Sciences. 41(8):1329–1364.

97) Kafui K.D., Thornton C. 2000. Numerical simulations of impact breakage of spherical crystalline agglomerate. Powder Technology 109(1-3) : 113–132

98) Thornton C., Liu L.2004. How do agglomerates break? Powder Technology 143–144:110–116

99) Thornton C., Ciomocos M.T., Adams M.J. 2004. Numerical simulations of diametrical compression tests on agglomerates. Powder Technology 140 (3): 258–267.

100) Ning Z, Boerefijn R, Ghadiri M, Thornton C. 1997. Distinct element simulation of impact breakage of lactose agglomerates. Adv Powder Technol 8:15–37.

101) Cleary P.W., Prakash M., Sinnott M.D., Rudman M., Das R. 2011. Large scale simulation of industrial, engineering and geophysical flows using particle methods, in: E.

Oñate, R. Owen (Eds.), Particle-Based Methods, Computational Methods, Springer Science + Business Media B.V. in Applied Sciences89–111

102) Djordjevic N., Shi F.N., Morrison R.D. 2003. Applying discrete element modelling to vertical and horizontal shaft impact crushers, Minerals Engineering 16 (10) 983–991

103) Naik, S., Malla R., Shaw M., Chaudhuri B. 2013. Investigation of Comminution in a Wiley Mill: Experiment and DEM Simulations Powder Technol. 237: 338-354

104) Cleary P.W 2001. Recent advances in DEM modelling of tumbling mills. Minerals Engineering 14: 1295‑1319

105) Powell M.S., Govender I., McBride A.T. 2008 Applying DEM outputs to the unified comminution model, Minerals Engineering 21: 744–750.

106) Tavares L.M., Carvalho R.M., 2010. A mechanistic model of batch grinding in ball mills, XXV International Mineral Processing Congress Brisbane, Australia. 1-11

107) Powell M.S., Weerasekara N.S. 2010. Building the unified comminution model, XXV International Mineral Processing Congress Brisbane Australia, 1133–1142

108) Delaney G.W., Cleary P.W. Morrison R.D., Cummins S., Loveday B. 2013. Predicting breakage and the evolution of rock size and shape distributions in AG and SAG mills using DEM. Minerals Engineering 50–51 :132–139

Tables

Table 1: Selection criteria for some mills[2,3]

Particle Description	Size (μm)	Universal And Pin mills	Hammer mills	High compression roller mills	Ball mills
Medium Fine	500-1000	Yes	Yes	No	No
Fine	150-500	Yes	Yes	No	No
Very fine	50-150	Yes	Yes	No	No
Super fine	10-50	Yes	Yes	Yes	Yes
Ultra fine	<10	No	No	Yes	Yes
Colloidal	<1	No	No	No	No

Table 2: Modeling techniques used in dry milling operation

Modeling tool	Information	Advantage	Short-comings
Energy based models[2, 40-41]	Based on semi-empirical relations between particle size and energy	Simple to operate	Not related to any material properties Cannot be extended to different mills
Population balance modelling (PBM)[43,53-55,59]	describes the evolution of populations of entities (particles, granules, droplets) over time. It gives the behavior of a population of particles from the analysis of behavior of single particle in local conditions	Population balances model the evolution of properties that may differ from particle to particle. Can model fine particles. Newer models incorporate material properties into model	A lot of experimental data is required Empiricism Challenging to extrapolate to different equipment design
Discrete Element Modeling (DEM) [78-82,,86,95-98,106-108]	Predict trajectories of all particles using Newton's equations of motions and Euler's law Combined with fracture mechanics and population balances provide a complete particle scale model	Provide dynamic information (transient forces energy spectra, power-consumption, stress distribution) which are difficult to calculate experimentally. Easily incorporates material properties and machine parameters.	Computationally very expensive and hence suitable for limited number of particles Doesn't account for account of the fine particles in milling applications

Figures

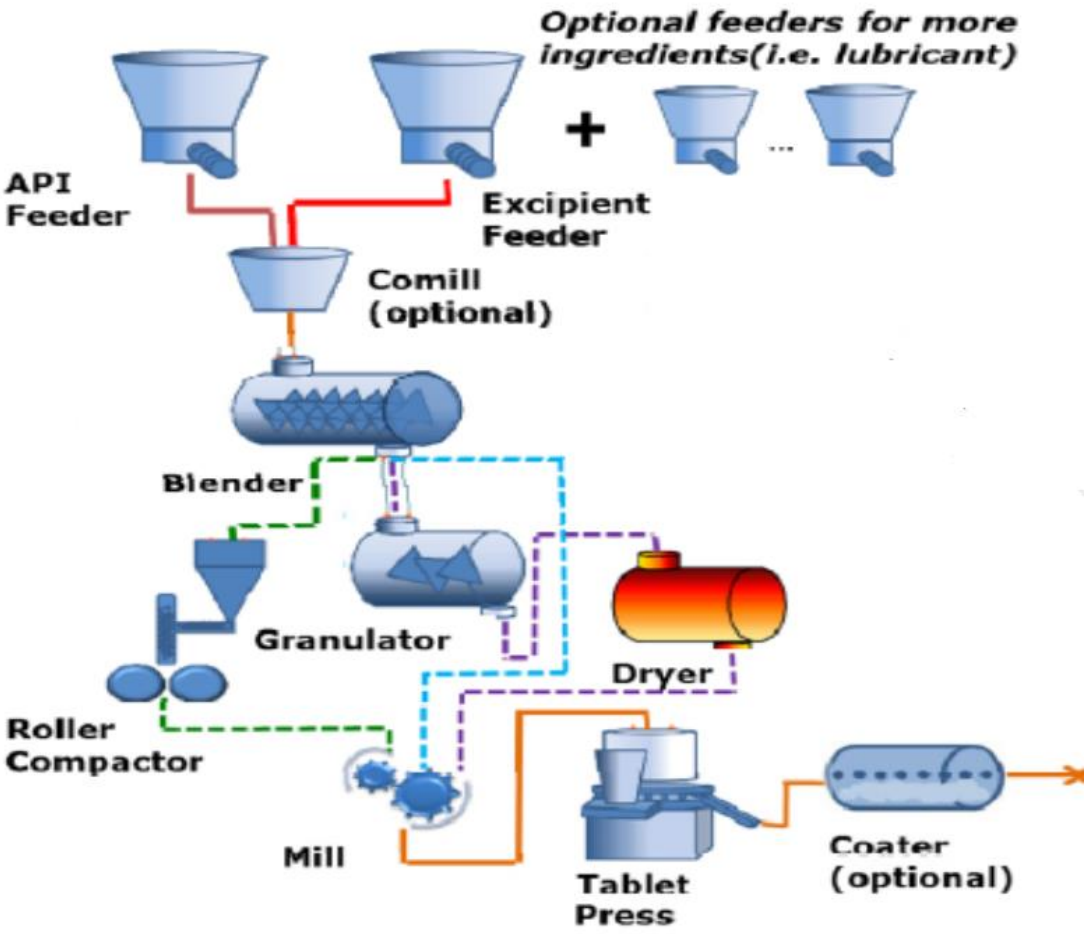

Figure 1: Process operations for solid dosage form [6]

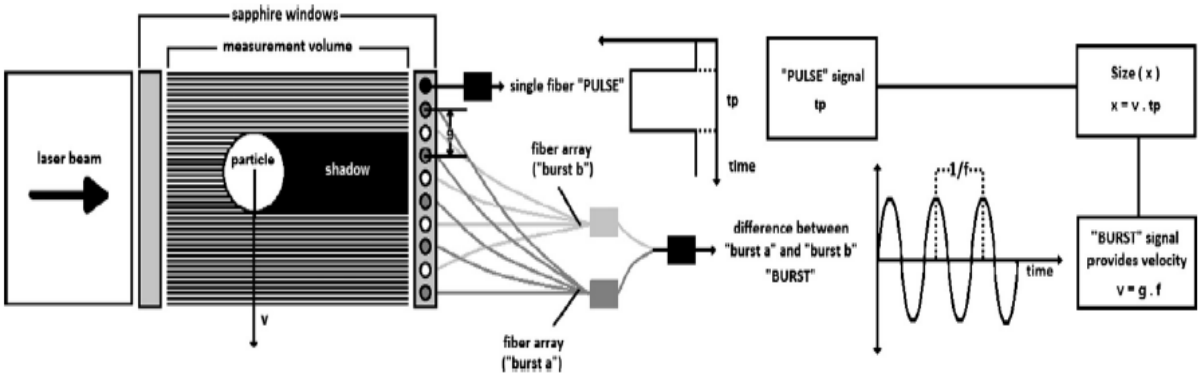

Figure. 2. Working principle of spatial field velocimetry (Parsum IPP70 probe).[13]

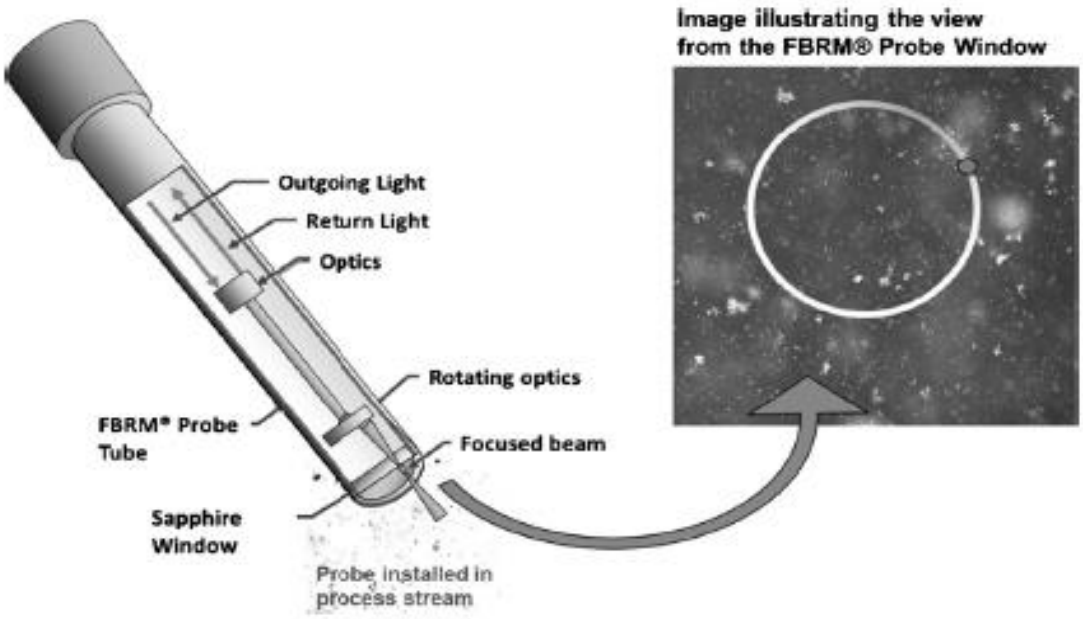

Figure 3: Working principle of the FBRM technology[26]

Chapter 7

Investigation of Comminution in a Wiley Mill: Experiments and DEM Simulations

Shivangi Naik [1], Ramesh Malla [2], Bodhisattwa Chaudhuri [1,3*]

[1]Department of Pharmaceutical Sciences, University of Connecticut, Storrs, CT 06269, USA

[2] Department of Civil Engineering, University of Connecticut Storrs, CT 06269, USA

[3] Institute of Material Sciences, University of Connecticut, Storrs, CT 06269, USA

*Corresponding Author

Email: bodhi.chaudhuri@uconn.edu

Abstract

Particle size reduction rate was studied by conducting parametric studies experimentally and computationally using Discrete Element Method (DEM). Studies were performed with lactose non-pareils to understand the effect of blade speed (rotational), feed rate, and blade-wall tolerance in a Wiley mill. The size of the resulting progeny of particles was analyzed by sieve analysis. Greater size reduction was observed at higher speeds and low feed rates owing to the greater centrifugal force experienced by the particles and longer mean free path lengths respectively. Increase in blade-wall tolerance resulted in accumulation of powder bed which was found to be higher at low impeller speeds. Single particle impact studies were performed using Dynamic Mechanical Analyzer to determine the force required to break the granule. In this method, the granules were subjected to a quasi-static compression process and the corresponding force was continuously recorded. The flow and fragmentation of non-pareil were simulated using DEM, an explicit numerical technique scheme, which calculates interaction forces between grains for each grain-grain contact, and the resulting motion of each grain.

Keywords: Comminution, Wiley Mill, Discrete element method, Fragmentation, DMA

1. Introduction

Particulate processing is commonly encountered in a wide variety of industries such as paper, ceramics, mineral, food and pharmaceutical industry. It has been estimated that roughly 70% of all manufactured products require some sort of particle processing [1]. Despite granular systems being so pervasive in industry, processes involving these types of materials are often poorly understood compared to their fluid processing counterparts [2]. This reality stems in part from the fact that there is a lack of a set of constitutive equations derived from first-principles that describe granular flows for a specified initial state and boundary conditions. This leads to broad assumptions during process design, poor identification of critical process parameters and scale-up complications [3]. The need for understanding the behavior of such complex particulate systems is of critical importance to the solid handling operations of the pharmaceutical industry; where close to 80% of pharmaceutical products are formulated as tablets, pills or capsules [4]. Tablets and capsules are manufactured as a result of different unit operations (mixing, granulation, drying, milling and compression) where reliable powder flow is crucial for the success of final product. Particle size reduction by mechanical means is an important unit operation as it determines the appropriate size distribution of the final product. For example the particle size distribution has significant impact on the performance and solubility of BCS II drugs whose solubility has been improved by micronization or milling [5-7].

The particle size distribution of the material after comminution depends on complex interaction between the operational parameters and material parameters. Surface characteristic and fracture pattern of the powder under an applied energy is influenced not only by material properties, but also by mill performance .The machine parameters depend on the mill involved and for impact mills typically consist of rotor speed, feed rate, screen size, impeller wall tolerance [8-9]. These operational conditions of the mill determine the number, intensity and the distribution of stress events within the particulate bed leading to fragmentation. The material properties of interest that determine their breakage during comminution include the Young's Modulus, Fracture toughness, Yield stress. Probably the most important characteristic governing size reduction is hardness because almost all size-reduction techniques involve somehow creating new surface area and this requires adding energy proportional to the bonds holding the feed particles together. Flow properties can be major factors, too, because many size-reduction processes are continuous, but

often have choke points at which bridging and flow interruption can occur [10-14]. Thus the knowledge of particle flow, granular fracture in a mill is very critical to optimize and to scale up this operation. Substantial effort has been expended in last three decades to understand the milling performance as a function to material properties, operational conditions and machine configuration. Kwan *et al.* [15] performed experiments and discrete element method (DEM) modeling of milling of pharmaceutical excipients in a very-small-scale, oscillatory, single-ball mill. Campbell [16] developed a relationship between the inlet and outlet particle size distribution in a roller-milling operation whereas the Hammer Mill has been investigated by Austin, Vogel and Djordjevic for different sorts of materials. Austin developed a simplified a analytical model of high-speed milling of limestone and cement in hammer mill and chose arbitrary parameter to match the model prediction to the experimental findings [17-18], whereas PMMA/Glass and rock were the materials of interest for Vogel [19] and Djordjevic [20]. A comprehensive understanding of the fragmentation mechanism from experiments helped the development of a series of mechanistic and population balance based models [17-19]. However, these models have some drawbacks such as computational complexity for which exact solutions may not be possible, and complete omission of inter-particle interaction. Moreover, such models are quite cumbersome for developing governing equations that handle influence of process parameters on particle size distribution.

Unlike population-based models, which ignore particle-particle interaction, DEM explicitly considers inter-particle and particle-boundary interactions, providing an effective tool to model fracture and fragmentation phenomena. Fragmentation of particles was modeled using a composite-particle approach by Khanal [21] and Thornton [22-23] where bigger primary particles were considered to be fabricated by gluing smaller particles with a cohesive bond. Their DEM was based on first principles (Newton's Law and Euler's Law for linear and angular motion) wherein particle breakage is not due to fracture or crack propagation but bigger particles (agglomerates) simply disintegrate into clusters of smaller particles. Comprehensive modeling of milling based on first principles was attempted by Djordjevic using DEM, where granular flow properties are considered [20]. The DEM-based direct modeling of the milling process is limited to a small number (a few hundred) of spherical particles, and derives essentially no conclusions regarding optimization, control or scale-up of milling performance. Mio *et al.* [24] used DEM to estimate the scale-up strategies of grinding gibbsite powder by using four different scales of

planetary mill, relating specific impact energy with grinding rate. In these DEM models, the breakage is being either modeled using a stochastic approach or empirical relations which are very material specific, instead of using kinetics, kinematics and theories of fracture mechanics.

This paper describes the use of Discrete Element Method (DEM) for studying particle flow and fracture under impact. The Discrete Element Method (DEM), proposed by Strack and Cundall [25] is a deterministic approach to investigate the particle dynamics. As DEM explicitly considers inter-particle and particle–boundary interactions along with kinematics of primary and secondary particles it provides an effective tool to model fragmentation. To the best of our knowledge no previous work has used 3D DEM of the comminution process for a realistic granular system in a Wiley mill which is the subject of our study. Experimentally validated particulate DEM has the capability to predict the particle size of fragments generated under different operational conditions. The DEM model can easily include physical properties of material of interest and operational conditions of comminution process.

2. Material and Methods:

2.1. Materials

Comminution studies were performed on Lactose non-pareils obtained from Paulaur Corporation (Cranbury, NJ) of diameter 1.2–1.4 mm. The non-pareils was selected as a model compound because of it's with well-known physical properties (stated in Table 1)

2.1. Dynamic Mechanical Analysis:

Breakage studies for single particles have been carried out using different approaches such as ultrafast load-cell [26], drop tests and quasi-static compression [27-28]. In this study a method similar to the testing procedure used by Antonyuk [28] et al. was used. Single particle breakage studies were performed in Dynamic Mechanical Analyzer (DMA) from TA instruments (Fig. 1a) to study the effect of the different loading conditions on granule properties. In this study the granule was placed on stationary clamp and compressed by a movable clamp that can be programmed to apply increasing load to sample. As the particle gets compressed, the applied force and corresponding change in granule properties (dimension change, displacement, and

stress) was continuously monitored on screen. Using this experimental approach the force required to crush the granule was determined. To investigate the effect of creep on breakage, the lactose granules were subjected to loading and unloading cycles and the corresponding breakage force for such treatment was monitored. To explore the effect of strain rate the particles were subjected to high loading rates (≈4N/min and 6N/min).

2.2. Experimental approach:

The milling equipment (Fig. 1b) (Thomas Wiley Mill, Thomas Scientific, Swedesboro, NJ) used in our study is a variable speed, digitally controlled, direct drive mill; that provides continuous variation of cutting speeds from 600 to 1140 rpm with constant torque maintained throughout the speed range. Parametric studies were conducted with lactose granules to study the effect of speed, impeller wall tolerance and feed rate on particle size reduction. In this study the material is fed from the hopper into the chamber and thrown out centrifugally by impact with the blades and ground by impact against the wall or hammers at the periphery. The material is retained until it is small enough to fall through the screen that forms the lower portion of the chamber. Particles fine enough to pass through the screen are discharged into a glass container. The experimental factors were studied at two or three levels. The operating conditions examined using the mill is enlisted in Table 2.

To quantify the effect of operational parameters on size reduction, particle size was computed by sieve analysis. The data obtained following sieve analysis was plotted in the form of d_{90}, d_{50} and d_{10} to understand the mechanism of comminution. The evolution of d_{90}, d_{50} and d_{10} was used to investigate the milling behavior of particles with coarse, average and fine sizes respectively [29-30].

3. Computational Model

Numerical simulations based on the Discrete Element Method (DEM). DEM, originally developed by Cundall and Strack [25] has been successfully used to simulate chute flow [31] hopper discharge [32] and flows in rotating drums [33-34]. In DEM, the total forces and torques acting on each particle are calculated. Each particle may interact with its neighbors or with the boundary only at the contact points through normal and tangential forces. The force on each particle is given by the sum of gravitational, inter-particle (normal and tangential F_N and F_T),

cohesive forces (F_c) and Eq. (1). The corresponding torque on each particle is the sum of the moment of the tangential forces (F_T) arising from inter-particle contacts (Eq. (3)). Hence, the forces and torques acting on each of the particles will be calculated as follows:

$$\sum F_i = m_i g + F_N + F_T \qquad (1)$$

$$\sum T_i = r_i \times F_T \qquad (2)$$

The flow chart of the simulation process is given in figure 2. Initially the force on each particle is given by the sum of gravitational and inter-particle (normal and tangential F_N and F_T) as indicated in Eq. (1). The normal forces (F_N) and the tangential forces (F_T) for inter-particle or particle-wall collision were calculated with the "latching spring model" and "incrementally slipping model" respectively, developed by Walton and Braun [35]. The normal forces between pairs of particles in contact are defined using a spring with constants K_1 and K_2 for compression and recovery: $F_N = K_1\mu_1$ (for compression), and $F_N = K_2(\mu_1 - \mu_0)$ (for recovery). Here μ represents the overlap during contact. The degree of inelasticity of collisions is incorporated in this model by including a coefficient of restitution $e = (K_1/K_2)^{1/2}$ ($0<e<1$, where $e=1$ implies perfectly elastic collision with no energy dissipation, $e=0$ implies completely inelastic collision

The major computational tasks of DEM in each time step are as follows: (i) add/delete contact between particles thus updating neighbor lists, (ii) compute contact forces from contact properties, (iii) sum all forces and torques on particles and update position and (v) determine the trajectory of the particle by integrating Newton's laws of motion (second order scalar equations in three dimensions) using a central difference scheme, Verlet's Leap Frog method. The DEM code was written in C language and was performed in 32 and 64 bit Linux clusters.

Grady [36] derived a simple model of dynamic fragmentation by balancing the available kinetic energy against the energy associated with the new surface created in the process. The fragments are supposed to be stress free upon their formation so that all the stored elastic energy is available for fragmentation. In this the paper, the model proposed by Djordevic [20] and Grady [36] was adopted to describe fragmentation in impact mills. However the breakage algorithm

was modified such that the particle breaks only when the contact forces between granule/hammer or granule/wall exceed the breakage force obtained from DMA studies.

Based on Grady's model the particle size of fragment following fracture is given in equation 4

$$D = \left(\frac{4.472 \times K_c}{\rho V_p S_r} \right)^{2/3} \qquad (4)$$

D is the diameter of the resultant progeny particle, K_{lc} is fracture toughness of material, (Pa $m^{0.5}$) V_p is propagation velocity (m/s) of longitudinal elastic waves in the material, S_r is the induced strain rate. The strain rate in the sample is defined as the difference in particle velocity at the point of impact and at the opposite end along the length of the sample.

The strain rate is calculated from the rotational velocity of the impeller and the radial distance between the center of the rotation and the impact point.

$$S_r = \frac{V_{pp1} - V_{pp2}}{L} \qquad (5)$$

Where V_{pp1} and V_{pp2} are particle peak velocities at the impact point and at the free end of the particle respectively, and L is the diameter of the particle sample (m). The peak velocity V_{pp1} at the interface of the impeller and particle is equal to the impeller velocity V_i, and that V_{pp2} at the free end of the particle sample is of the opposite sign of V_{pp1}, thus the strain rate can be represented [20] as

$$S_r = \frac{2V_i}{L} \qquad (6)$$

Following fragmentation, the resultant particles are considered as spheres, obeying the laws of conservation of total mass and momentum [37]. Besides predicting the particle size, DEM simulations were performed to illustrate the effect of speed, feed rate and impeller wall tolerance. The value of DEM parameters are given in table 1

4. Results and Discussion

4.1. Experimental Results

4.1.1. Breakage force and Creep

Granule breakage on impact with a rigid surface depends upon material properties of the granule and the impact surface. It is plausible that for any given granule there is a specific force required to cause the granule to fracture under dynamic conditions and a different specific force required under static compression. This belief in the inequality between static failure force and dynamic failure force is largely due to the acceptance of creep (permanent deformation caused when certain materials experience low static forces) and high strain rate effects(increased resistance to deformation in some materials when exposed to high forces over very short periods) [38]. Also, in a rotating bed depending upon mill speed and mass flow rate not all particles maybe subjected to forces of similar magnitude. To investigate these effects, the breakage force using DMA was determined. As illustrated in Fig. 3a, this force was found to vary between 6-7 N for the granules. To evaluate the effect of creep, the non-pareils were subjected to at most three cyclic loading and unloading tests. As demonstrated in Fig. 3b when the material was subjected to smaller cyclic static forces, the breakage force did not change and the granule fractured completely around 7N. Thus in this case there was no permanent deformation that could cause the material to fail under lower loads when subjected to static forces. Moreover the breakage force did not change upon varying the loading rate from 4 N/min for the first cycle and 6 N/min for the next cycle depicted in figure 3c. Thus a creep cycle (Fig. 3b) and high strain rate effect (Fig. 3c) do not seem to affect the breakage force of the material. An initial hysteresis was observed in the first cycle that disappeared in the subsequent cycles. This hysteresis might be due to surface asperities on particles which deform plastically upon loading and loading.

4.1.2. Parametric Studies

4.1.2.1. Effect of Feed rate

The feed rate determines the hold up of material in sizing chamber. For each impeller speed, there exists a value of feed rate above which the chamber becomes flooded. At high feed rates, the hold-up of mill may increase beyond its nominal capacity thereby compromising its

comminution rate. As a consequence, the particle size distribution at the outlet becomes coarser. To understand the effect of feed rate, experiments were performed at three different levels; 60g/min, 120g/min and 200g/min while the blades were rotated at 600 rpm and 1140 rpm. The clearance between the stationary and rotating knives was kept constant at 1.9 mm. As depicted in Fig. 4, as the feed rate increased from 60g/min to 200g/min the fragmentation rate declined as there was a significant decrease in d_{90} (≈ 8 fold). Hence, the larger particles are not rapidly being broken which manifests into a decline in d_{90} and d_{50} rate. Thus, the mechanism of comminution changed more towards attrition from impact. This can also be concluded from the rate of decline of d_{10}. As the feed rate was increased from 60g/min to 200g/min the decline in d_{10} increased to by at least three times. Thus, because of low impeller speed and higher feed rate there is accumulation of the particles in the milling chamber. This can consequently lead to flood feed conditions. As a result same particles might come in contact with the blades resulting in production of fines.

A similar result was observed at 1140 rpm. As the feed rate was increased from 60g/min to 200g/min Fig. 5 the fragmentation rate decreased (≈ 2.75 fold) with respect to d_{90}, however this decline was not as steep as 600 rpm. Moreover the change in d_{10} rate was not very steep (≈ 1.2 fold). Thus, because of higher impeller speed rapid, fragmentation of particles dominates even at higher feed rates. This suggests that no flood feed conditions were observed at 1140 rpm under the current experimental parameters.

4.1.2.3. Effect of blade clearance

The blade clearance is determined by the intrusion of four knives from the inner wall of mill. A very large distance can result in continuous rolling of particles and hence significantly reduce the rate of size reduction. A very small tolerance on the other hand can result in unwarranted fines formation. For these experiments, a clearance of 1.9 mm and 3.6 mm was chosen. As shown in Fig.6, the size reduction rate declined with increasing impeller wall tolerance. The effect seemed to be more substantial at 600 rpm than at 1140 rpm. Owing to the lower impact velocities particle–wall fragmentation may not contribute significantly to milling at 600 rpm. This change in clearance can also influence the mechanism of size reduction, perhaps changing it from impact to a combination of rolling and attrition and hence reducing the overall milling rate.

4.2. Simulations

The flow and fragmentation of particles in the Wiley mill is simulated using DEM as described in section 3. Initially 30,000 spherical particles with material properties described in table 1 are deposited in the hopper with a closed outlet. The impeller chamber and the blades were made by gluing particles together. After deposition, particles are discharged from hopper into the mill. The blades are then set into motion at prescribed velocity of 600 rpm and/or 1140 rpm. Color-coding is based on particle size in order to visually track the evolution of size in simulations. Figure 7 illustrates the entire simulation model contour chart represents size of particles in meters.

4.2.1. Effect of impeller speed

As presented in the simulation axial snapshots in Fig. 8A and Fig. 8B, size reduction is slower at 600 rpm than at 1140 rpm. This is apparent from the larger number of broken particles in the range of 600 to 350 μm at 1140 rpm. The parent particle are red in color as opposed to the broken particles which range from orange (900 μm) to blue (300 μm) as fragmentation occurs. This effect is due to the greater strain rate in accordance to Grady‘s algorithm, experienced by the particles which results in a smaller particle size at 1140 rpm. It is evident. that the velocity (Fig. 9) of particles was higher throughput the chamber for particles at 1140 rpm which results in rapid fragmentation.

4.2.2. Effect of feed rate

Similar to the experimental design, the effect of feed rate on milling was studied at 1140 and 600 rpm. As illustrated from the simulation snapshots (Fig. 10), at 600 rpm the size distribution become coarser as the feed rate is increased. It increased from (580-710μm) at 60 g/min to around (750-900 μm) at 200 g/min. Moreover at 200 g/min the size distribution was also slightly bimodal (Fig 11). This can be as a result of flood feed conditions due to which the movement of powder bed gets impeded and same particles can come in contact with hammers. To further explore the effect of feed rate the average velocity at different time points were compared (figure 12). In these snapshots, the particles have been color coded for velocity. From the snapshots one can observe that as the feed rate was increased the velocity of the particle decreased gradually

with time. Thus, the higher feed rates perhaps decrease the mean free path length and hence reduce comminution rate.

At 1140 rpm (Fig 13), the lower feed rates generated a smaller size distribution (370-580μm). As the feed rate was increased to 200 g/min the distribution tends to become coarse (Fig. 14). However unlike the effect at 600rpm, no flood feed condition was observed at higher feed rates. This suggests that due to greater centrifugal forces movement of powder bed is not obstructed and hence there is no much accumulation of particles.

4.2.3. Effect of impeller-wall clearance

The effect of impeller wall tolerance Fig. 15 was approximated by creating short hammers (3200 glued particles) thereby providing a tolerance of 4.8 mm approximately. The operational speed during the simulation has been kept constant at 600rpm and 1140 rpm. As the impeller tolerance was increased the comminution rate slowed down Fig. 16. The snapshots indicate that there is accumulation of particles near the base of mill. This is because as length of blade is reduced the particles don't strike the surrounding chamber/blade easily especially at lower speeds as centrifugal forces go down. Thus, the powder bed tends to collapse easily. Since at 600 rpm the size reduction rate is slow, the effect of clearance was more substantial than at 1140 rpm. These results underscore the importance of equipment design which can be easily studied by DEM simulations.

5. Model verification

As the parent particle size in simulation (2mm) differs from experimental (1.3 mm) a dimensionless size was computed and plotted against time. The simulation data for earlier time period displays a trend similar to experimental parameters viz. effect of feed rate and blender speed (Fig. 17). In some cases, deviations are observed and are mainly attributed to nature of the soft particle algorithm. In these studies, the stiffness of the particles was reduced to obtain a reasonable time-step as it involves smaller particles; thereby resulting in very minute time steps. Nevertheless, the simulations could capture the differences observed in milling as the operation parameters were varied.

6. Conclusions

Experimental and DEM simulation model have been employed to study comminution of granular bed in a Wiley mill. Granular flow and mechanical properties of lactose are taken into account in order to develop a fundamental understanding of their effect on milling performance. DEM simulations were used to examine the breakage rate in the granular materials processed in a lab scale Wiley mill. It was found that the speed and mass flow rate play an important role in comminution of powder bed. Very high mass flow rates resulted in flood feed conditions at lower speeds that can cause the mode of breakage to change from fragmentation to attrition. Increasing the impeller wall clearance reduced particle size reduction at both speeds. However the effect was more significant at lower speeds. In these simulations, the breakage algorithm does not depict the effect of attrition on particle size distribution as it does not account for mechanism of surface removal. However, the simulations could still qualitatively capture the difference in breakage behavior upon changing the experimental conditions. This suggests that simulations can be used to direct future experimental and equipment design to provide a better understanding of the process. To facilitate a priori prediction warrants the need to extend the simulation model to other materials.

7. Acknowledgement

We gratefully acknowledge the support of NSF-Center for Pharmaceutical Processing Research (CPPR) for funding this project.

8. References

1. Bridgewater, J., The dynamics of granular materials – towards grasping the fundamentals. Granular Matter, 4(2003), 175–181.
2. Meier, S.W., R.M. Lueptow, and J.M. Ottino, A dynamical systems approach mixing and segregation of granular materials in tumblers. Advances in Physics, 56(2007), 757-827
3. Geldart, D., Powder Processing - The Overall View, in Principles of Particle Technology, John Wiley & Sons Ltd,1-7(1990).
4. Muzzio, F.J., T. Shinbrot, and B.J. Glasser, Powder technology in the pharmaceutical industry: the need to catch up fast. Powder Technology, 124(2002),1-5
5. A.J. Jounela, P.J. Pentikainen, A. Sothmann. Effect of particle size on the bioavailability of digoxin. European Journal of Clinical Pharmacology 8, (1975), 365-370.
6. M. Vogt, K. Kunath, J.B. Dressman, Dissolution enhancement of fenofibrate by micronization, co-grinding and spray-drying: Comparison with commercial preparations. European Journal of Pharmaceutics and Biopharmaceutics 68, (2008), 283-288.
7. G.G. Liversidge, K.C. Cundy, Particle size reduction for improvement of oral bioavailability of hydrophobic drugs: I. Absolute oral bioavailability of nanocrystalline danazol in beagle dogs. International Journal of Pharmaceutics 125, (1995), 91-97.
8. L. Vogel, W. Peukert, Breakage behaviour of different materials—construction of a mastercurve for the breakage probability. Powder Technology 129 (2003) 101– 110
9. M. Meier, E. John, D. Wieckhusen, W. Wirth, W. Peukert, Influence of mechanical properties on impact fracture: Prediction of the milling behaviour of pharmaceutical powders by nanoindentation, Powder Technology 18 (2009) 301–313.
10. P.W. Clearly, Predicting charge motion, power draw, segregation, wear and particle breakage in ball mills using discrete element method, Miner. Eng., 11, (1998), 1061-1080.
11. H. Watanbe, Critical rotation speed for ball-milling, Powder Technology, 104, (1999), 95-99.
12. B.K. Misra, R.K. Rajamani, Simulation of charge motion in ball mills, Part 2: numerical simulations, Int. J. Miner. Processing, 40, (1994), 187-197.

13. O. Hlungwani, J. Rikhotso, H. Dong, m.H. Moys, Further validation of DEM modeling of milling: effects of linear profile and mill speed, Minerals Engineering, 16, (2003), 993-998.
14. L.G. Austin, P.T. Lucker, A simulation model for air-swept ball mill grinding coal, Powder Technology, 38, (1984), 255-266
15. C.C. Kwan, H. Mio, Y.C. Chen, Y.L. Ding, F. Saito, D.G. Papadopoulos, A.C. Benthem, M. Ghadiri, Analysis of the milling rate of pharmaceutical powders using distinct element method, Chemical Engineering Science, 60, (2005), 1441-1448.
16. G.M. Campbell, P.J. Bunn, C. Webb, S.C.W. Hook, On predicting roller mill performance, Part II. The breakage function, Powder Technology, 115, (2001), 243-255.
17. L. Austin, A preliminary simulation model for fine grinding in high speed hammer mills, Powder Technology, (2004), 240-252.
18. C. Gotsis, L.G. Austin, Batch grinding kinetics in the presence of a dead space as in a hammer mill, Powder Technology 41 (1985) 91–98.
19. L. Vogel, W. Peukert, From single particle impact behavior to modeling of impact mills, Chemical Engineering Science 60 (2005) 5164–5176.
20. N. Djordjevic, F.N. Shi, R.D.Morrison, Applying discrete element modeling to vertical and horizontal shaft impact crushers, Minerals Engineering 16 (2003) 983–991.
21. M. Khanal, W. Schubert, J. Tomas, Discrete element method simulation of bed comminution, Minerals Engineering 20 (2007) 179–187.
22. C. Thornton, K.K. Yin,M.J. Adams, Numerical simulation of the impact fracture and fragmentation of agglomerates, Journal of Physics D: Applied Physics 29 (1996) 424–435.
23. Thornton, M.T. Ciomocos, M.J. Adams, Numerical simulation of agglomerate impact breakage, Powder Technology 105 (1999) 74–82.
24. H. Mio, J. Kano, F. Satio, Scale-up method of planetary ball mill, Chemical Engineering Science 59 (2004) 5909–5916.
25. P.A. Cundall, O.D.L. Strack, A discrete numerical model for granular assemblies, Geotechnique 29 (1979) 47.
26. L.M. Tavares, R.P. King, Single-particle fracture under impact loading, International Journal of Mineral Processing 54 (1998) 1–28.

27. ASTM, in: Standard drop shatter test for coal, Annual Book of ASTM Standards, 5.05, 1991, p. 214.
28. S. Antonyuk, J. Tomas, S. Heinrich, L. Mörl, Breakage behaviour of spherical granulates by compression, Chemical Engineering Science 60 (2005) 4031–4044
29. R. Pitchumani, G. Meesters, B. Scarlett, Breakage behaviour of enzyme granules in a repeated impact test, Powder Technology 130 (2003) 421–427.
30. Y. Chen. Energy-Based Analysis of Milling a-Lactose Monohydrate, Journal of Pharmaceutical Sciences 93 (2004) 886–895.
31. S. Dippel, G.G. Batrouni, D.E. Wolf, Collision-induced friction in the motion of a single particle on a bumpy inclined line, Physical Review E 54 (1996) 6845.
32. P.S. Thompson, G.S. Grest, Granular flow: friction and the dilatancy transition, Physical Review Letters 67 (1991) 1751.
33. G.H. Ristow, Dynamics of granular material in a rotating drum, Europhysics Letters 34 (1996) 263.
34. B. Chaudhuri, A. Mehrotra, F.J. Muzzio, M.S. Tomassone, Cohesive effects in powder mixing in a tumbling blender, Powder Technology 165 (2006) 103–112.
35. O. Walton., R. Braun. Viscosity, granular-temperature and stress calculations for shearing assemblies of inelastic, frictional disks.J.Rheol.30 (1986) 949–980.
36. D.E. Grady, Fragmentation under impulsive stress loading, in: W.L. Fourney, et al., (Eds.), Fragmentation by blasting, Society for Experimental Mechanics, Connecticut, USA, 1985, pp. 63–72.
37. T. Poschel, T. Schwager, in: Computational Granular Dynamics: Model and Algorithms, Springer Verlag, Berlin, Germany, 2005, p. 110.
38. R.E. Maxim, A.D. Salman, M.J. Hounslow, Predicting dynamic failure of dense granules from static compression tests, International Journal of Mineral Processing 79 (2006) 188–197.

Tables

Table 1.The Parameters used in DEM simulations

DEM Parameters	Values
Total number of particles	30000-90000
Size	2 mm- 600 μm
Coefficient of restitution Particle/particle	0.5
Coefficient of restitution Particle/wall	0.5
Friction coefficient: particle/particle	0.5
Friction coefficient: particle/wall	0.2
Fracture toughness	0.5-0.8 MPa $m^{0.5}$
Time step	$1.0 * 10^{-6}$

Table 2. Conditions examined for the milling experiments

Speed (rpm)	600, 1140
Clearance (mm)	1.9, 3.6
Feed rate (g/min)	60 ,120, 200

Figures

Figure1a: Compression clamp of Dynamic Mechanical Analyzer

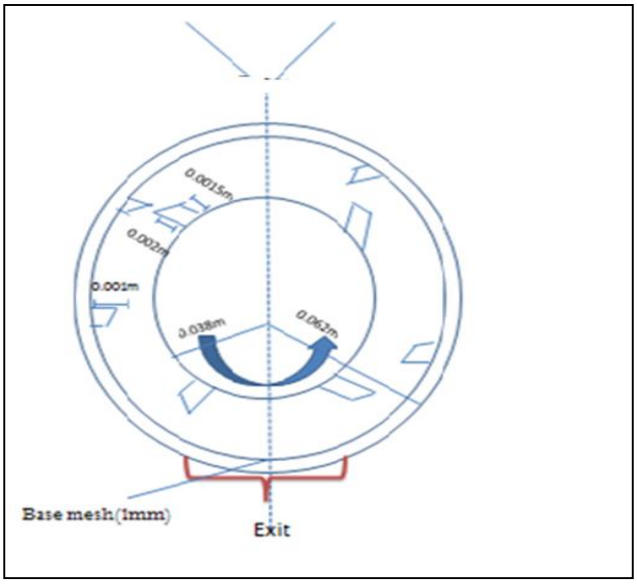

Figure1b: Schematic of Wiley Mill

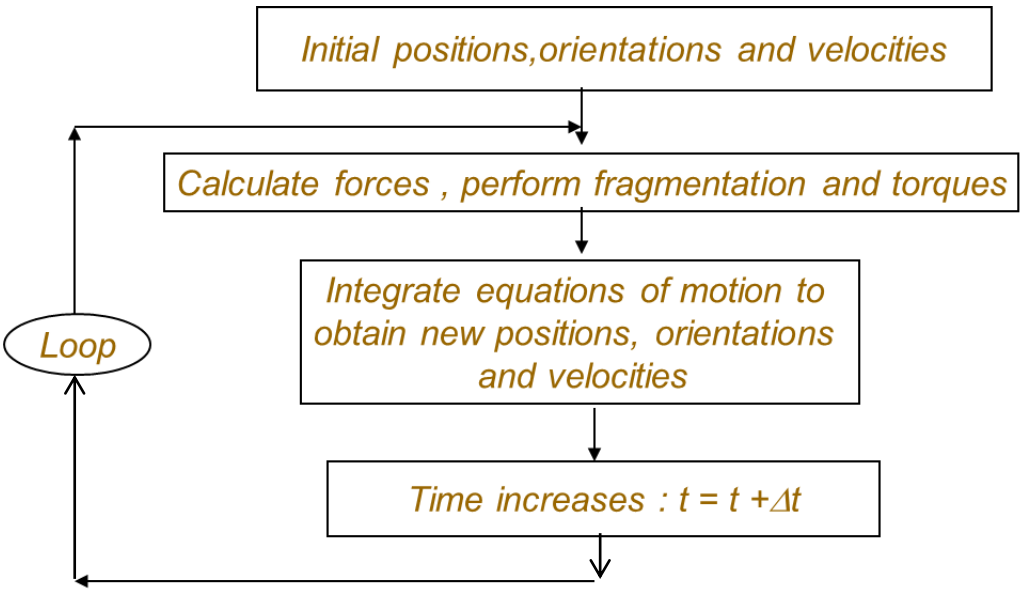

Figure 2. Flow chart for DEM simulations

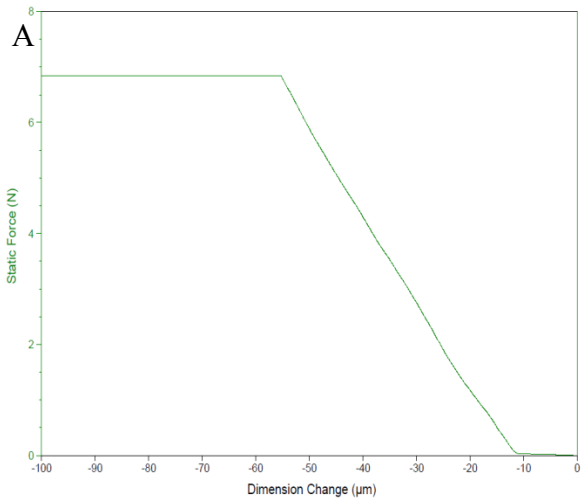

Figure 3A: Breakage forces under static compression

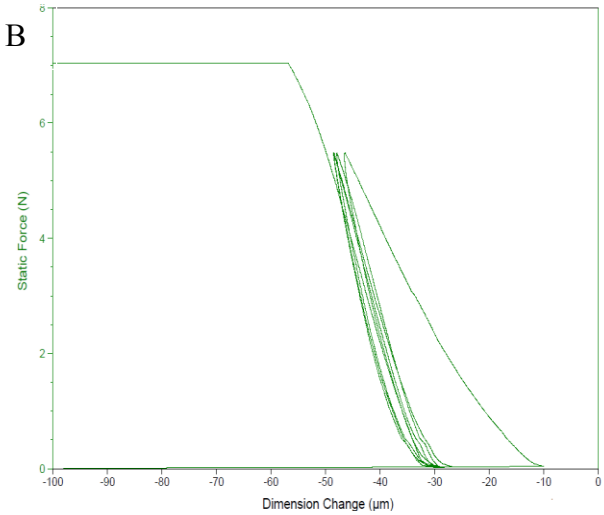

Figure 3B: Force displacement behavior under cyclic loading and unloading

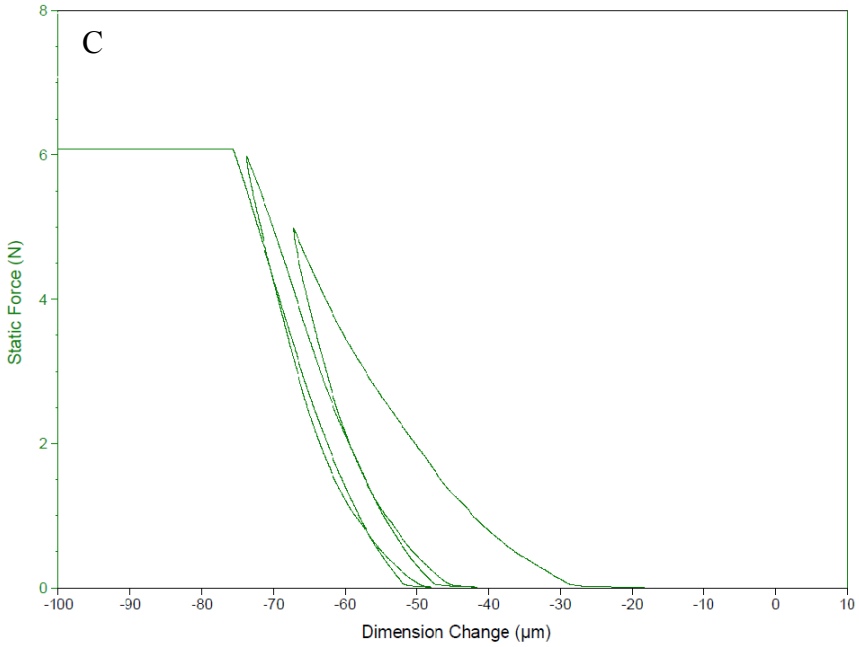

Figure 3C: Force displacement behavior under different loading rates

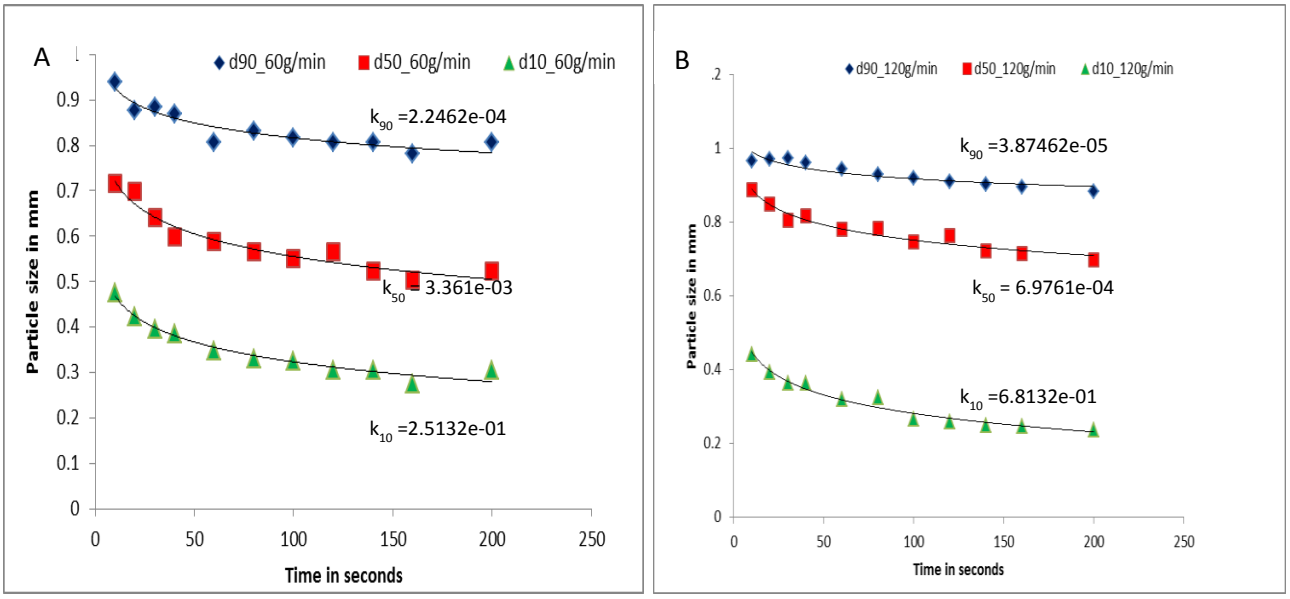

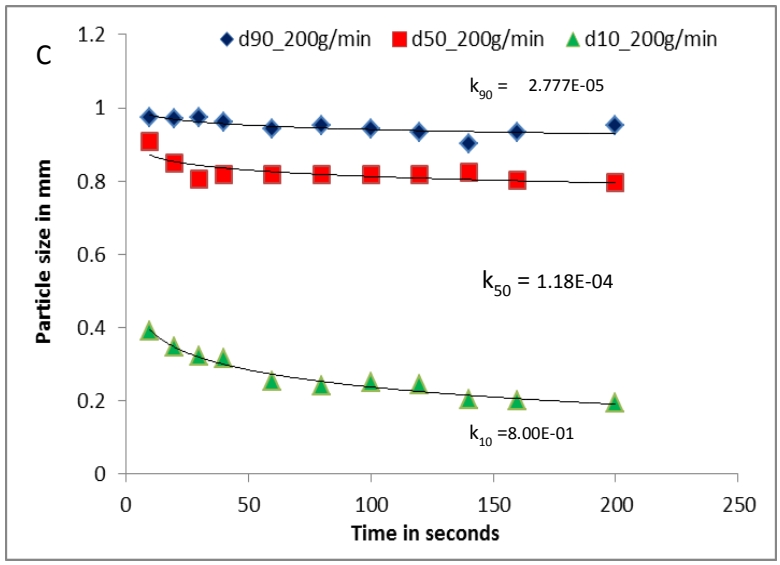

Figure 4 Size reduction behavior at impeller speed of 600 rpm under feed rate A) 60 g/min B) 120 g/min C) 200 g/min

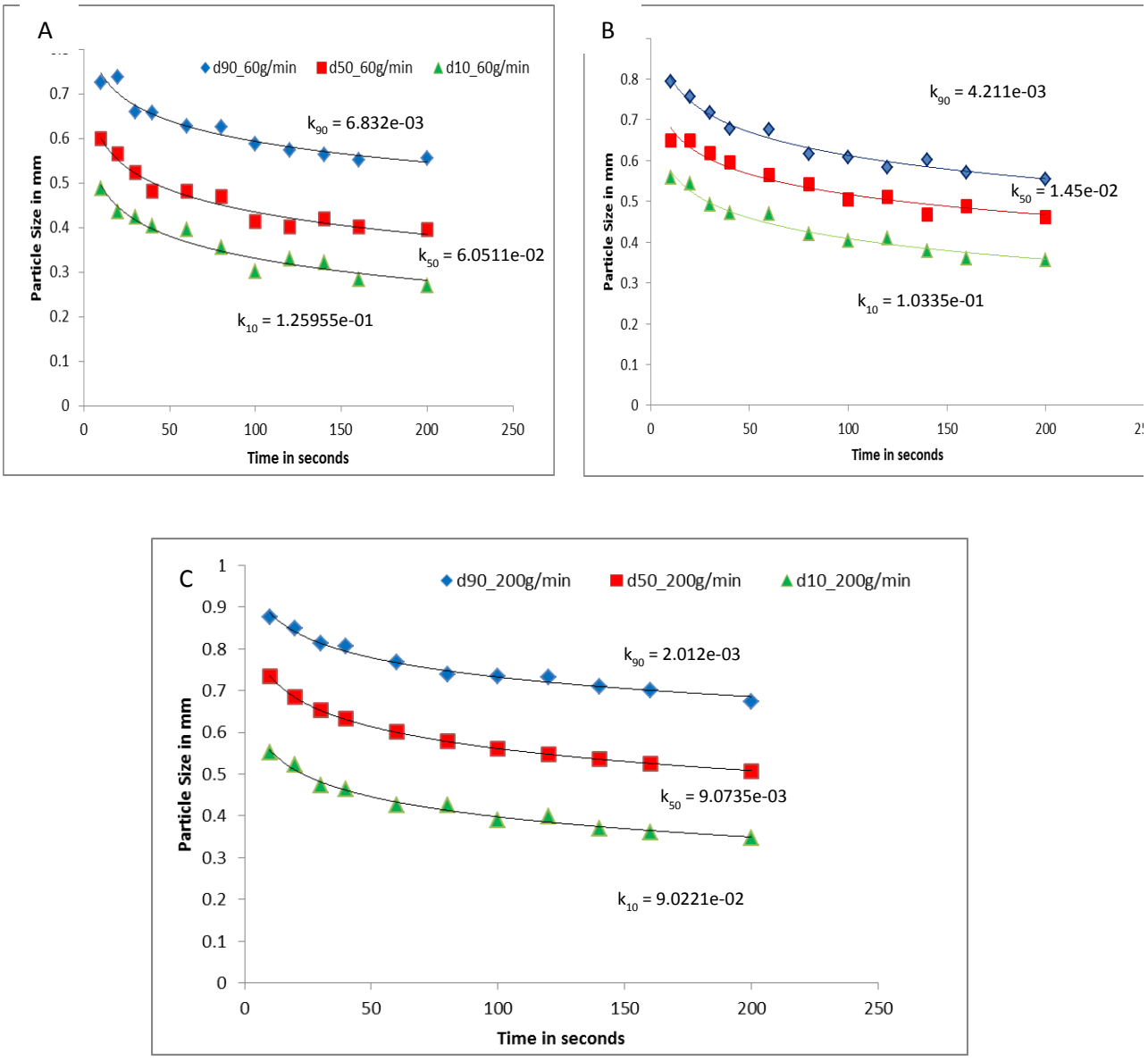

Figure 5 Size reduction behavior at impeller speed of 1140 rpm under feed rate A) 60 g/min B) 120 g/min C) 200 g/min

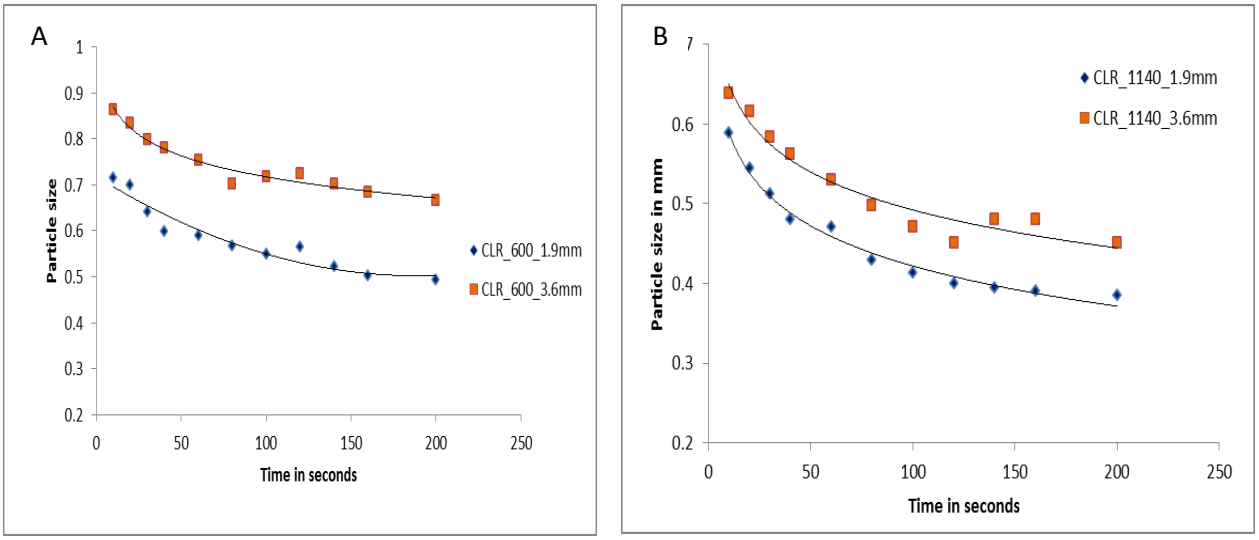

Figure 6 Effect of impeller wall tolerance on size reduction at A) 600 rpm B) 1140rpm

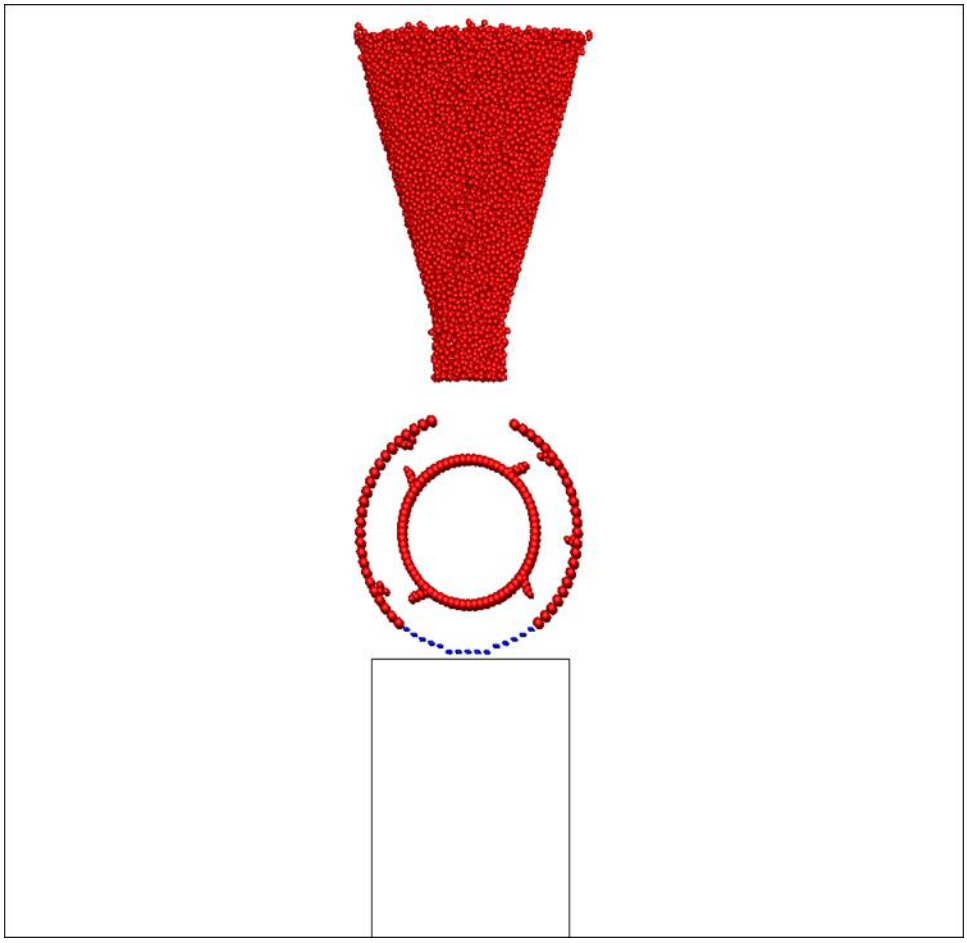

Figure 7: Full frame of Wiley hammer mill

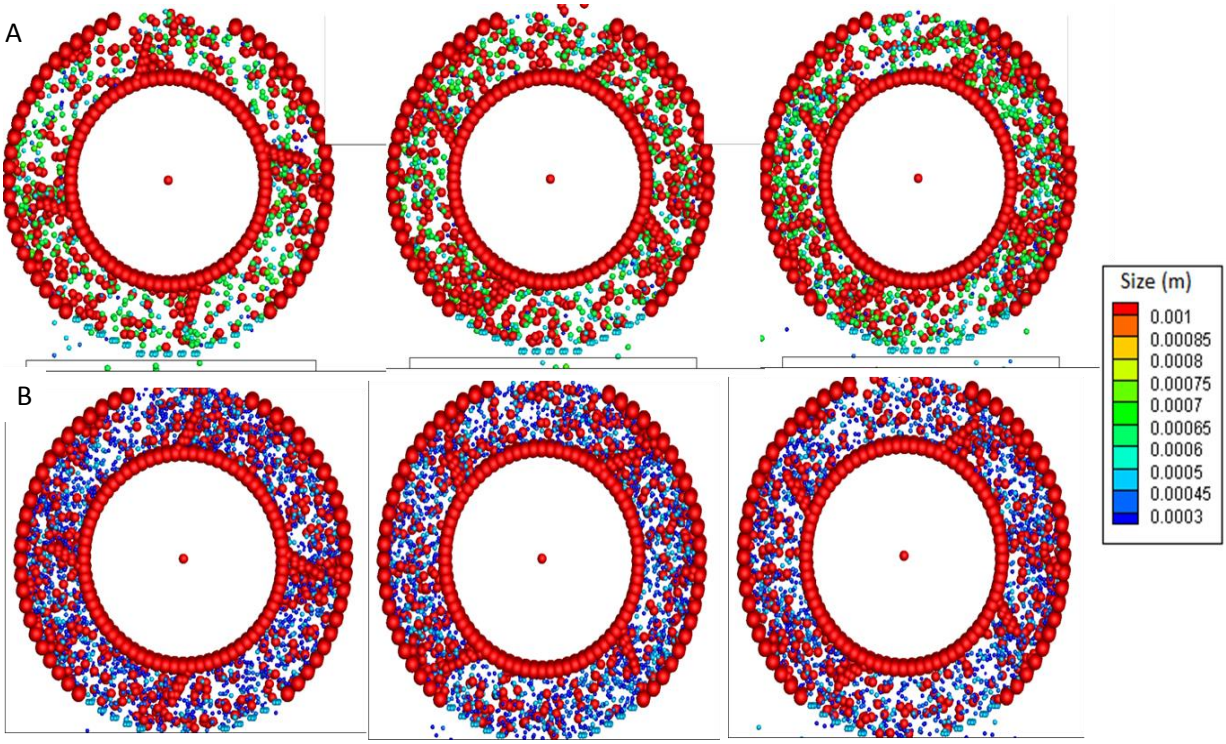

T =5.0000 s T =10.0000 s T = 15.0000 s

Figure8 Temporal evolution of particle size under impeller speed of A) 600 rpm B) 1140 rpm

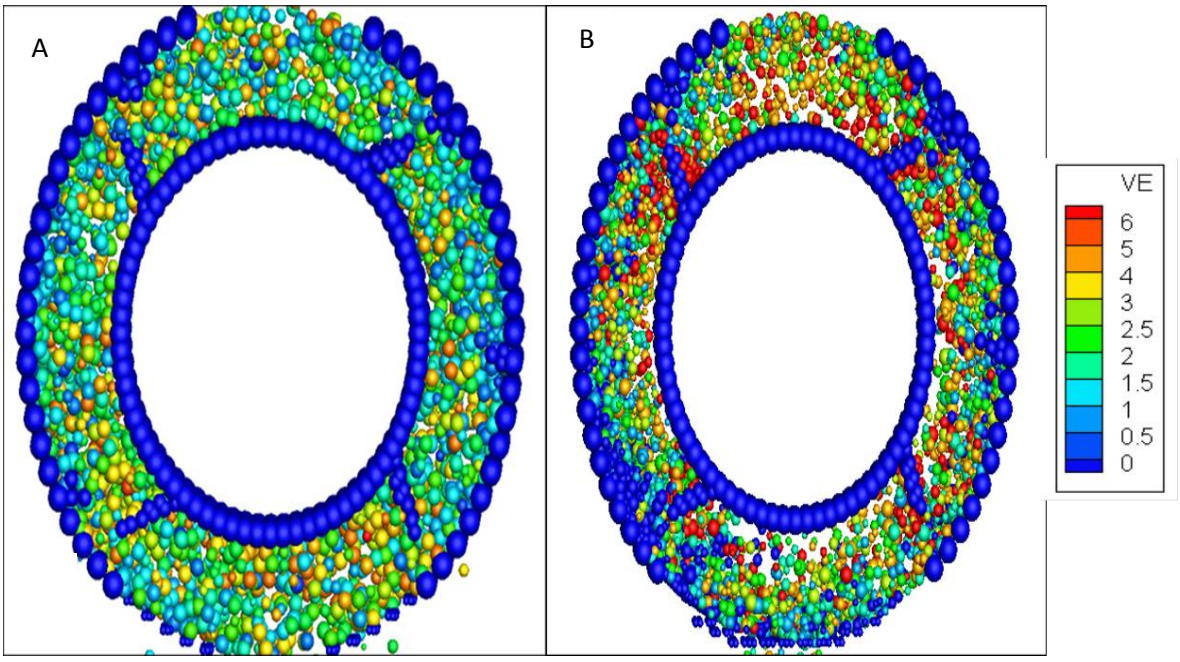

T=15.0000 s T=15.0000 s

Figure 9: Spatial distribution of velocity under impeller speed A) 600 rpm B) 1140 rpm

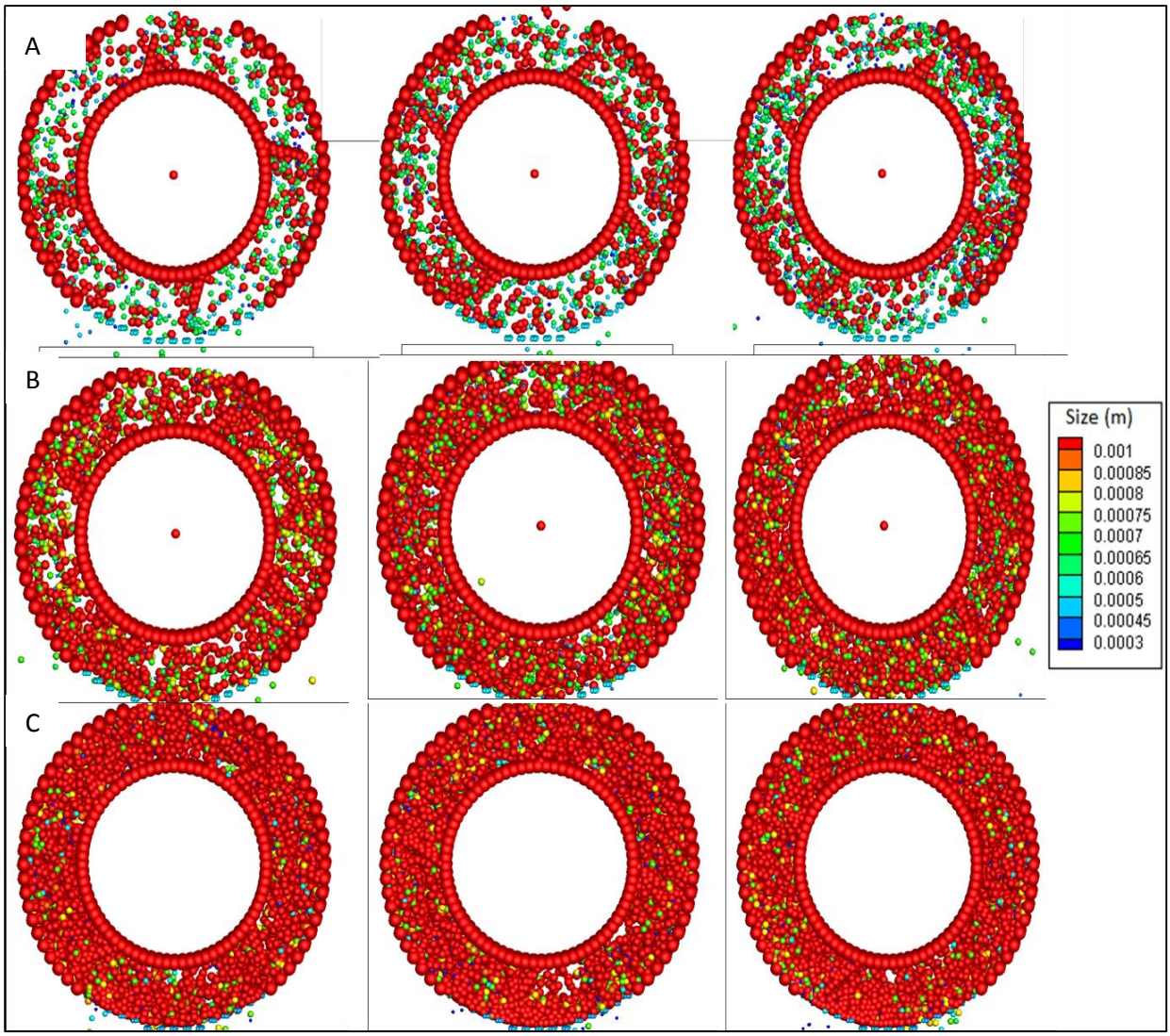

T=5.0000 secs T=10.0000 secs T=20.0000 secs

Figure 10: Temporal evolution of particle size under impeller speed of 600rpm A) 60 g/min B) 120 g/min C) 200 g/min

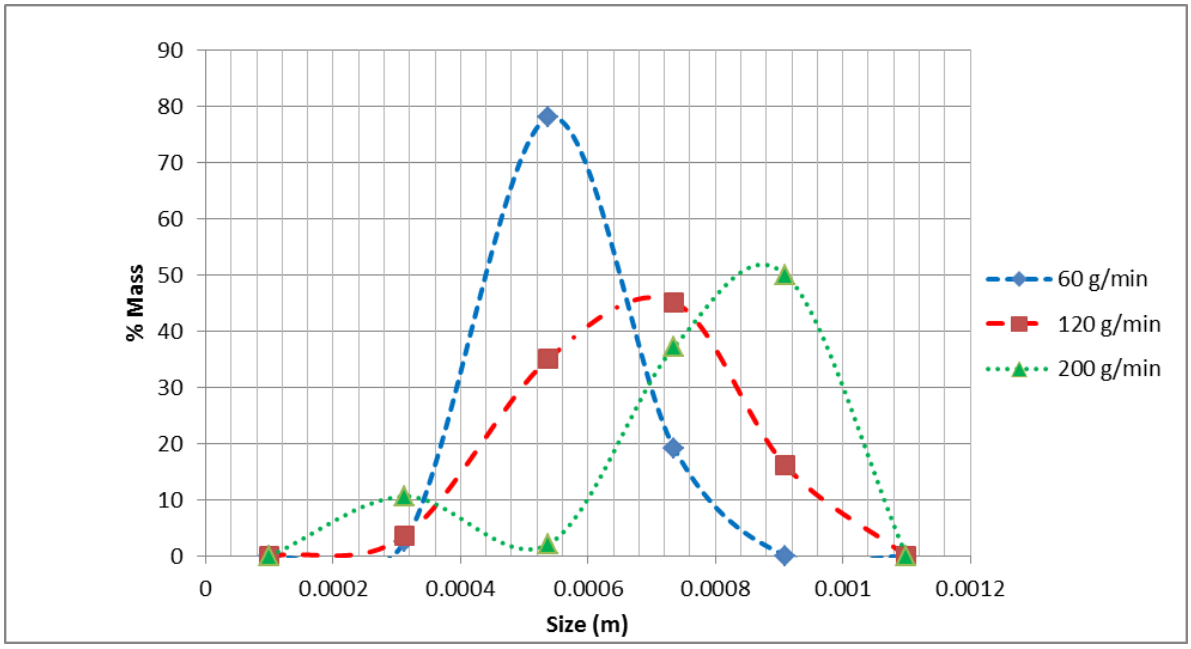

Figure 11: Particle size distribution at different feed rates for an impeller speed of 600rpm

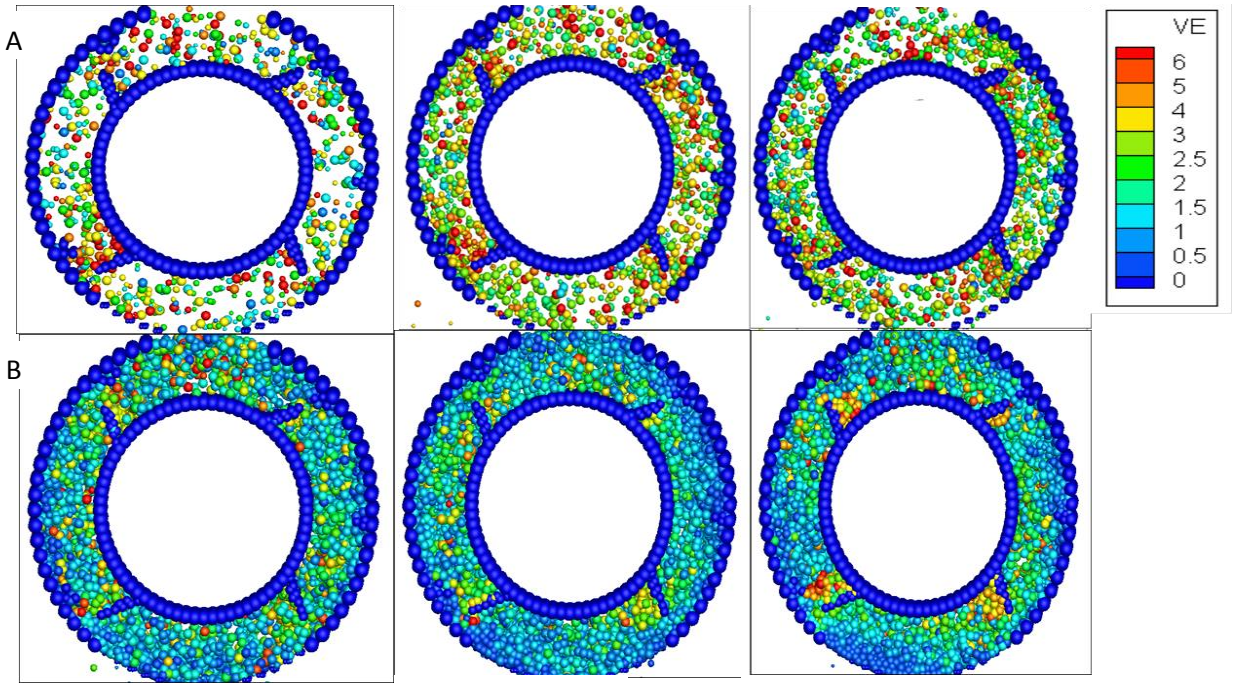

Figure 12: Temporal distribution of velocity under impeller speed of 600rpm

A) 60g/min B) 200 g/min

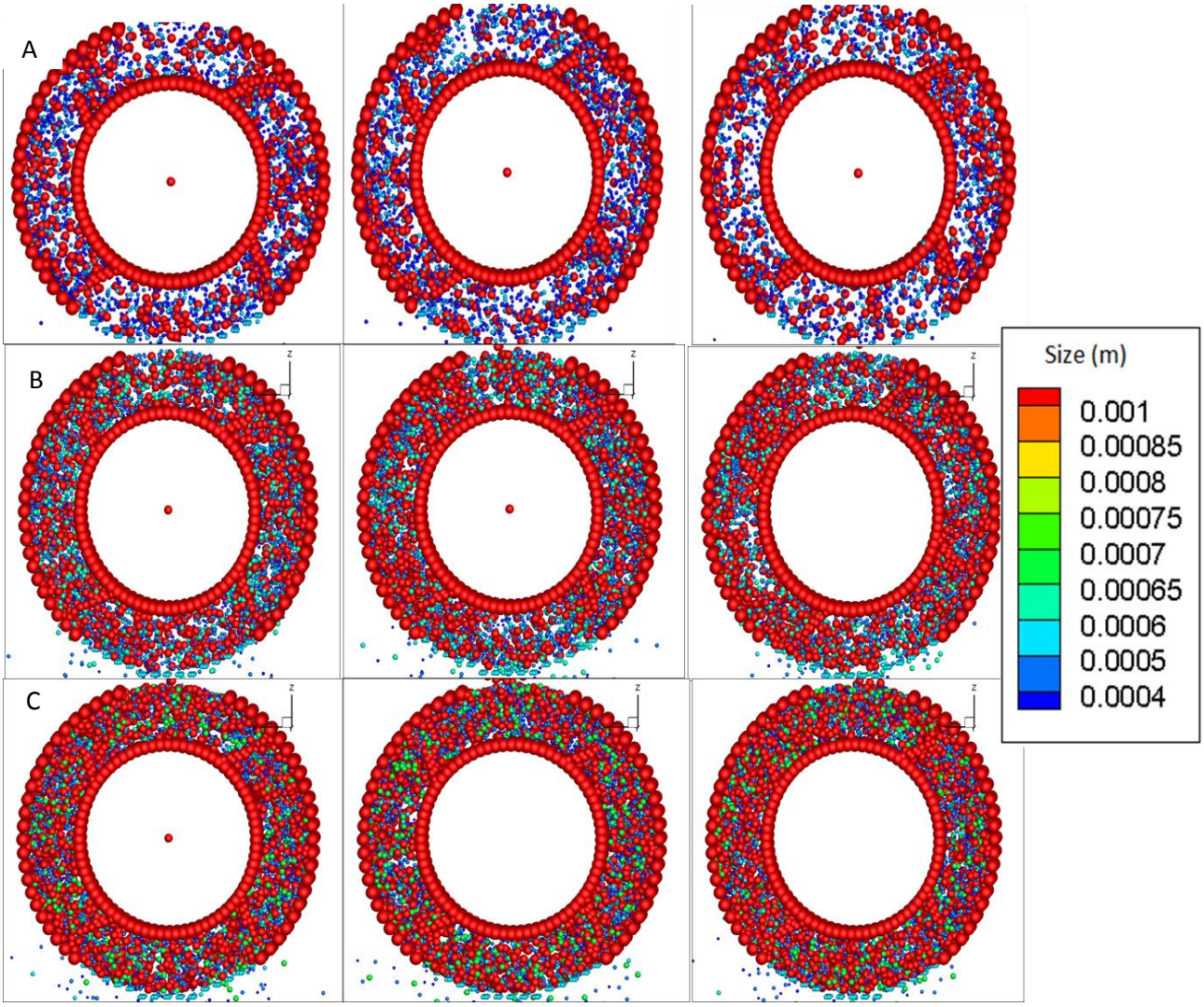

Figure 13: Temporal evolution of particle size under impeller speed of 1140rpm A) 60g/min B) 120 g/min C) 200 g/min

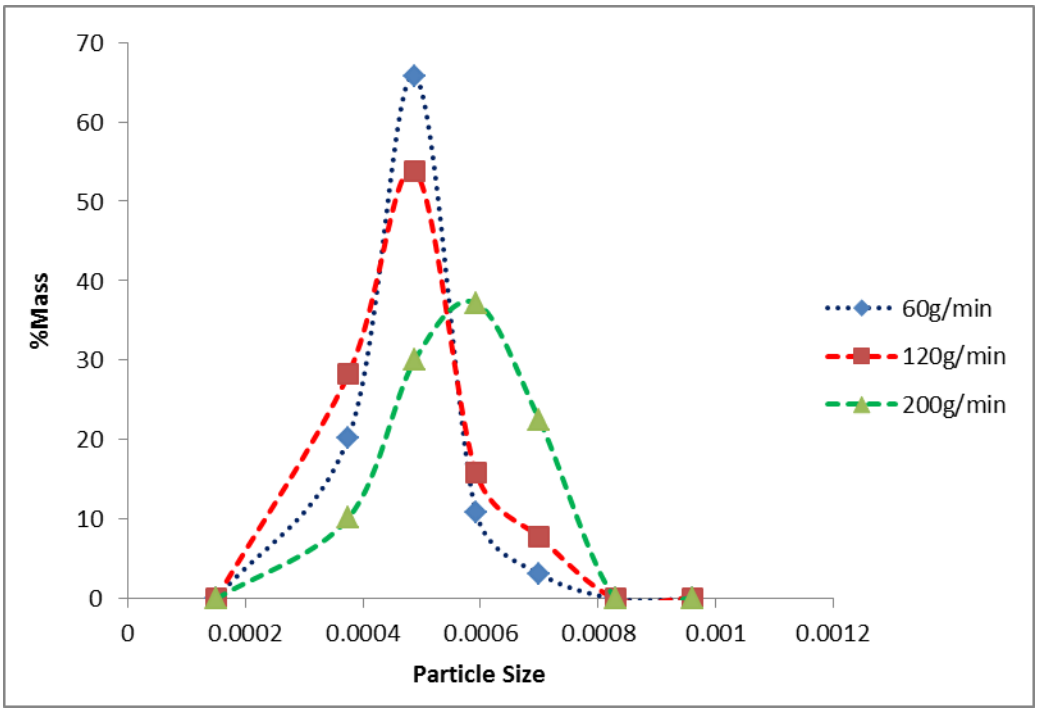

Figure 14: Particle size distribution at different feed rates for an impeller speed of 1140 rpm

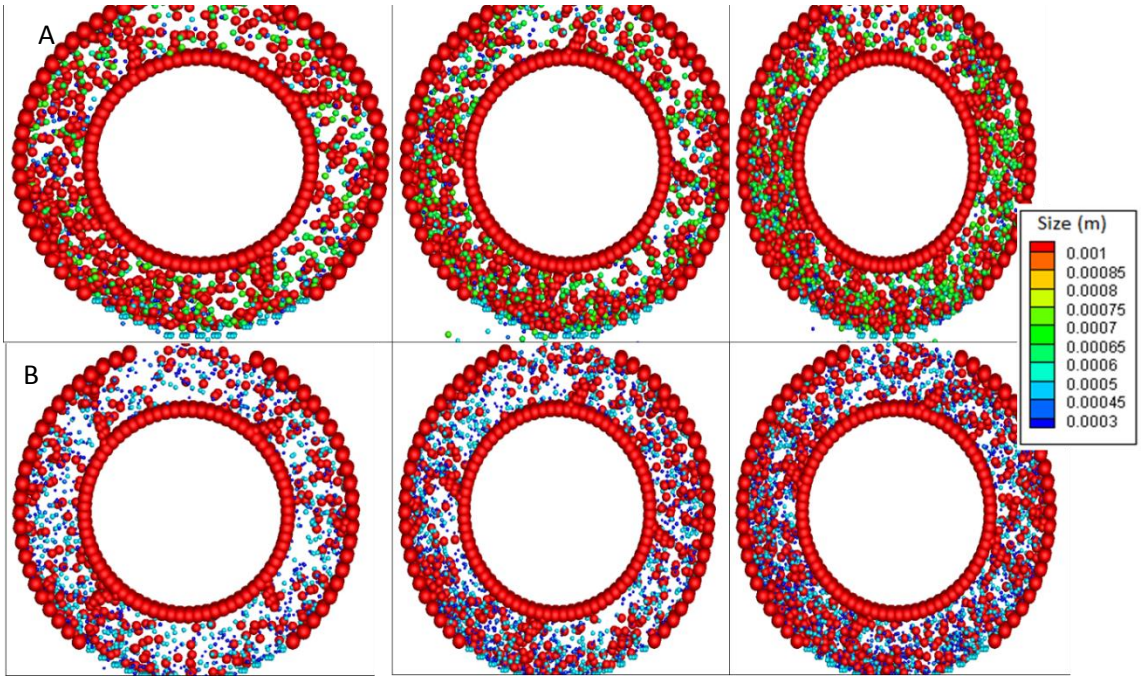

Figure 15 Temporal distribution of particle size at impeller wall tolerance 4.8 mm A) 600 rpm B) 1140 rpm

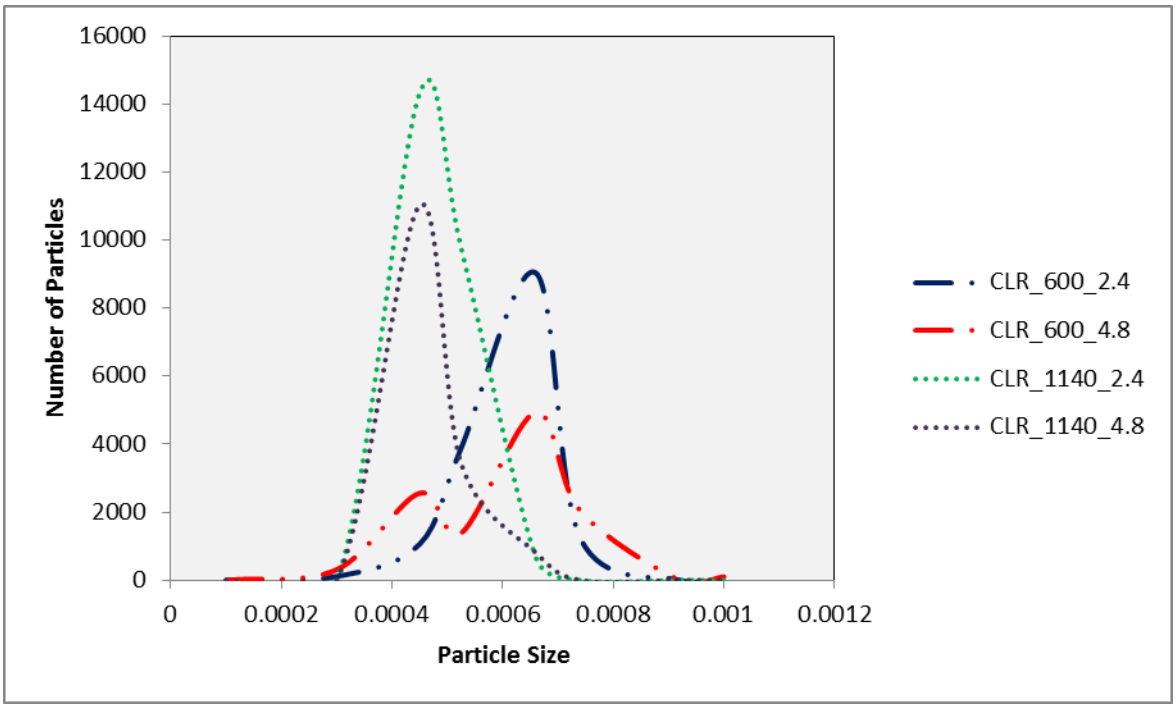

Figure 16. Effect of impeller wall tolerance on size reduction at 600 rpm and 1140 rpm

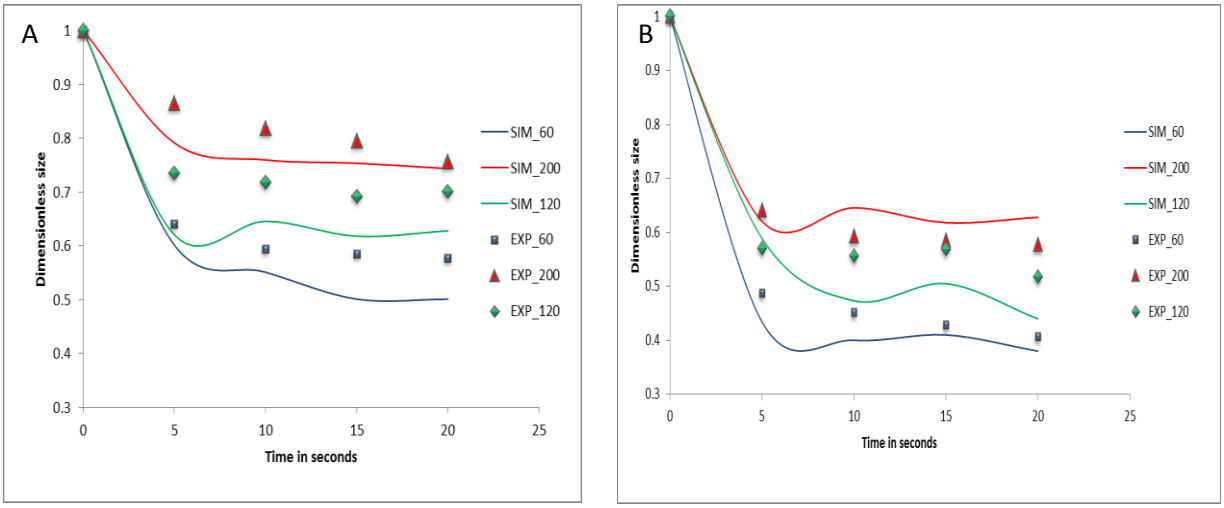

Figure 17 Comparison of DEM simulations and experimental data A) 600 rpm B) 1140 rpm

Chapter 8

Summary and Future Studies

Manufacturing is a critical step in procuring safe medication since it comprises of series of complex operations before the drug product is marketed. An improved understanding of these unit operations with the aid of first principle models could help in circumventing some of process development concerns. The focus of this dissertation has been triboelectrification and particle size reduction during pharmaceutical processing. Thus, the objective of this study was to elucidate and address the effect of process variables and material properties by employing experimentally validated discrete element model. Triboelectrification of powders is a multifaceted process that has been recognized to play a substantial role in powder processing. A review of current experimental and numerical methods employed for measuring electrostatic charges has been outlined in **Chapter 2**. Experimental evidence suggests that cleanliness and environmental conditions play an important role and should be carefully controlled. The need for reliable experimental and numerical models has also been emphasized. A brief description has been provided of the current DEM models used in quantifying tribocharging.

As triboelectrification is a complex process, **Chapter 3** employs a simplified experimental setup to quantify charging. A hopper-chute and a faraday pail system have been employed to develop an experimental method for tribocharging. The effect of contact time, relative humidity and contact surface on electrification of particles was evaluated. With respect to humidity, the difference observed in specific charge of sucrose particles upon changing the RH from 20% to 60% was found to be practically insignificant. However statistically significant results were obtained in the case of MCC due to greater moisture sorption. The different interacting surfaces viz. aluminum and PVC produced charges of opposite polarity owing to difference in work function. The contact mechanical aspects of tribocharging were investigated using a 3D DEM model incorporating charge transfer and electrostatic forces. The effect of bouncing and continuous contacts revealed that the latter are more effective in charge transfer. Overall, a synergistic experimental and multi-scale approach was found to be more useful in quantifying electrostatic charging.

In **Chapter 4**, the tribocharging in a V-blender system has been investigated by both experiments and DEM simulations. The study was more elaborate with 2 API viz. Ibuprofen and

theophylline and 2 excipients i.e. MCC and lactose monohydrate. Secondly, a larger set of contact surfaces were employed viz. Aluminum, PVC, PMMA, Nylon and Teflon. Material characterization studies were performed to estimate particle size, surface area, moisture content and surface energy. Additionally, the experimental method developed in the previous chapter had to be modified since ibuprofen had a high initial charge. Hence, in this case all powders were spread into thin layer on aluminum foils and grounded for 36 hrs. The effect of contact time and blender speed was investigated. All powders displayed an initial rise in charge followed by a plateau. For all cases considered, Ibuprofen was found to charge the most. These saturation effects are expected in the DEM model as it incorporates the effect of the increasing potential of the particle as they charge in terms of its electric field. However there are quite significant differences between the experimental and simulation data for Ibuprofen. Thus the smaller particle size can be partly responsible for this enhanced tribocharging against all surfaces. However, there might be other material properties involved in charging efficiency of these powders that can be responsible for excessive charge accumulation on Ibuprofen as compared to other powders. For instance, the polar surface energy of Ibuprofen, estimated by Surface Energy Analyzer Chromatography, was found to be the highest as compared to other powders. Moreover a comparison of cohesive energy density (CED) suggests that Ibuprofen seems to deform the most and hence can accumulate a significant amount of charge as compared to other powders.

The approach presented **in Chapter 5** was aimed in understanding triboelectrification of binary mixtures. In this study it was observed that considerable charge mitigation occurs for different drug excipient combinations. To elucidate these effect furthers DEM simulations were performed. The electrostatic model developed in chapter 3 was extended to incorporate particle-particle charge transfer. The simulations results suggest that inter-particle charge transfer is considerable. The drug particles were found to charge positively at higher excipient concentrations due to more particle-particle collisions. Such interactions could also be involved in DPI formulations were charge reversal has been reported.

The Chapter 6 reviews the current state of knowledge encompassing the experimental and modeling approaches to understand particle size reduction. Besides the traditional techniques to measure particle size distribution viz. Laser diffraction and sieve analysis, new PAT tools have been highlighted. Additionally, benefits of simulations as a potential tool have been discussed. In most cases, the method of choice is contingent to the nature and extent of

information desired. An integrated approach however, of experimental and process modeling was recommended to understand the process meticulously.

The Chapter 7 involves an experimental and numerical based approach to study particle size reduction in a Wiley mill. Single particle breakage studies have been performed to understand the effect of damage accumulation. Moreover, experimental runs were conducted for parameters such as feed rate and impeller speeds. These effects have been simulated by employing a numerical model based on Grady's approach for fragmentation in impact mills, where DEM has been used to model flow of the material. Both simulation and experimental data suggest that flood feed conditions are observed for higher feed rate at impeller speed of 600 rpm. Velocity distributions at such high feed rates indicate that the particle bed almost becomes stagnant which overall reduces any particle-wall collisions. The simulations result suggests that DEM can be employed as a process development tool since it provides an insight on the effect of process parameters and equipment design.

Further investigation should be performed to develop a comprehensive understanding of both processes. For instance, in case of tribocharging effect of shape, surface roughness, and surface energy should be tested over a wide range of materials. The effect of humidity on triboelectrification has not yet been addressed the exact reason has not yet been elucidated. Future approaches could combine DEM-CFD to understand the effect of humidity on tribocharging. Moreover, the effect electrostatic discharge at higher RH also needs to be quantified. These phenomenon are not addressed in the current developed model. In case of milling, efforts should be directed towards incorporating the effect of shape and extending the model to other materials and. Furthermore, the effect of attrition or shear should also be incorporated. These modifications could also enhance the applicability of the existing models.